FACULTY OF TECHNOLOGY

DEPARTMENT OF MECHANICAL ENGINEERING

SCHOOL OF GRADUATE STUDIES

THERMAL ENGINEERING STREAM

AEROTHERMODYNAMICS ANALYSIS OF AXIAL FLOW AIRCRAFT GAS TURBINE ENGINE COMPRESSOR

A THESIS

By

TILAHUN NIGUSSIE GEMECHU

ADVISOR:

Dr. TESFAYE DAMA

IN PARTIAL FULFILMENT OF THE REQUIREMENTS OF MASTER'S OF SCIENCE DEGREE IN MECHANICAL ENGINEERING (SPECIALIZED IN THERMAL ENGINEERING).

October 5, 2009

FACULTY OF TECHNOLOGY

DEPARTMENT OF MECHANICAL ENGINEERING

SCHOOL OF GRADUATE STUDIES

THERMAL ENGINEERING STREAM

AEROTHERMODYNAMICS ANALYSIS OF AXIAL FLOW AIRCRAFT GAS TURBINE ENGINE COMPRESSOR

By:

Tilahun Nigussie Gemechu

Approved By Board of Examiners:

1	**Dr. Ing. Edessa Dribsa**		
Chairman, ME Department Graduation Committee		**Signature**	**Date**
2	**Dr. Tesfaye Dama**		
Advisor		**Signature**	**Date**
3	**Dr.Ing. Edessa Dribsa**		
Internal Examiner		**Signature**	**Date**
4	**Dr.Ing. Abebayehu Assefa**		
External Examiner		**Signature**	**Date**

ACKNOWLEDGEMENT

First I thank God for giving me strength to finish my work and also the works described not have been possible with out the valuable assistance of many people. I would like to express my deepest gratitude to my thesis advisor, Dr.Tesfaye Dama, for his skillful guidance, encouragement, enormous patience and willing attitude throughout the course of this research.

I would also like to thank Dr. - Ing. Edessa Dribsa for providing me with useful directions and discussions in my quest for solutions as well as for showing the scientific path in order to enrich my knowledge.

I am indebted to the Technology faculty of Addis Ababa University for the financial assistance towards some expenditure incurred in the preparation of this thesis. I also want to appreciate all of my instructors / colleague in the Department of Mechanical Engineering, Addis Ababa University for their continuous encouragement.

I regret if any acknowledgement that is due has been missed out or found inadequate.

Finally, I would like to thank my family for the unending confidence, constant support and endless love.

"If we knew what it was we were doing, it would not be called research, would it?"

Albert Einstein

ABSTRACT

The axial flow type compressor is one of the most common compressor types in use today. It finds its major application in large aircraft gas turbine engine like those that power today's jet aircraft.

Early axial flow aircraft engine compressors had pressure ratio of around 5:1 and require about 10 stages. Over the years the overall pressure ratios available exceed 30: 1 due to continued aerodynamic development that resulted in a steady increase in a stage pressure ratio with reduced number of stages. There has been in consequence a reduction in engine weight for a specific level of performance, which is particularly important for aircraft engines. These potential gains have now been fully realized as the result of intensive research into the Aero-thermodynamics Analysis of Axial Flow Aircraft Gas Turbine Engine Compressor. Therefore, careful design of compressor blading based on aero-thermodynamic theory, experiment and computational fluid dynamic (CFD) analysis is necessary not only to prevent useful losses but also to insure a minimum of stalling troubles.

The complete analysis of this thesis is done to provide some part of design of an axial compressor suitable for a simple low-cost and low weight turbojet Aircraft Gas Turbine Engine Compressor by using different research work on the aero-thermodynamic analysis of the compressor.

Details of CFD analysis on the models of the compressor, using a commercial software "FLUENT", will be presented. The CFD simulation predictions were validated quantitatively against the experimental data and the theoretical (calculated values) were then used to obtain further insights into the characteristics of the flow behaviors.

To calculate the work and power required by the compressor to sustain the flight, the blades of the compressor will be modeled, and the required equations will be developed. Finally a small scale computer program will be developed to calculate the power (work) required by the compressor and to determine other performance measuring parameters.

LIST OF CONTENTS

CHAPTER THREE

LITERATURE REVIEW

CHAPTER FOUR

AERO-THERMODYNAMIC ANALYSIS OF COMPRESSOR STAGES

CHAPTER FIVE

AERO-THERMODYNAMIC ANALYSIS FOR AXIAL FLOW AIRCRAFT GAS TURBINE ENGINE COMPRESSOR DESIGN

CHAPTER SIX

CFD ANALYSIS AND PERFORMANCE EVALUATION OF AXIAL FLOW AIRCRAFT GAS TURBINE ENGINE COMPRESSOR

CHAPTER SEVEN

SUMMARY, CONCLUSIONS AND RECOMMENDATIONS FOR FUTURE WORK

LIST OF FIGURE

LIST OF TABLE

NOMENCLATURE

For velocity triangle notation (U, C, V,α,β) see figure 4.2

For cascade notation (α, δ, ε, ζ, θ, I ,S,C) see figure 3.1

C_D Overall drag coefficient

C_{DA} Annulus drag coefficient

C_{DP} Profile drag coefficient

C_{DS} Secondary loss coefficient

C_L Lift coefficient

C_P Specific heat constant at constant pressure

W_C Work of compressor

P_C Power of compressor

T_C Torque of compressor

D Diffusion factor

U Blade speed

γ Ratio of specific heats

h Blade height, specific enthalpy

n Number of blades

N Number of stages, rotational speed of the shaft

r Radius

R r/r_m as well as pressure ratio and gas constant

w, Stagnation pressure loss

h/C Aspect ratio

S/C pitch/chord ratio

λ Work-done factor

Λ Degree of reaction

ϕ Flow coefficient

ψ Temperature coefficient, stage loading coefficient

V Relative velocity

C Absolute velocity

η Efficiency

Suffixes

a, w axial, whirl component

b blade row

m mean, vector mean

S stage

R root radius, radial component

t tip radius

Subscript

0 stagnation conditions

1 inlet station of compressor rotor blade for a stage or stage 1

2 exit station of compressor rotor blade for a stage or stage 2

3 exit station of compressor stator blade for a stage or stage 3

CHAPTER ONE

INTRODUCTION

A compressor is one of a turbo machine operate on the principal of acceleration of the working fluid followed by diffusion to convert the acquired kinetic energy to a pressure rise. Its primary importance in aircraft gas turbine engine is to increase the pressure of the mass of air entering the engine inlet and discharge it to the exit of the compressor and then to combustion section at the correct velocity, temperature and pressure.

In the following sections of this chapter, different types of aircraft gas turbine engine compressors, the objective of this thesis, methodology used and the outline of the thesis will be presented.

1.1 Classification of Aircraft Engine Compressors

The desire of having a compressor is the most fully meeting all the requirements in specific conditions that led to creation of several types of aircraft engine compressor. The two principal types of compressors used in turbojet aircraft engines are centrifugal and axial flow type. The following section will briefly describe the two types of compressors.

1.1.1 Centrifugal Flow Compressors

The centrifugal flow compressor is sometimes referred to as a radial out flow compressor. It is the oldest design and still in use today. Many small engines, as well as the majority of auxiliary gas turbine power plants, use this design.

In a centrifugal engine, the compressor performs its duties by receiving air at the center of the impeller in an axial direction and accelerating the air outwards by a centrifugal reaction due to its rotational speed. The air is then allowed to expand into divergent duct, called diffuser, and according to Bernoulli's principle, as the air speeds slow and static pressure builds.

1.1.2 Axial Flow Compressors

Axial flow aircraft engine compressors are rotating, aerofoil based compressors in which the working fluid principally flows parallel to the axis of rotation. This is in contrast with other rotating compressors such as centrifugal, axis-centrifugal and mixed-flow compressors where the air may enter axially but will have a significant radial component on exit.

In general, the importance of a high overall pressure ratio, in reducing specific fuel consumption from an early stage in history of the gas turbine was recognized that the axial flow compressor had the potential for both high-pressure ratio and high efficiency than the centrifugal compressors. Another major advantage, especially for jet engines, was the much larger airflow rate for a given frontal area.

1.2 Objective of the Thesis

Axial flow jet engine manufacturers are continuously seeking to produce engines that are lighter and smaller in order to reduce manufacturing and operating costs. Part of the approach is to design a compressor with fewer stages while maintaining the required overall pressure rise and efficiency. This can be achieved by the aerothermodynamics analysis of the compressor. Therefore, the objective of this thesis is to present the complete aero-thermodynamic analysis of an axial flow compressor which is suitable for a simple low-cost and low weight turbojet aircraft engine.

The specific objectives of the thesis are to formulate a knowledge-driven process that facilitates the design of axial flow aircraft engine compressors by achieving the following:

- Carryout a literature survey on the different work done on axial flow compressor cascade by different researcher.
- Highlight, the three different design approaches for the blade of the compressor.
- Decide on the air angles likely to lead to a satisfactory design of compressor.
- Discuss methods of obtaining the blade shape and determine the correct geometry of the blade forms.

- Present computational fluid dynamic analysis (CFD) using FLUENT software on the model of the compressor after determining the correct geometrical forms of the blades.
- Present numeric results, simulations and discussion on the model of the compressor based on FLUENT results.
- Develop a small scale computer program using C++ high programming language in order to reduce the preliminary design effort of axial flow compressor for determining its performance.

1.3 Methodology

The blades of the compressor can be modeled to carry out the analysis of the thesis by following an assumed design point under sea-level static conditions since the compressor performance vary with altitude (air density). The see-level design performance is quoted for maximum power (that is at maximum turbine inlet temperature) which must meet the aircraft take-off requirements in order to have short take-off distance.

The complete aero-thermodynamic analysis will encompass the following steps:

- Choice of rotational speed and annulus dimensions;
- Determination of number of stages, using an assumed efficiency;
- Calculation of air angles for each stage at the mean radius;
- Determination of the variation of air angles from root to tip;
- To accurately model the systems of interest and to solve the governing continuum equations without making any arbitrary assumptions, the commercial Computational Fluid Dynamics (CFD) package FLUENT is utilized.
- The entire system that includes a rotor and stator (stage of compressor) will be modeled to investigate compressibility effect, to see the velocity and pressure distributions through the system.

- The numerical results are then presented and validated with experimental and theoretical (calculated) data.
- Developing of small scale computer program using C++ high programming language.

1.4 Outline of the Thesis

This thesis has seven chapters and it starts with a detail discussion of fundamentals, hypothesis of operation and applications of axial flow compressors in ***chapter 2***.

Chapter 3 deals with previous research work done on axial flow compressors. The literature survey presented in chapter 3 consists of published theoretical models, experimental investigations, blade designs, loss analysis.

Chapter 4 describes the aero-thermodynamic analysis of axial compressor stage which is the basis for the overall analysis of axial flow compressor. Basic assumptions, governing equations are also given.

Chapter 5 deals with the aero-thermodynamic analysis of axial flow compressor to get a simple, low-cost and low weight turbojet engine compressor design.

Chapter 6 describes basic numerical computation scheme, which is CFD analysis using FLUENT and developing of small scale computer program using C++ high programming language. The major part of this chapter study deals with analysis on the model of one stage compressor with FLUENT. However, the methods used are suitable for any of an axial compressor stage simulation using FLUENT. The analysis and interpretation of the results is discussed in Chapter 6 by using graphical displays and empirical reporting of results.

In the last chapter conclusions are drawn based on results obtained and some recommendations are given in regard to the long-term objectives.

CHAPTER TWO

CONSTRUCTIONAL AND OPERATIONAL FEATURES OF AXIAL FLOW COMPRESSORS

The objective of this chapter is to present constructional feature of axial compressors, to present the working principle of axial compressor and to describe the application of axial compressors in different sectors.

2.1 Constructional Feature of Axial Compressors

The two main elements of an axial-flow compressor are the rotor and stator. The rotor is the rotating element of the compressor. The stator is the fixed element of the compressor. The rotors and stators are enclosed in the compressor casing. Modern engines use a casing that is horizontally divided into upper and lower halves. The halves are normally bolted together with either dowel pins or fitted bolts. On some older engines, the cases are a one-piece cylinder open on both ends. The one-piece compressor case is simpler to manufacture; however, any repair or detailed inspection of the compressor rotor is impossible. The engine must be removed and taken to a shop where it can be dis-assembled for repair or inspection of the rotor or stators. On many split-case engines, either the upper or lower case can be removed for maintenance and inspection with the engine in place.

The compressor case is usually made of aluminum or steel. The material used will depend on the engine manufacturer and the accessories attached to the case.

Rotor blades are usually made of stainless or iron-based, super-strength alloys. Methods of attaching the blades in the rotor disk rims vary in different designs, but they are commonly fitted into disks by either bulb (Figure. 2-1, view A) or fir-tree (Figure 2-1, view B) type roots. The blades are then locked with grub screws, lock wires, pins, or keys.

The stator vanes project radially toward the rotor axis and fit closely on either side of each stage of the rotor. The stator vanes are usually made of steel with corrosion- and erosion-resistant qualities. Frequently, the vanes are shrouded by a band of suitable material to simplify the fastening

problem. The vanes are welded into the shrouds, and the outer shrouds are secured to the inner wall of the compressor case by retaining screws.

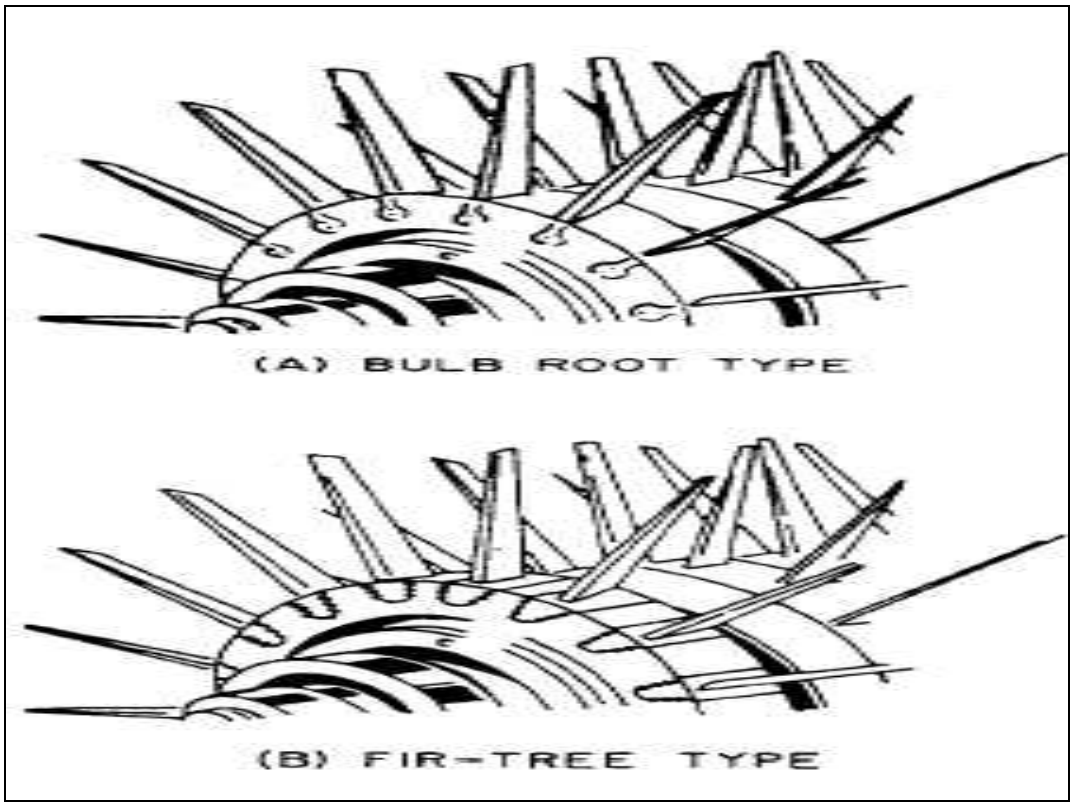

Figure 2-1 Methods of attaching the blades in the rotor disk rims [4]

Each consecutive pair of rotor and stator blades constitutes a pressure stage, and each successive rotor-stator pair is called a compressor stage, as shown in Figures 2.2 and 2.3.

Preceding the stators and the first stage of the compressor rotor, there may be a row of IGVs. The function of the IGVs is to straighten the airflow and direct it to the first-stage rotor.

The very low pressure ratio attainable in a single axial stage requires that, for most aircraft engine applications, a multiple stage compressor be used.

In principle the preceding treatment of single stage performance is adequate for the study of a multistage compressor which is, after all, just a series of single stages.

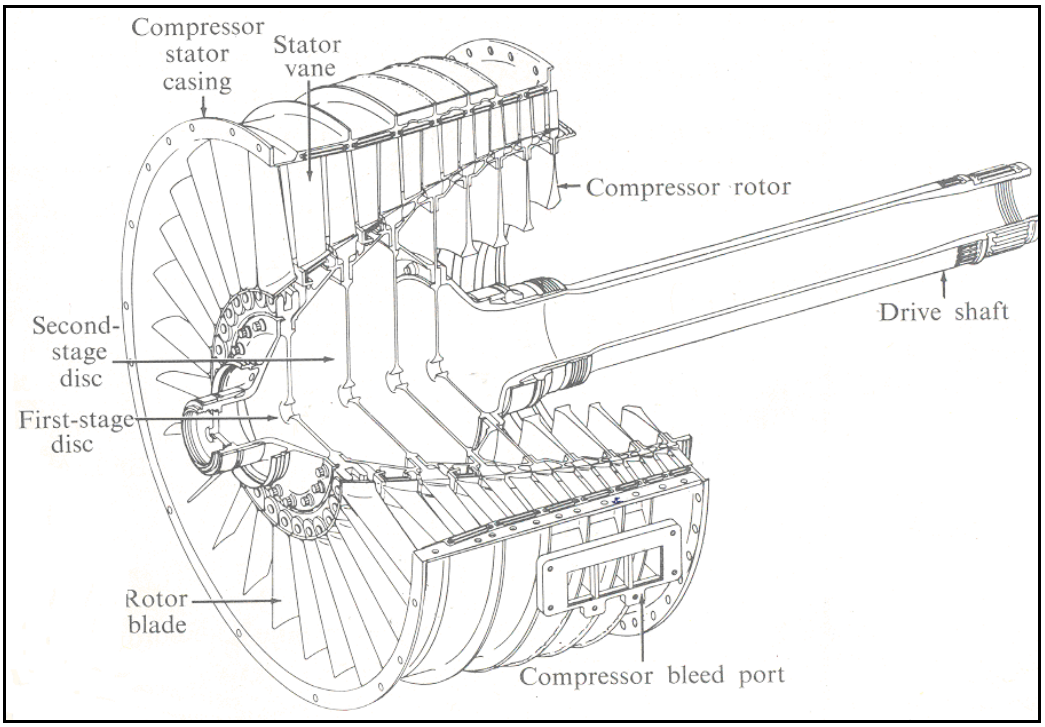

Figure 2.2: **A cutaway sketch of a typical multistage axial flow compressor assembly: the general Electric J85 compressor. (Courtesy General electric Co.) [2]**

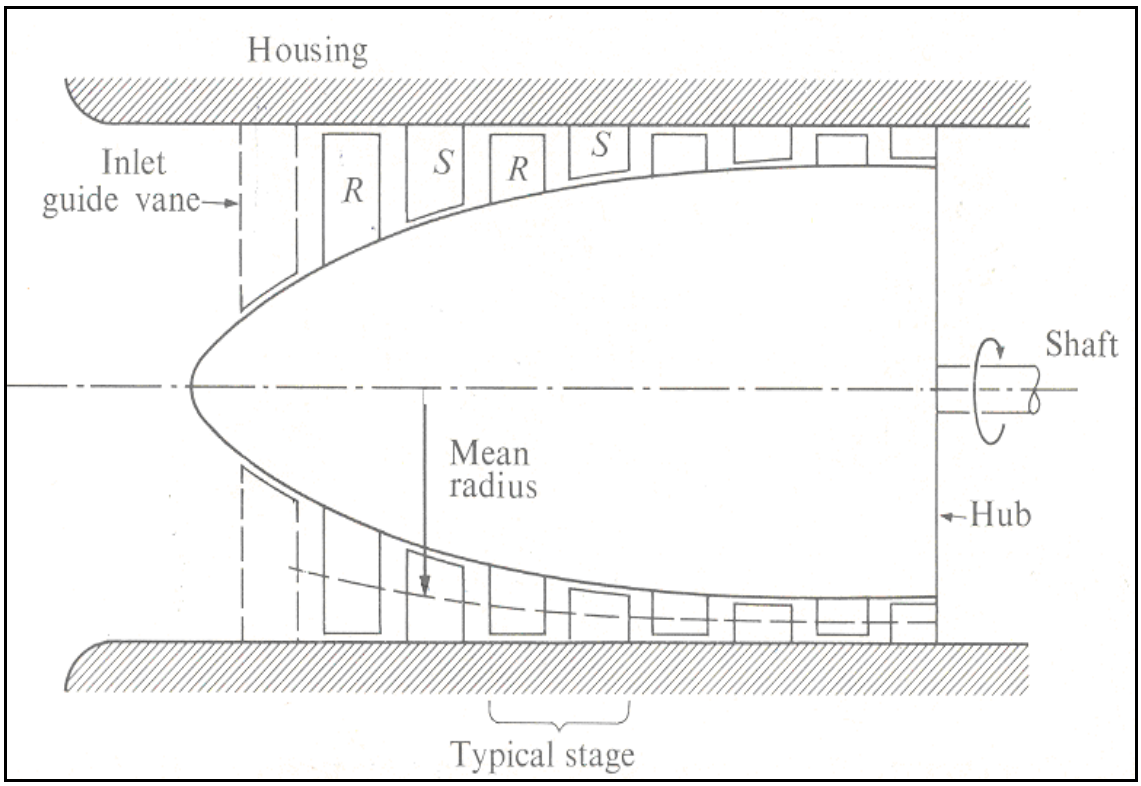

Figure 2.3: Schematic of a section of multistage axial flow compressor. [2]

2.2 Basic Principle of Operation

The compressor section is that portion of an aircraft gas turbine engine which produces an air pressure rise. Its operating principle is as follows:-

First, air is drawn into the system through the intake and enters the first row of moving blades. These blades are attached to the periphery of the rotor, mounted on the shaft and, due to the rotation, have a mean tangential velocity. The blade inlet angle is so designed that the entry of air is smooth and as shock-free as possible when the compressor is running under the designed optimum conditions. In passing through the ring of moving blades the air is given a certain tangential velocity in the direction of rotation of the blades, so that it emerges from the ring with its original axial velocity parallel to the rotor axis plus a tangential velocity component. If these two velocities are added vectorially it will be seen that the resultant velocity, which is the absolute velocity of the air leaving the moving rings is greater than the original absolute velocity of the air on the entry to the ring, and that the direction of this absolute velocity is no longer parallel to axis of the rotor, but is inclined to it at an angle. Thus, the absolute velocity of the air is increased due to its passage through the ring of moving blades.

On leaving the moving blade-ring the air enters the first row of the fixed blades, attached to the compressor casing. The entry angle of these fixed blades is so designed that the air is picked up smoothly and without shock loss, which means that the inlet edges of the blades are in line with the direction of the air leaving the moving blade-ring. The function of these fixed blades is to guide the air back to its original direction parallel to the axis of the rotor, so that it enters the second moving blade-ring in the same direction in which it entered the first moving blade-ring .In so doing, the tangential velocity component which the air acquired during its passage through the moving blade-ring is destroyed and the air leaves the fixed blades in an axial direction with the same absolute velocity with which it entered the first ring of moving blades .Thus ,the absolute velocity of the air is decreased during its passage through the fixed blade-ring. The air then enters the second moving blade-ring passes to the second fixed blade-ring and the process is repeated until it finally reaches the compressor outlet.

2.3 Applications of Axial Flow Compressors

Axial compressors are widely used in gas turbines, such as jet engines, high speed ship engines, and small scale power stations. They are also used in industrial applications such as large volume air separation plants, blast furnace air, fluid catalytic cracking air, and propane dehydrogenation.

Axial compressors, known as superchargers, have also been used to boost the power of automotive reciprocating engines by compressing the intake air, though these are very rare.

CHAPTER THREE

LITERATURE REVIEW

3.1 Introduction

As mentioned in section 2.3 axial flow compressors have found many applications in different sectors. Despite this, there was much research conducted in the past. But, the numbers of publications existing in literatures for axial flow aircraft engine compressor are very few comparing to other applications of axial flow compressor and most of the researches conducted in axial flow aircraft engine compressor are experimental rather than other areas of research. Hence, the literature review presented in this chapter can be categorized as:-

- Cascade Nomenclature and Terminology
- Stage losses and Efficiency
- Experimental Work
- Theoretical Models
- CFD Work
- Unsteady operation of compressor (compressor stall).

3.2 Cascade Nomenclature and Terminology

A cascade blade profile can be conceived as a curved camber line upon which a profile thickness distribution is symmetrically superimposed. A cross-section of three blades forming a part of a typical cascade is shown in Figure 3.1, which is reproduced from Howell's early paper [1, 10] on cascade theory and performance, shows the standard nomenclature, related to aerofoil in cascade, which is used throughout this thesis analysis.

In practice the shape of the camber line is usually either a circular arc or a parabolic arc defined by the maximum camber located at a distance 'a' from the leading edge of the blade. The profile thickness distribution may be that of a standard aerofoil section but, more usually, is one of the sections specifically developed by the various research establishments for compressor.

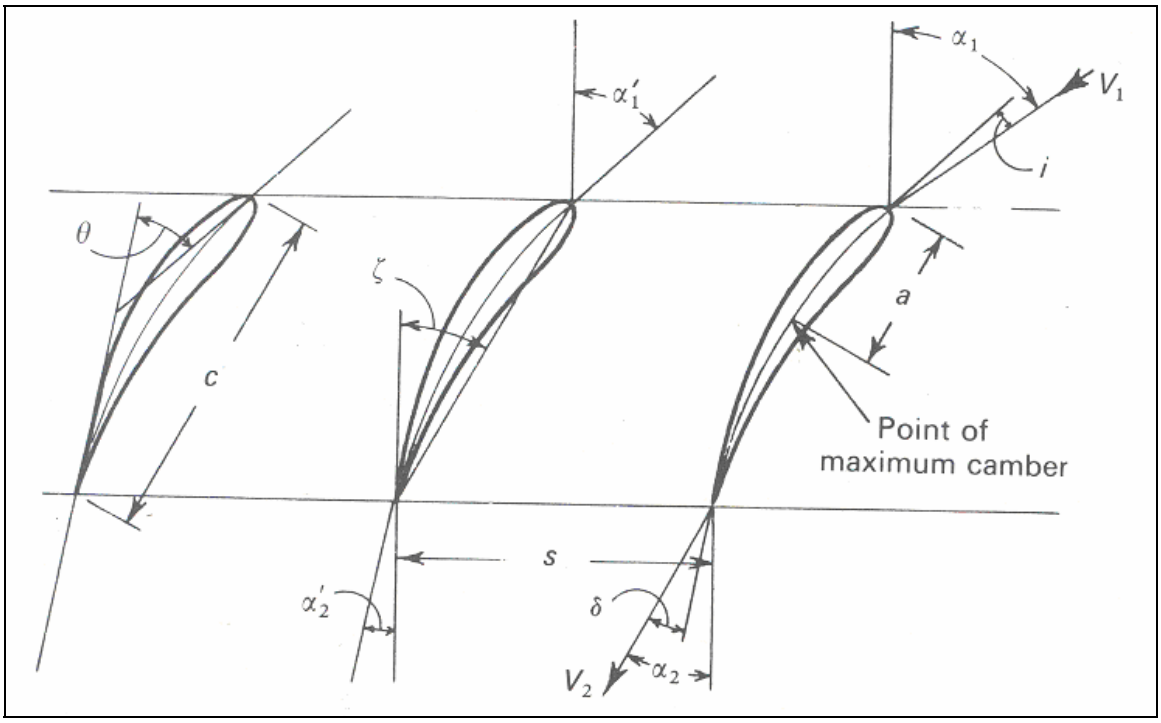

Figure 3.1 Compressor cascade and blade notation (A.R. Howell (10) Courtesy H.M.S.O-Crown copyright reserved) [1, 16]

α'_1=blade inlet angle,
α'_2=blade outlet angle,
α_1=air inlet angle,
α_2=air outlet angle,
θ=blade camber angle,
$=\alpha'_1-\alpha'_2$
ε=deflection=$\alpha_1-\alpha_2$
$=\alpha_1-\alpha_2$

ζ=setting or stagger angle C (or l) =Chord
S=pitch (or space)
V_1=air inlet velocity
V_2=air outlet velocity
i=incidence angle
$=\alpha_1-\alpha'_1$
δ=deviation angle
$=\alpha_2-\alpha'_2$

3.3 Stage Losses and Efficiency

Cascades losses occurring in axial compressor depend on a number of aerodynamic and cascade geometrical parameters. In a complete compressor, stage losses due to bearing and disc friction (shaft losses) also occur. Figure 3.2 shows the energy flow diagram for an axial compressor stage. Figures in brackets indicate the order of energy or losses corresponding to 100 units of energy supplied at the shaft. The values shown in the energy flow diagram are only to give an example.

The stage work ($h_{03}-h_{01}$) is less than the energy supplied to the shaft by the prime mover on account of bearing and disc friction losses. All the stage work does not appear as energy at the stator entry on

account of aerodynamic losses in the rotor blade row. After deducting the stator (diffuser) blade row losses from the energy at its entry, the value of the ideal or isentropic work required to obtain the stage pressure rise is obtained. The ratio of the isentropic work and the actual stage work gives the stage efficiency, whereas the overall efficiency is directly obtained as 82%.

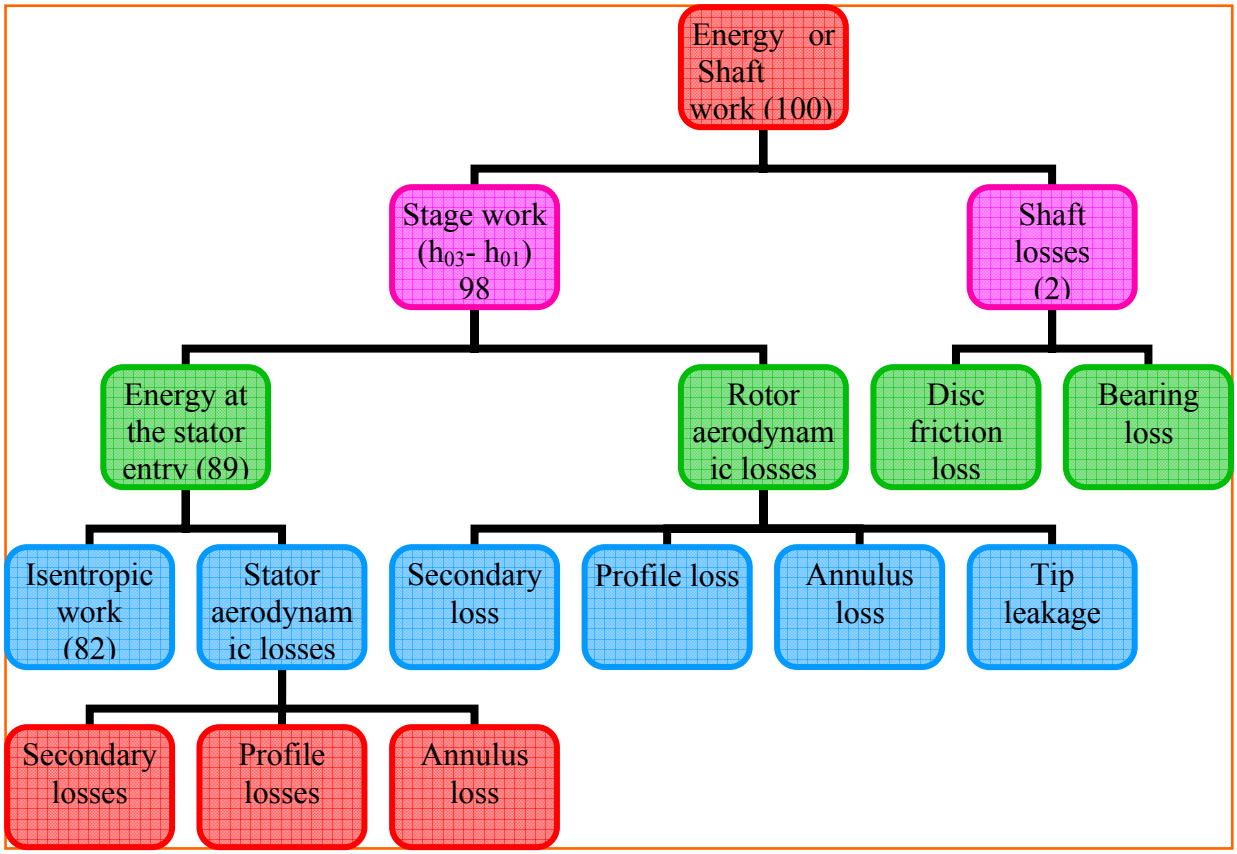

Figure 3.2 Energy flow diagrams for an axial flow compressor stage [3]

3.4 Experimental Work

The results obtained from numerous cascade wind tunnel tests have been used to establish design criteria. For example, Howell [1,10] has given ‘’mean work-done factors’’ for compressors with varying numbers of stages, as in Figure 3.3 based on his experimental work as the number of stage increases the work done factor decrease and finally it become constant for large number of stages. He suggested that the stagnation enthalpy rise across a stage could be expressed as:-

$h_{03} - h_{01} = \lambda U (\Delta C_w)$. Where λ is a ‘’work-done factor which is used to compensate the reduction in the work capacity of a stage’’, U is the blade speed, ΔC_w is change in whirl velocity.

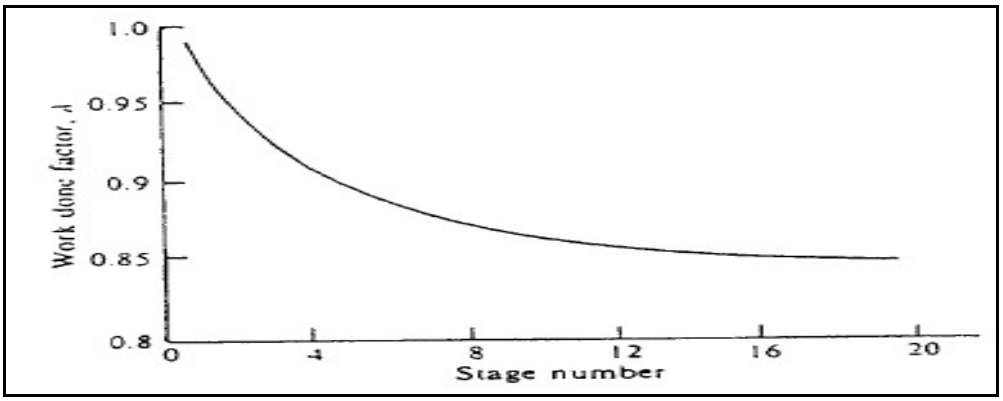

Figure 3.3 Mean work-done factors in compressors (Howell and Bonham (1, 10)) (Courtesy of the Institution of Mechanical engineers)

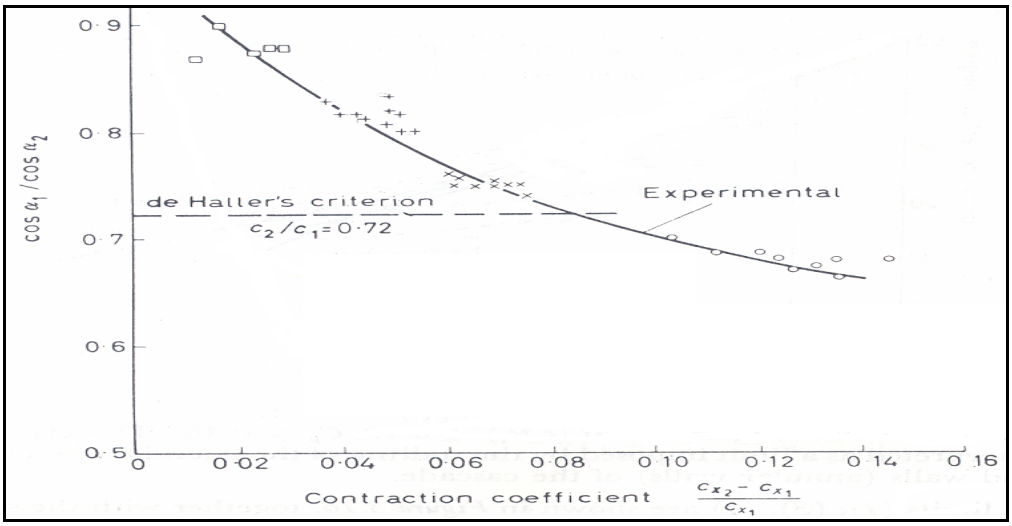

Figure 3.4 Contraction coefficients in cascades [1]

A plot of the contraction ratio (which is the ratio of the change in the mainstream axial velocity and the entry axial velocity, $(C_{x2}-C_{x1})/C_{x1}$) obtained by Rhoden [1]. Figure 3.4 shows the increase in C_{x2}/C_{x1} at high incidence (and pressure coefficient C_p). The outlet angle (α_2) is the same for all the cascades tested and a limit $C_2/C_1=0.72=\cos\alpha_1/\cos\alpha_2$ may be drawn on the graph to indicate de Haller's limit on cascade performance. [1]

Howell [3, 10] obtained design conditions for a compressor cascade from plots of experimentally obtained values of cascade losses and deflection against incidence. Figure 3.5 shows curves for the variations of the lift coefficient, deflection angle and total pressure loss coefficient with incidence. It is observed that high losses occur at maximum values of deflection and lift coefficient. Therefore

Howell suggested that the chosen value (nominal value,ε^*) of the deflection must be fairly away from the stalling point (stalling incidence i_s, deflection ε_s). Though it is difficult to specify the stall point, here it is defined as a condition at which the total cascade loss is twice its minimum value.

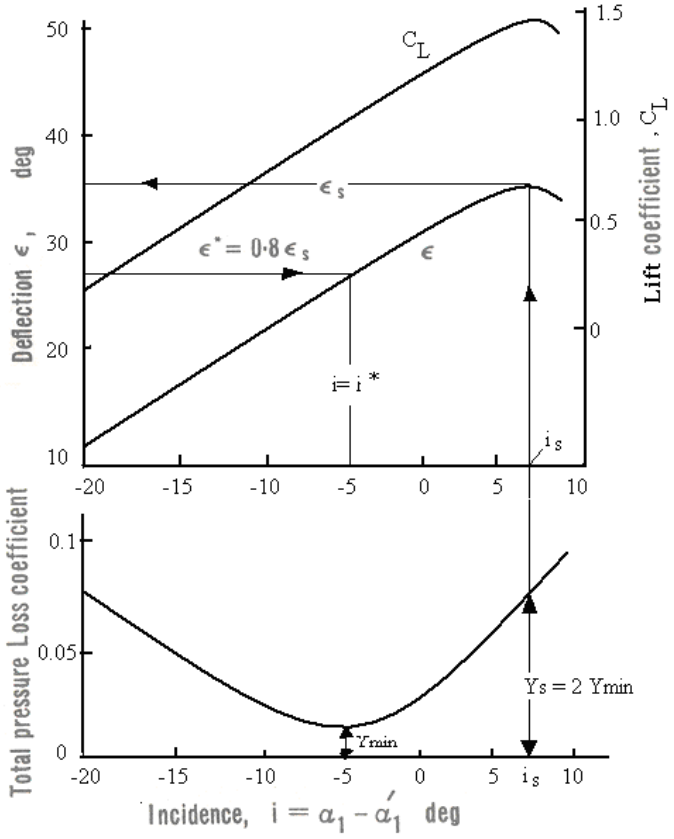

Figure 3.5 Variation of lift, deflection and pressure loss with incidence for a compressor cascade (Howell (3, 9)). (By Courtesy of the controller of H.M.S.O) crown copyright reserved.

A typical set of low-speed compressor cascade results made by Howell [3, 9] for a blade cascade of specified geometry is shown in Figure 3.6. These results are presented in the form of a pressure loss coefficient, $\Delta Po/(1/2\rho C^2_1)$ and the fluid deflection $\varepsilon=\alpha_1-\alpha_2$ against incidence $i=\alpha_1-\alpha'_1$ (refer to Figure 3.1 for nomenclature). It is seen from the graph that there is a pronounced increase in total pressure loss as the incidence rises beyond a certain value and the cascade is stalled in this region.

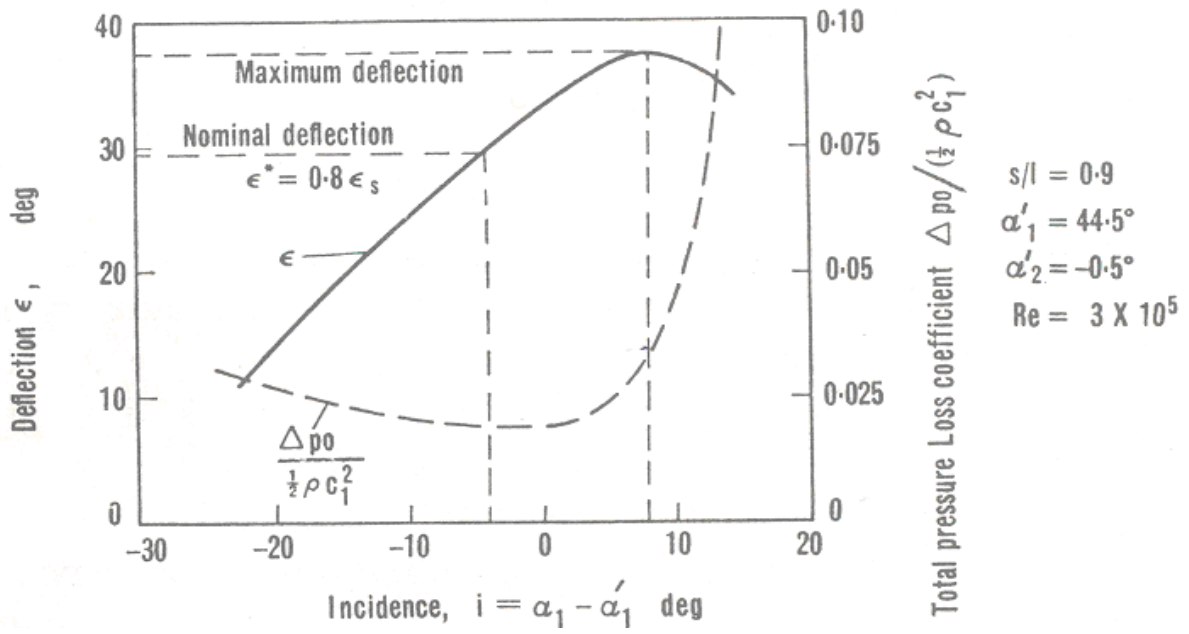

Figure 3.6 Compressor cascade characteristics (Howell (1, 9)). (By Courtesy of the controller of H.M.S.O) crown copyright reserved.

Physically, stall is characterized (at positive incidence) by the flow separating from the suction side of the blade surfaces. With decreasing incidence, total pressure losses again rise and a ‘’negative incidence’’ stall point can also be defined as above.

Howell again states that the working range is conventionally defined as the incidence range between these two limits at which the losses are twice the minimum loss. An accurate knowledge of the extent of the working range, obtained from two-dimensional cascade tests, is of great importance when attempting to assess the suitability of blading for changing conditions of operation.

Howell [1, 9] suggested that the different losses could be estimated using the following drag coefficients.

For the annulus walls loss,

$$C_{Da}=0.02\ S/h \qquad [3.1]$$

And for the so-called ‘’secondary’’ loss,

$$C_{Ds}=0.018\ C^2_L \qquad [3.2]$$

Where, S and h are the blade pitch and blade height respectively, and C_L the blade lift coefficient. Calculations of this type were made by Howell and others to estimate the efficiency of a complete compressor stage.

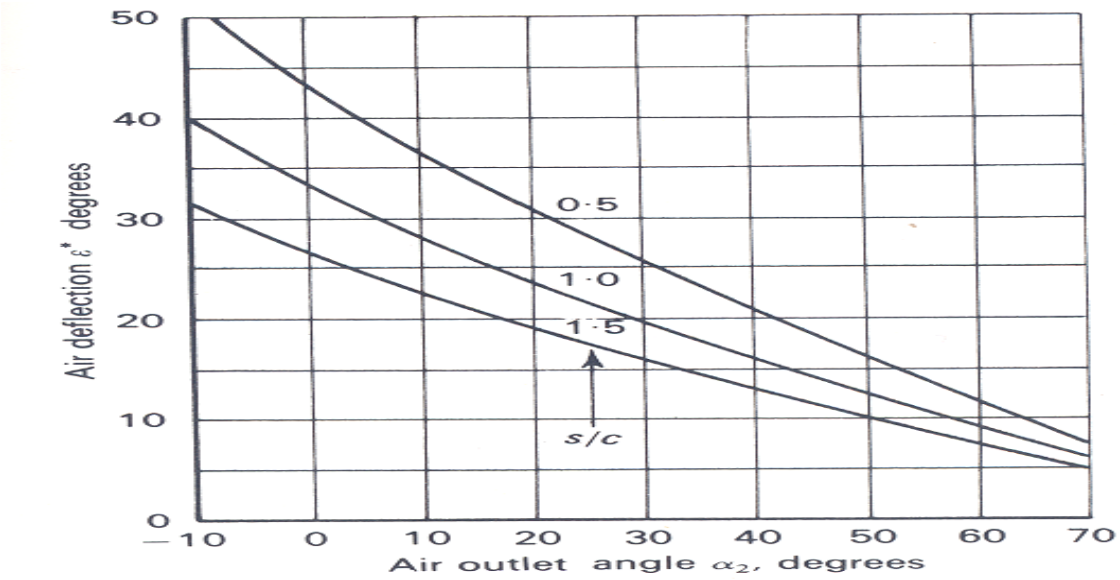

Figure 3.7 Variation of nominal deflection with nominal outlet angle for several Space/chord ratios (adapted from Howell (1, 3, and 10)).

Figure 3.7 shows the variation of ε* found by Howell, [5] against α_2 for several space-chord ratios. The dependence on Reynolds number is small for $Re>3\times10^5$, based on blade chord.

Referring to Figure 3.1, the deviation $\delta=\alpha_2-\alpha'_2$ is drawn as positive, almost without exception, it is in such a direction that the deflection of the fluid is reduced. The deviation may be of considerable magnitude and it is important that an accurate estimate is made of it. Howell used an empirical rule to relate nominal deviation δ* to the camber and space-chord ratio,

$$\delta^*=m\,\theta(\delta/c)^n \qquad [3.3]$$

The value of 'm' depends up on the shape of the camber line and the blade setting. For compressor cascade (that is diffusing flow). Where n=0.5 for compressor cascades.

$$m=0.23\,(2a/C)^2+\alpha_2/500 \qquad [3.4]$$

Where, a, is the distance of maximum camber from the leading edge. Frequently a circular arc camber-line is chosen so that 2a/C=1, thereby simplifying the formula for m, but as given in Equation (3.4) embraces all shapes including a parabolic arc which is sometimes used. (For inlet guide vanes, which are essentially nozzle vanes giving accelerating flow, the power of S/C in Equation (3.3) is taken as unity instead of 0.5 and m is given a constant value of 0.19.)

To obtain the performance of a given cascade at conditions removed from the design point generalized performance curves of Howell (9) shown in Figure 3.8 may be used. If the nominal deflection ε* and nominal incidence i* are known the off-design performance (deflection, total pressure loss coefficient) of the cascade at any other incidence is readily calculated.

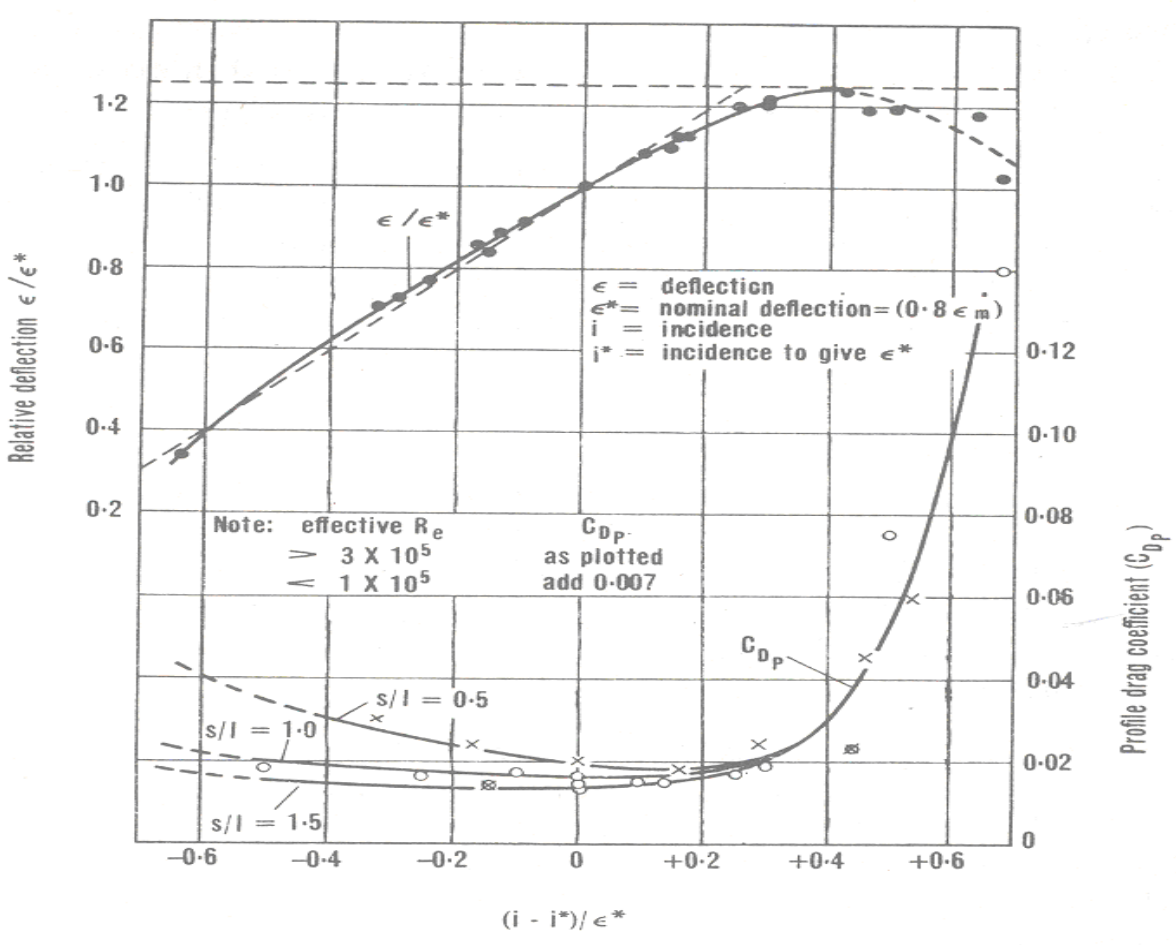

Figure 3.8 The off-design performance of a compressor cascade (Howell (1, 9, 16)) (By courtesy of the controller of H.M.S.O, crown copyright reserved.)

3.5 Theoretical models

The development of flow theories through a row of blades started in the 1920's when axial compressor blades began to be designed by considering each blade as isolated airfoils. Various methods were employed later for determining the effects of neighboring blades [3].The following section will briefly describes the governing equation for flow through blades row.

3.5.1 Equations of motion-Cartesian coordinate system

Figure 3.9 shows that the axes of references are X, Y, and Z. The origin is located at the trailing edge of the blade at its root. The Z-axis is along the blade height, Y-axis along the blade pitch and X-axis along the axial direction. These directions are also referred to as span –wise, pitch wise and stream-wise directions.

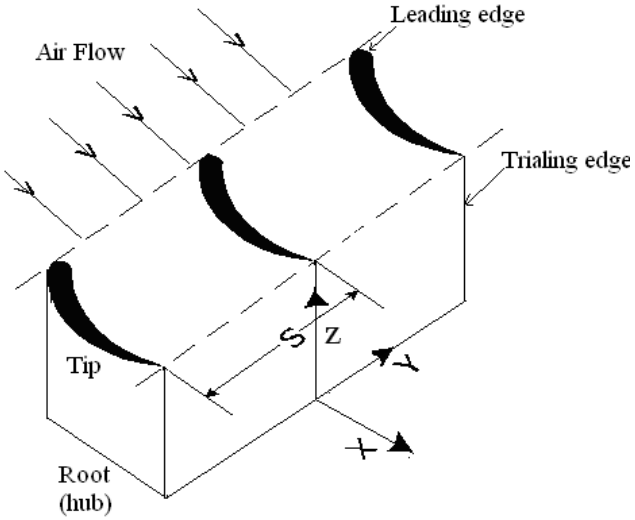

Figure 3.9 A rectilinear cascade of an axial compressor in Cartesian coordinates.

A point in the flow field through the blades is specified by its coordinates X, Y, and Z. Various fluids dynamic parameters at this point are:

- **Coordinates** X Y Z
- **Velocities** **Cx (Ca)** **Cy** **Cz**
- **Vorticities** ξ η ζ
- **Body forces** **x** **y** **z**

3.5.1.1 Continuity Equation

This simply states the law of conservation of mass mathematically. In three dimensions it is given by:-

$$\frac{\partial}{\partial x}(\rho C_x)+\frac{\partial}{\partial y}(\rho C_y)+\frac{\partial}{\partial z}(\rho C_z)+\frac{\partial \rho}{\partial t}=0 \qquad [3.5]$$

Its modified form for the following conditions is given below:

(A) Steady flow

There is no change in any flow parameter with time in steady flow that is:-$\frac{\partial \rho}{\partial t}=0$ .Therefore for steady, three-dimensional and compressible flow,

$$\frac{\partial}{\partial x}(\rho C_x)+\frac{\partial}{\partial y}(\rho C_y)+\frac{\partial}{\partial z}(\rho C_z)=0 \qquad [3.6]$$

(B) Incompressible flow

The change in the fluid density is negligible in incompressible flow, that is, ρ≈constant. Therefore,

$$\frac{\partial}{\partial x}(C_x)+\frac{\partial}{\partial y}(C_y)+\frac{\partial}{\partial z}(C_z)=0 \qquad [3.7]$$

(C) Two-dimensional flow

The flow in an infinitesimally thin slice of the flow field in the cascade shown in the Figure 3.9 will be two dimensional; the variations in the third direction (Z-direction are absent). Therefore for steady, two-dimensional incompressible flow,

$$\frac{\partial}{\partial x}(C_x)+\frac{\partial}{\partial y}(C_y)=0 \qquad [3.8]$$

(D) One-dimensional steady flow

For one-dimensional steady flow, $\frac{\partial}{\partial x}(C_x) = 0$

Therefore, ρA Cx =constant [3.9]

A is the cross-sectional area perpendicular to the velocity Cx (Ca).

3.5.1.2 Momentum Equations

The momentum equation in a given direction is a mathematical statement of Newton's second law of motion. If only viscous body and pressure forces are considered the following equations are obtained:-

$$C_x \frac{\partial C_x}{\partial x} + C_y \frac{\partial C_x}{\partial y} + C_z \frac{\partial C_x}{\partial C_z} + \frac{\partial C_x}{\partial t} - X + \frac{1}{\rho}\frac{\partial P}{\partial x} = \frac{\mu}{\rho}\left(\frac{\partial^2 C_x}{\partial x^2} + \frac{\partial^2 C_x}{\partial y^2} + \frac{\partial^2 C_x}{\partial z^2}\right) \quad [3.10]$$

$$C_x \frac{\partial C_y}{\partial x} + C_y \frac{\partial C_y}{\partial y} + C_z \frac{\partial C_y}{\partial C_z} + \frac{\partial C_y}{\partial t} - Y + \frac{1}{\rho}\frac{\partial P}{\partial y} = \frac{\mu}{\rho}\left(\frac{\partial^2 C_y}{\partial x^2} + \frac{\partial^2 C_y}{\partial y^2} + \frac{\partial^2 C_y}{\partial z^2}\right) \quad [3.11]$$

$$C_x \frac{\partial C_z}{\partial x} + C_y \frac{\partial C_z}{\partial y} + C_z \frac{\partial C_z}{\partial C_z} + \frac{\partial C_z}{\partial t} - Z + \frac{1}{\rho}\frac{\partial P}{\partial z} = \frac{\mu}{\rho}\left(\frac{\partial^2 C_z}{\partial x^2} + \frac{\partial^2 C_z}{\partial y^2} + \frac{\partial^2 C_z}{\partial z^2}\right) \quad [3.12]$$

These are the well known Navier-stokes equations for three dimensional, unsteady and viscous flows.

(A) Three-dimensional inviscid flow

The above equations for non-viscous or inviscid flow reduce to the following form:

$$C_x \frac{\partial C_x}{\partial x} + C_y \frac{\partial C_x}{\partial y} + C_z \frac{\partial C_x}{\partial C_z} + \frac{\partial C_x}{\partial t} - X + \frac{1}{\rho}\frac{\partial P}{\partial x} = 0 \quad [3.13]$$

$$C_x \frac{\partial C_y}{\partial x} + C_y \frac{\partial C_y}{\partial y} + C_z \frac{\partial C_y}{\partial C_z} + \frac{\partial C_y}{\partial t} - Y + \frac{1}{\rho}\frac{\partial P}{\partial y} = 0 \quad [3.14]$$

$$C_x \frac{\partial C_z}{\partial x} + C_y \frac{\partial C_z}{\partial y} + C_z \frac{\partial C_z}{\partial C_z} + \frac{\partial C_z}{\partial t} - Z + \frac{1}{\rho}\frac{\partial P}{\partial z} = 0 \quad [3.15]$$

These are the three Euler's momentum equations.

(B) Three-dimensional, inviscid and steady flow without body forces

$$C_x \frac{\partial C_x}{\partial x} + C_y \frac{\partial C_x}{\partial y} + C_z \frac{\partial C_x}{\partial C_z} + \frac{\partial C_x}{\partial t} + \frac{1}{\rho}\frac{\partial P}{\partial x} = 0 \quad [3.16]$$

$$C_x \frac{\partial C_y}{\partial x} + C_y \frac{\partial C_y}{\partial y} + C_z \frac{\partial C_y}{\partial C_z} + \frac{\partial C_y}{\partial t} + \frac{1}{\rho}\frac{\partial P}{\partial y} = 0 \quad [3.17]$$

$$C_x \frac{\partial C_z}{\partial x} + C_y \frac{\partial C_z}{\partial y} + C_z \frac{\partial C_z}{\partial C_z} + \frac{\partial C_z}{\partial t} + \frac{1}{\rho}\frac{\partial P}{\partial z} = 0 \quad [3.18]$$

3.5.1.3 Vorticity Components

Circulation is the line integral of velocity around a closed contour. Vorticity is the circulation per unit area. The three vorticity components in the Cartesian coordinates are:

$$\xi = \frac{\partial C_z}{\partial y} - \frac{\partial C_y}{\partial z} \quad (Stream-wise\ vorticity) \quad [3.19]$$

$$\eta = \frac{\partial C_x}{\partial z} - \frac{\partial C_z}{\partial x} \quad (Pitch-wise\ vorticity) \quad [3.20]$$

$$\zeta = \frac{\partial C_y}{\partial x} - \frac{\partial C_x}{\partial y} \quad (Span-wise\ vorticity) \quad [3.21]$$

3.5.1.4 The Potential Function Equation

The velocity potential function (ϕ) is a point function whose derivative in a given direction gives the velocity component in that direction. This function exists for an irrotational flow ($\xi=\eta=\zeta=0$). The velocity components in terms of the potential function are:-

$$C_x = \frac{\partial \phi}{\partial x}, C_y = \frac{\partial \phi}{\partial y}, \; C_z = \frac{\partial \phi}{\partial z}$$

The differential equation for three-dimensional steady flow in terms of the potential function is:

$$\left[1 - \frac{1}{a^2}\left(\frac{\partial \phi}{\partial x}\right)^2\right]\frac{\partial^2 \phi}{\partial x^2} + \left[1 - \frac{1}{a^2}\left(\frac{\partial \phi}{\partial z}\right)^2\right]\frac{\partial^2 \phi}{\partial z^2} = \frac{2}{a^2}\left[\frac{\partial \phi}{\partial x}\frac{\partial \phi}{\partial y}\frac{\partial^2 \phi}{\partial x \partial y} - \frac{\partial \phi}{\partial y}\frac{\partial \phi}{\partial z}\frac{\partial^2 \phi}{\partial y \partial z} - \frac{\partial \phi}{\partial z}\frac{\partial \phi}{\partial x}\frac{\partial^2 \phi}{\partial z \partial x}\right]$$

[3.22]

In incompressible flows the fluid velocity components are small compared to the velocity of sound. Therefore, Equation (3.22) reduces to the Lap lace's equation

$$\frac{\partial^2 \phi}{\partial x^2} + \frac{\partial^2 \phi}{\partial y^2} + \frac{\partial^2 \phi}{\partial z^2} = 0 \qquad [3.23]$$

3.5.1.5 The Stream Function Equation

If the continuity equation for two-dimensional steady flow is satisfied, a point function called the stream function (ψ) is defined by:

$$C_x = \frac{\rho_o}{\rho}\frac{\partial \psi}{\partial y}, \; C_y = \frac{\rho_o}{\rho}\frac{\partial \psi}{\partial x}$$

An equation of motion can be obtained in terms of the stream function for two dimensional, steady and irrotational flows.

$$\left[1 - \frac{1}{a^2}\left(\frac{\rho_o}{\rho}\right)^2\left(\frac{\partial \psi}{\partial y}\right)^2\right]\frac{\partial^2 \psi}{\partial x^2} + \left[1 - \frac{1}{a^2}\left(\frac{\rho_o}{\rho}\right)^2\left(\frac{\partial \psi}{\partial x}\right)^2\right]\frac{\partial^2 \psi}{\partial y^2} + \frac{2}{a^2}\left(\frac{\rho_o}{\rho}\right)^2\frac{\partial \psi}{\partial x}\frac{\partial \psi}{\partial y}\frac{\partial^2 \psi}{\partial x \partial y} = 0$$

For incompressible flow, putting velocity of sound (a)≈∞ in the above equation reduces to:

$$\frac{\partial^2 \psi}{\partial x^2} + \frac{\partial^2 \psi}{\partial y^2} = 0 \qquad [3.24]$$

3.5.1.6 Energy Equation

The energy equation derived from the first law of thermodynamics as:-

Heat transfer=Work+ change in energy,

$Q=W+(E_2-E_1)$ [3.25a]

For applications in compressor, the energy terms will include internal energy, gravitational potential energy and kinetic energy.

$E=U + m (g Z) +1/2(mc^2)$ [3.25b]

$dE = dU +m (g dZ) +m d (1/2c^2)$ [3.26]

The change in the energy in a finite process between two states is given by:-

$E_2-E_1= (U_2-U_1) + m g (Z_2-Z_1) +1/2 m (c_2^2-c_1^2)$ [3.27]

Substituting Equation (3.27) in Equation (3.25(a)) a general form of the energy equation is obtained.

$Q=W+ (U_2-U_1) +m g (Z_2-Z_1) +1/2 m (c_2^2-c_1^2)$ [3.28]

Dividing throughout by m,

$$q = w + (u_2 - u_1) + g(Z_2 - Z_1) + \frac{1}{2}(c_2^{\,2} - c^2{}_1)$$ [3.29]

A. Steady-Flow Energy Equation

For steady flow energy equation through compressor, the work term in Equations (3.28) and (3.29) contains shaft work and flow work. Thus,

$W=Ws + (P_2V_2-P_1V_1)$ [3.30]

Substituting Equation (3.30) in Equation (3.28) and rearranging, we get

$Q=Ws + (U_2+P_2V_2)-(U_1+P_1V_1) + m g (Z_2-Z_1) + ½ m (c^2{}_2-c^2{}_1)$

Writing enthalpy, H, for the quantity, U+PV.

$$H_1 + m g Z_1 + \frac{1}{2} m c^2{}_1 + Q = H_2 + m g Z_2 + \frac{1}{2} m c^2{}_2 + Ws$$ [3.31]

In terms of specific quantities,

$$h_1 + g Z_1 + \frac{1}{2} c_1^{\,2} + q = h_2 + g Z_2 + \frac{1}{2} c_2^{\,2} + w_s$$ [3.32]

Equation (3.32) is the steady flow energy equation for a control volume or an open system.

B. Compressible Flow Equation

Axial compressors are adiabatic machines, that is Q=0. In these machines the change in potential energy (Z_1-Z_2) is negligible as compared to changes in enthalpy (h_1-h_2) and kinetic energy (c^2_1-c^2_2)/2.

Therefore, Equation (3.32) yields:-

$$h_1 + \frac{1}{2}c_1^{\,2} = h_2 + \frac{1}{2}c_2^{\,2} + w_s \qquad [3.33]$$

The shaft work is given by $w_s = \left(h_1 + \frac{1}{2}c_1^{\,2}\right) - \left(h_2 + \frac{1}{2}c_2^{\,2}\right)$

If the entry and exit velocities are small or the difference between them is negligible, then shaft work is given by the difference between the static enthalpies at the two states.

$$w_s = h_1 - h_2 \qquad [3.34]$$

C. Energy Transformation

Energy transfer (shaft work input or out put) in compressor stage is possible only in the rotor, whereas energy transformation can occur both in moving and fixed blades. A special application of the energy equation is in the stationary components of compressors. These components are nozzle blade rings and diffusers. The shaft work is absent in these components and the flow is almost adiabatic. Therefore Equation (2.52) gives

$$h_1 + \frac{1}{2}c_1^{\,2} = h_2 + \frac{1}{2}c_2^{\,2} = cons\tan t \qquad [3.35]$$

D. Stagnation Enthalpy

In an adiabatic energy transformation process if the initial state is represented by h,T, c, etc. and the final gas velocity is zero, the resulting value of the enthalpy (h_2=h_0) has a special significance. Under these conditions, Equation (3.35) yields:-

$$h_0 = h + \frac{1}{2}c^2 \qquad [3.36]$$

Since the gas is stagnant or stationary in the final state, the quantity (h_0) in Equation (3.36) is known as the stagnation enthalpy.

E. Stagnation Temperature

For a perfect gas, a stagnation temperature is defined through stagnation enthalpy. From equation (3.36),

$$c_p T_0 = c_p T + \frac{1}{2}c^2 \quad \Rightarrow \quad T_0 = T + \frac{c^2}{2c_p} \qquad [3.37]$$

T_0 is known as the stagnation temperature, T is the static temperature and $c^2/2c_p$ is the velocity temperature (T_c).

$$T_c = \frac{c^2}{2c_p} \qquad [3.38]$$

$$T_0 = T + T_c \qquad [3.39]$$

Equation (3.37) can be used to obtain an important relation for compressible flow machines

$$\frac{T_o}{T} = 1 + \frac{c^2}{2c_p T}$$

Substituting, $c_p = \frac{\gamma}{\gamma - 1}R$

$$\frac{T_0}{T} = 1 + c^2\left(\frac{2\gamma}{\gamma - 1}RT\right)$$

The velocity of sound in a gas at a local temperature T is given by:-

$$a = \sqrt{\gamma RT} \qquad [3.40]$$

The Mach number of the flow is defined as the ratio of the local velocity of the gas and the local velocity of sound.

$$M = \frac{c}{a} = \frac{c}{\sqrt{\gamma RT}} \qquad [3.41]$$

Therefore,

$$\frac{T_0}{T} = 1 + \left(\frac{\gamma - 1}{2}\right)\left(\frac{c^2}{a^2}\right) = 1 + \left(\frac{\gamma - 1}{2}\right)M^2 \qquad [3.42]$$

F. Stagnation Pressure

The pressure of a gas or fluid which is obtained by decelerating it in a reversible adiabatic (isentropic) process to zero velocity is known as the stagnation pressure.
The ratio of the stagnation and static pressures can be obtained from Equation (3.42).

$$\frac{P_0}{P} = \left(\frac{T_0}{T}\right)^{\frac{\gamma}{\gamma-1}} \qquad [3.43a]$$

$$\frac{P_0}{P} = \left(1 + \frac{\gamma-1}{2} M^2\right)^{\frac{\gamma}{\gamma-1}} \qquad [3.44b]$$

3.6 Computational Fluid Dynamic (CFD) work

Computational studies give investigators the ability to examine many flow and heat transfer phenomena that may not be possible to study through experimentation. This study is no exception to that rule. Questions' concerning what occurs in areas such as the tip gap, gutter, rim, and microcircuit are extremely difficult if not impossible to examine by an experimentalist.

Fortunately, a CFD model that has been benchmarked by experimental data can provide many incites and answers into the underlying physics of a problem. The analysis of data obtained from CFD is critical to explaining the occurrences within a flow.

Experimental investigations can prove to be expensive, may be unsafe and limited by the existing available techniques. Computational Fluid Dynamics (CFD) simulations are being increasingly employed to overcome these limitations. It has to be acknowledged that assumptions need to be made to simplify the conditions that are to be modeled. These introduce approximation errors into the simulations. In an attempt to reduce the effect of such simplifications and approximations, the models first need to be verified and validated against experimental data to ensure their accuracy. They can then be used to investigate the effects of changing the experimental conditions. Therefore, this technique is finding increased acceptance for the study of fluid flows. It is attractive to industry since it is more cost-effective than physical testing. This obviously drives the researcher to use CFD coded software to tackle the problem.

3.7 Unsteady Operation of Axial Flow Compressor (Compressor Stall)

Compressor stalls cause air flowing through the compressor to slow down, to stagnate (stop) or to reverse direction depending on the stall intensity. The unsteady or stalling operation of the compressor manifests itself in heavy fluctuations of the air flow velocity and pressure, which is accompanied by a considerable drop of the air pressure average value at the compressor outlet, dangerous vibration of the compressor. Surging occurs when volumetric airflow through the compressor diminishes below a definite magnitude and is usually accompanied by air back flow surges from the compressor to the engine inlet ducts.

Stall conditions can result from many causes, the most common of which are as follows:

- Turbulent or disrupted airflow to the engine inlet (reduces the velocity vector).
- Excessive fuel flow caused by abrupt engine acceleration (reduces the velocity vector by increasing combustor back pressure).
- Damaged turbine components, causing loss of power to the compressor.
- Engine operation above or below designed revolutions per minute (increases or decreases the revolution per minute vector).
- Contaminated or damaged compressor (increases the velocity by reducing compression).

The pilot will know that an engine is experiencing compressor stall by an audible noise, by fluctuation in revolutions per minute, by an increase in exhaust gas temperature or by a combination of these three. This reaction will probably be to reduce power, so that the inlet air velocity and revolutions per minute will return back to their proper relationship.

Generally to prevent surging and ensure a steady state operation of the compressor within the entire operational range of the rotational speed, the following methods are used:-

- Bleed valve or blow off valve
- Variable geometry inlet duct or exhaust duct
- Unti-surge unit (fuel feed interruption system)

CHAPTER FOUR

AERO-THERMODYNAMICS ANALYSIS OF COMPRESSOR STAGES

This chapter deals with the aerothermodynamics analysis of flow through complete axial flow aircraft gas turbine engine compressor stages.

Flow problems through both long (low pressure stages) and short blades (high pressure stages) and factors affecting stage pressure ratio have been considered. Methods of estimating the stage work, efficiency, lift and drag coefficients through a row of cascade blades are also given here.

4.1 Two-Dimensional Flow

The analysis which follows is applicable to axial flow aircraft gas turbine engine compressor and it is assumed that the working fluid is air.

A sketch of a typical stage is shown in Figure 4.1. Applying the steady flow energy equation to the rotor, and recognizing that the process can be assumed to be adiabatic, it can readily be seen that the power input is given by:

$$P = \dot{m} C_P \left(T_{02} - T_{01}\right) \qquad [4.1]$$

Where $\dot{m}$ is the mass flow rate of air, Cp is the specific heat capacity. Repeating with the stator, where the process can again be assumed adiabatic and there is zero work input, it follows that $T_{02}=T_{03}$. All the power is absorbed in the rotor, and the stator merely transforms kinetic energy to an increase in static pressure with the stagnation temperature remaining constant.

A T-S diagram for the stage, showing the effect of losses in both the rotor and the stator, is also shown in Figure 4.1.

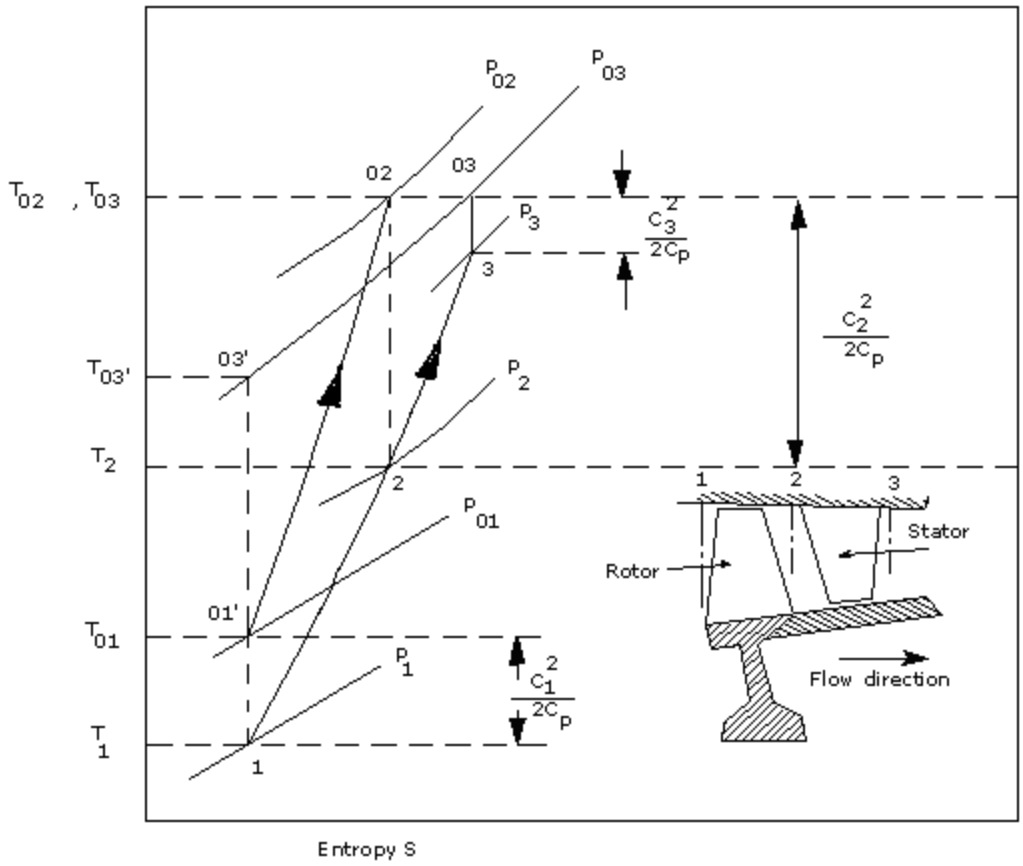

Figure 4.1 Compressor stage and T-S diagram [3].

Obtaining the power input to the stage from simple thermodynamics is no help in designing the blading. For this purpose we need to relate the power input to the stage velocity triangles. Initially attention will be focused on a simple analysis of the flow at the mean height of a blade where the peripheral speed is U, assuming the flow to occur in a tangential plane at the mean radius. This two-dimensional approach means that in general the flow velocity will have two components, one axial (denoted by subscript a) and one tangential (denoted by subscript w, implying a whirl velocity).

The velocity vectors and associated velocity diagram for a typical stage are shown in Figure 4.2. The air approaches the rotor with a velocity C_1 at angle α_1 from the axial direction; combining C_1 vectorially with the blade speed U gives the velocity relative to the blade, V_1, at angle β_1 from the axial direction. After passing through the rotor, which increases the absolute velocity of the air, the fluid leaves the rotor with a relative velocity V_2 at an angle β_2 determined by the rotor blade out let angle. Assuming that the design is such that the axial velocity Ca is kept constant, the value of V_2 can be obtained and the outlet velocity triangles constructed by combining V_2 and U vectorially to

give C_2 at angle α_2. The air leaving the rotor at α_2 then passes to the stator where it is diffused to a velocity C_3 at angle α_3; typically the design is such that $C_3 \approx C_1$ and $\alpha_3 \approx \alpha_1$ so that the air is prepared for entry to another similar stage.

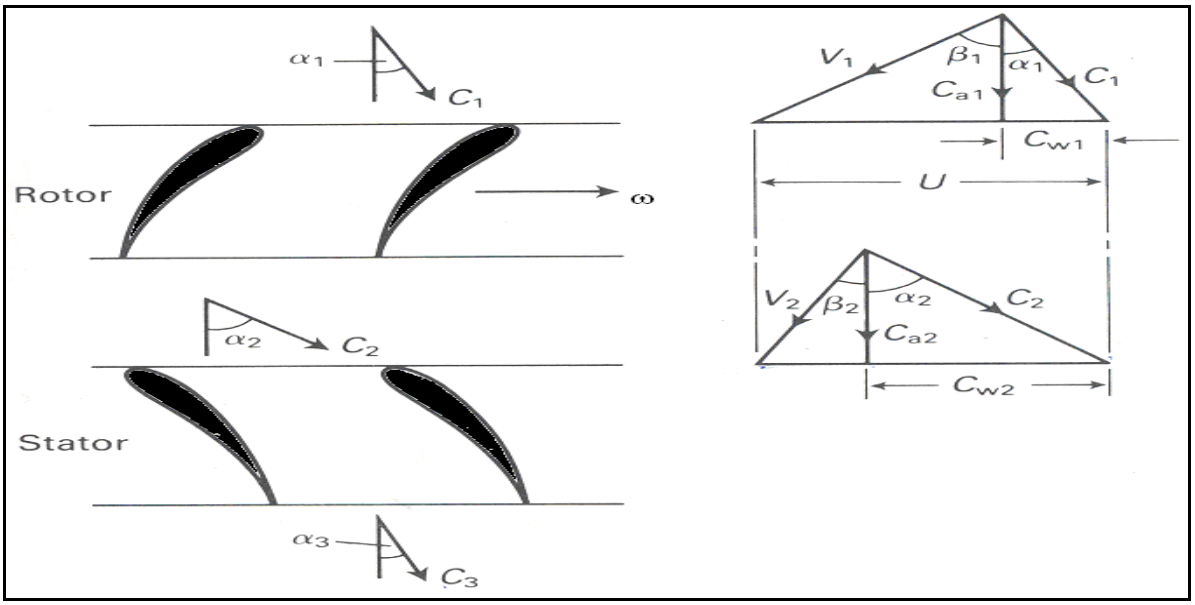

Figure 4.2 Velocity triangles for one stage [3]

Assuming that $C_a = C_{a1} = C_{a2}$, two basic equations follow immediately from the geometry of the velocity triangles. These are:

$$\frac{U}{C_a} = \tan\alpha_1 + \tan\beta_1 \qquad [4.2]$$

$$\frac{U}{C_a} = \tan\alpha_2 + \tan\beta_2 \qquad [4.3]$$

By considering the change in angular momentum of the air in passing through the rotor, the expression for the power input to the stage can be deduced as follows:

Figure 4.2 shows the velocity triangles at the entry and exit of a rotor. All the velocity vectors are in the same plane and are assumed to remain constant over the entire entry and exit sections of the rotor.

The angular speed of the rotor is ω radians per second given by:- $\omega = \frac{2\Pi N}{60}$

The peripheral velocities of the blades at the entry and exit at a section (or station 'r') is U=ωr as shown in Figure 4.3. The directions of the relative velocity vectors are assumed to corresponding to the rotor blade angles.

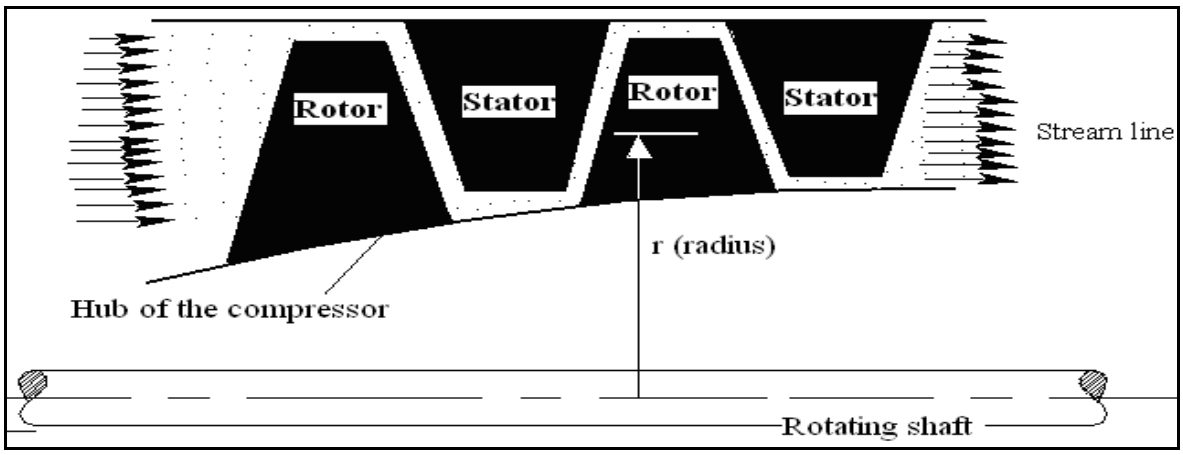

Figure 4.3 some stages of a multistage compressor with streamline of axially symmetrical flow pattern (schematic).

The three velocity vectors C, V and U at a section (or station) are related by simple vector equation.

C=U+V

The torque on the rotor (exerted by the rotor or by the fluid) is obtained by employing Newton's second law of motion for the change of moment of momentum.

Torque=rate of change in moment of momentum

The tangential momentum at a given station 'r' from the center of the compressor is $\dot{m}C_w$ and its moment is $\dot{m}rC_w$.

Therefore, the rate of torque on the rotor is given by:- $\tau = \dot{m}_2 r C_{w2} - \dot{m}_1 r C_{w1}$

For constant flow rate through a rotor, $\dot{m} = \dot{m}_1 = \dot{m}_2\ kg/s$

$\tau = \dot{m}(r C_{w2} - r C_{w1})$ This is the rate of torque that is exerted by the rotor blades on the fluid, which is supplied by the prime mover.

The power input is given by:-

Power input =rate of torque × angular velocity of the rotor

Therefore, the specific work at a given radial section (r) is given by:-

$W = U\,(C_{w2}-C_{w1})$ [4.4]

$$P = \tau\omega = \dot{m}\left(\omega r C_{w2} - \omega r C_{w1}\right) = m\left(UC_{w2} - UC_{w1}\right)$$

Where, C_{w1} and C_{w2} are the tangential components of fluid velocity before and after the rotor. This expression can be put in terms of the axial velocity and air angles to give:

$W = U\,C_a\,(\tan\alpha_2 - \tan\alpha_1)$

It is more useful, however, to express the power in terms of the rotor blade air angles, β_1 and β_2. It can readily be seen from Equations (4.2) and (4.3) that $\tan\alpha_1 + \tan\beta_1 = \tan\alpha_2 + \tan\beta_2$. Thus the power input and work input is given by Equation (4.5) and (4.6) respectively.

$$P = \dot{m}UC_a\left(\tan\beta_1 - \tan\beta_2\right) \quad [4.5]$$

$W = U\,C_a\,(\tan\beta_1 - \tan\beta_2) = U\,C_a\,(\tan\alpha_2 - \tan\alpha_1)$ [4.6]

This input energy will be absorbed usefully in raising the pressure of the air and wastefully in overcoming various frictional losses.

4.1.1 Blade Loading and Flow Coefficients

The blade loading coefficient for an axial compressor stage is defined as the ratio of stage work to the rotor speed squared.

$$\Psi = \frac{W}{U^2} \quad [4.7]$$

This is a dimensionless quantity used for comparing stages of differing sizes and speeds.

The flow coefficient for an axial compressor stage is defined as the ratio of axial velocity to the rotor speed.

$$\phi = \frac{C_a}{U} \quad [4.8]$$

For modern axial-flow compressors of aircraft gas turbine engine the flow coefficients are in the range of 0.45 to 0.57 at the mean radius [3].

Equation (4.4) and (4.6) when put in Equation (4.7) give successively

$$\Psi = \frac{C_{w2}}{U} - \frac{C_{w1}}{U}$$

$$\Psi = \phi(\tan\alpha_2 - \tan\alpha_1) = \phi(\tan\beta_1 - \tan\beta_2) \qquad [4.9a]$$

From the velocity diagram we have the following relation: $\tan\alpha_2 = \frac{1}{\Phi} - \tan\beta_2$

Therefore, substituting in Equation (4.9a) we have:

$$\psi = 1 - \phi(\tan\beta_2 + \tan\alpha_1) \qquad [4.9b]$$

The quantity ($\tan\beta_2 + \tan\alpha_1$) can be assumed constant in a wide range of incidence up to the stalling value is. This is justified in view of small variations in the air angles at the rotor and stator exits.

If the constant in Equation (4.9b) is $A = \tan\beta_2 + \tan\alpha_1$, then the design values are identified by the superscript *, Equation (4.9b) can be written as

$\Psi^* = 1 - A\phi^*$

At off-design conditions the expression becomes $\Psi = 1 - A\phi$, and this also implies that

$$\Psi = 1 - (1 - \Psi^*)\frac{\phi}{\phi^*} \qquad [4.9c]$$

This equation also gives the off-design characteristics of an axial-flow compressor.

4.1.2 Static Pressure Rise

The static pressure rise in the stage depends on the flow geometry and the speed of the rotor. The total static pressure rise across the stage is the sum of static pressure rises in the rotor and diffuser (stator) blade rows; expressions for these values are derived here assuming reversible adiabatic flow and constant axial velocity through the stage.

Further, in view of the small pressure rises over blade rows of axial compressor stages the flow is assumed incompressible, i.e. $\rho \approx cons\tan t$.

The Bernoulli equation across the rotor blade row gives:-

$$P_1 + \frac{1}{2}\rho V_1^2 = P_2 + \frac{1}{2}\rho V_2^2$$

$$(\Delta P)_R = P_2 - P_1 = \frac{1}{2}\rho\left(V_1^2 - V_2^2\right) \qquad [4.10]$$

Using velocity triangles of Figure 4.2,

$V_{W1}=V_1 \sin \beta_1 = C_{a1} \tan \beta_1$

$$\left(V_1^2 - V_2^2\right) = C^2_{a1} + V_{w1}{}^2 - C^2_{a2} - V_{w2}{}^2 = \left(V_{w1}{}^2 - V_{w2}{}^2\right)$$
$$\left(V_1^2 - V_2^2\right) = C^2_a(\tan^2 \beta_1 - \tan^2 \beta_2)$$

This when put in Equation (4.10) gives the pressure rise across the rotor as

$$(\Delta P)_R = P_2 - P_1 = \frac{1}{2}\rho C^2{}_a\left(\tan^2 \beta_1 - \tan^2 \beta_2\right) \qquad [4.11]$$

Similarly, the Bernoulli equation across the diffuser blade row gives

$$(\Delta P)_D = P_3 - P_2 = \frac{1}{2}\rho\left(C_2{}^2 - C_3{}^2\right) \qquad [4.12]$$

$$(\Delta P)_D = \frac{1}{2}\rho\left(C_{w2}{}^2 - C_{w3}{}^2\right)$$

$$(\Delta P)_D = \frac{1}{2}\rho C^2{}_a\left(\tan^2 \alpha_2 - \tan^2 \alpha_3\right)$$

Assuming $\alpha_3 = \alpha_1$,

$$(\Delta P)_D = \frac{1}{2}\rho C^2{}_a\left(\tan^2 \alpha_2 - \tan^2 \alpha_1\right) \qquad [4.13]$$

The stage pressure rise is:-

$P_3 - P_1 = \Delta P_{st} = \Delta P_R + \Delta P_D$

Substituting from Equations (4.11) and (4.13)

$$(\Delta P)_{st} = \frac{1}{2}\rho C^2{}_a[(\tan^2 \beta_1 - \tan^2 \beta_2) + \left(\tan^2 \alpha_2 - \tan^2 \alpha_1\right)]$$

Using Equation (4.6)

$$(\Delta P)_{st} = \frac{1}{2}\rho C_a(\tan \beta_1 - \tan \beta_2)\{Ca\left(\tan \beta_1 + \tan \beta_2\right) + C_a\left(\tan \alpha_2 + \tan \alpha_1\right)\ \}$$

This on rearrangement and using the following relations from the velocity triangles,

$U = C_{a1}(\tan \alpha_1 + \tan \beta_1)$ and $U = C_{a2}(\tan \alpha_2 + \tan \beta_2)$ we have:

$$(\Delta P)_{st} = \rho C_a U\left(\tan \beta_1 - \tan \beta_2\right) \qquad [4.14]$$

$$(\Delta P)_{st} = \rho C_a U(\tan\alpha_2 - \tan\alpha_1) \quad [4.15]$$

These relations for isentropic flow can also be obtained direct from Equation (4.6).For such a flow, changes in pressure and enthalpy and work are related by:-

$$\frac{\Delta P_{st}}{\rho} = \Delta h_{st} = W \quad [4.16]$$

4.1.3 Efficiencies

The efficiencies of the compression process can now be defined on the basis of ideal (isentropic) and actual (adiabatic) processes defined in the previous section. The ideal specific work in the stage is:-

$W_s = h_{03'} - h_{01} = C_p (T_{03'} - T_{01})$ [4.17]

This is the minimum value of the stage work required to obtain a static pressure rise of:-

$(\Delta P)_{st} = P_3 - P_1$

However, the actual process on account of losses and the associated irreversibilities will require a larger magnitude of work for the same pressure rise. This is given by:-

$W_a = h_{02} - h_{03} = h_{03} - h_{01} = Cp (T_{03} - T_{01})$ [4.18]

Thus the total –to –total efficiency of the stage is defined by:-

$$\eta_{tt} = \frac{ideal\ \ stage\, work\ \ between\ \ total\ \ conditions\ \ at\ \ entry\ \ and\, exit}{actual\ \ stage\, work}$$

$$\eta_{tt} = \frac{W_s}{W_a} = \frac{h_{03'} - h_{01}}{h_{03} - h_{01}} = \frac{T_{03'} - T_{01}}{T_{03} - T_{01}} \quad [4.19]$$

Assuming a perfect gas with constant specific heat, the overall stagnation pressure ratio can be written as:

$$\frac{P_{03}}{P_{01}} = \left(1 + \eta_c \frac{\Delta T_0}{T_{01}}\right)^{\frac{\gamma}{(\gamma-1)}} \qquad [4.20]$$

The compressor efficiency can be calculated from the estimated efficiencies of the stages.
Consider an incremental pressure rise from Po to $P_0 + dP_o$ as shown on a T-S diagram in Figure 6 in Appendix 'A'. The temperature rise accompanying this pressure rise is dT_o, while the temperature rise for an isentropic process would be (dT_{os}).

The polytropic compression efficiency, η_{pc} is defined for this incremental process just as the overall efficiency is defined for a finite compression:

$$\eta_{pc} = \frac{dT_{os}}{dT_o} \qquad [4.20]$$

For the isentropic process,

$$dT_{os} = T_o\left[\left(\frac{Po + dPo}{Po}\right)^{(\gamma-1)/\gamma} - 1\right]$$

Using the binomial expansion for dPo/Po<<1

$$\left(1 + \frac{dPo}{Po}\right)^{(\gamma-1)/\gamma} = 1 + \frac{\gamma - 1}{\gamma}\frac{dPo}{Po}$$

Thus equation (4.20) can be written as:

$$\eta_{pc}\frac{dTo}{To} = \frac{\gamma - 1}{\gamma}\left(\frac{dPo}{Po}\right)$$

For overall compression from state 1 to state 3, this may be integrated (for constant η_{pc}) to give:-

$$\frac{T_{03}}{T_{01}} = \left(\frac{P_{03}}{P_{01}}\right)^{(\gamma-1)/\gamma\,\eta_{PC}} \qquad [4.21]$$

Combining Equation (4.21) and (4.20) we can get the relationship between overall pressure ratio, isentropic efficiency and polytropic efficiency of the compressor:

$$\eta_c = \frac{\left(P_{03}/P_{01}\right)^{(\gamma-1)/\gamma} - 1}{\left(P_{03}/P_{01}\right)^{(\gamma-1)/\gamma\eta_{pc}} - 1} \qquad [4.22]$$

For a MATLAB plot of η_c verses pressure ratio for various values of η_{pc}, see Appendix 'A' Figure 2. For pressure ratio as low as those encountered in a single stage, it can be seen that, $\eta_c = \eta_{st} \approx \eta_{pc}$; hence the polytropic and stage efficiencies are about the same for a small pressure ratio compressor. With the reasonable assumption that maximum attainable stage efficiency is independent of the number of stages (or at least that η_{pc} does not increase as the number of stages increase), it can be seen that overall compressor efficiency decrease as compressor pressure ratio increases.

4.1.4 Degree of Reaction

The degree of reaction Λ provides a measure of the extent to which the rotor contributes to the overall static pressure rise in the stage. It is normally defined in terms of enthalpy rise as follows,

$$\Lambda = \frac{isentropic\ \ change\ \ of\ \ enthalpy\ \ in\ \ the\ \ rotor}{isentropic\ \ change\ \ of\ \ enthalpy\ in\ the\ stage} \qquad [4.23]$$

But, because the variation of Cp over the relevant temperature ranges is negligible, the degree of reaction can be expressed more conveniently in terms of temperature rises.

The degree of reaction is a useful concept in compressor design, and it is possible to obtain a formula for it in terms of the various velocities and air angles associated with the stage. This will be done for most common case in which it is assumed that:-

- Ca is constant through the stage, and
- The air leaves the stage with the same absolute velocity with which it enters that is $C_3=C_1$ and hence, $\Delta Ts=\Delta T_{os}$.

If ΔT_A and ΔT_B denote the static temperature rises in the rotor and stator respectively, then equating (4.1) and (4.5) we have the stagnation temperature rise in the stage, ΔT_{os}, is given by $\Delta T_{os} = \frac{UC_a}{C_p}\left(\tan\beta_1 - \tan\beta_2\right)$ and then this gives per unit mass flow,

$$W=Cp\ (\Delta T_A+\Delta T_B) = Cp\ \Delta Ts = U\ Ca\ (\tan\beta_1-\tan\beta_2) = U\ Ca(\tan\alpha_1-\tan\alpha_2) \qquad [4.24]$$

Since, all the work input to the stage takes place in the rotor, the steady flow energy equation yields

$W=Cp\ \Delta T_A+\frac{1}{2}\left(C_2{}^2-C_1{}^2\right)$

So that with Equation (4.24)

$$C_p\Delta T_A=UC_a\left(\tan\alpha_2-\tan\alpha_1\right)-\frac{1}{2}\left(C_2{}^2-C_1{}^2\right)$$

But C_2=Ca sec α_2 and C_1=Ca sec α_1, hence

$$C_p\Delta T_A=UC_a\left(\tan\alpha_2-\tan\alpha_1\right)-\frac{1}{2}C_a{}^2\left(\sec^2\alpha_2-\sec^2\alpha_1\right)$$

$$C_p\Delta T_A=UC_a\left(\tan\alpha_2-\tan\alpha_1\right)-\frac{1}{2}C_a{}^2\left(\tan^2\alpha_2-\tan^2\alpha_1\right)$$

From the definition of Λ,

$$\Lambda=\frac{\Delta T_A}{\Delta T_A+\Delta T_B}=\frac{UC_a\left(\tan\alpha_2-\tan\alpha_1\right)-\frac{1}{2}C_a{}^2\left(\tan^2\alpha_2-\tan^2\alpha_1\right)}{UC_a\left(\tan\alpha_2-\tan\alpha_1\right)}$$

$$=1-\frac{C_a}{2U}\left(\tan\alpha_2+\tan\alpha_1\right)$$

By the addition of Equations (4.2) and (4.3),

$$\frac{2U}{C_a}=\tan\alpha_1+\tan\beta_1+\tan\alpha_2+\tan\beta_2$$

Hence,

$$\Lambda=\frac{C_a}{2U}\left[\frac{2U}{C_a}-\frac{2U}{C_a}+\tan\beta_1+\tan\beta_2\right]=\frac{C_a}{2U}\left[\tan\beta_1+\tan\beta_2\right] \qquad [4.25]$$

It must be pointed out that in deriving Equation (4.25) for,Λ, a work-done of unity has implicitly been assumed in making use of Equation (4.24).

For a real or actual compressor stage the degree of reaction is defined as:-

$$\Lambda=\frac{actual\ change\ of\ \ enthalpy\ in\ the\ rotor}{actual\ change\ of\ enthalpy\ in\ the\ stage}$$

$$\Lambda=\frac{h_2-h_1}{h_3-h_1}=\frac{T_2-T_1}{T_3-T_1} \qquad [4.26]$$

For $C_1=C_3$, $h_3-h_1=h_{03}-h_{01}=U\ (C_{w2}-C_{w1})$

Equation (4.25) can be rearranged to give:

$$\Lambda = \frac{C_a}{2U}\left[(\tan\beta_1 + \tan\alpha_1) - (\tan\alpha_1 - \tan\beta_2)\right]$$

From Equation (4.2)

$$\tan\beta_1 + \tan\alpha_1 = \frac{U}{C_a}$$

Therefore

$$\Lambda = \frac{1}{2} - \frac{1}{2}\frac{C_a}{U}\left(\tan\alpha_1 - \tan\beta_2\right) \qquad [4.27]$$

This is a useful relation in terms of the geometry of flow and can be used to study the effect of air angles and the required cascade geometry (to provide these air angles) on the degree of reaction of an axial compressor stage.

4.1.5 Low Reaction Stages

A low reaction stage has a lesser pressure rise in its rotor compared to that in the diffuser, that is in such a stage the quantity (tan α_1-tan β_2) is positive or in other words $\alpha_1 > \beta_2$ [Figure 4.2 and Equation (4.27)].

The same effect can be explained in another manner:-

$$\left.\begin{array}{l} C_a \tan\alpha_1 = C_{w1} = U - V_{w1} \\ C_a \tan\beta_2 = V_{w2} = U - C_{w2} \end{array}\right\} \text{ from Figure (4.2).}$$

Therefore, after substituting these values in Equation (4.27) we can get that:-

$$\Lambda = \frac{1}{2} - \frac{1}{2}\left(\frac{C_{w1}}{U} - \frac{V_{w2}}{U}\right) \qquad [4.28]$$

$$\Lambda = \frac{1}{2} - \frac{1}{2U}\left(C_{w2} - V_{w1}\right) \qquad [4.29]$$

This equation relates the degree of reaction to the magnitude of swirl or the whirl components approaching the rotor and the diffuser. Thus a low degree of reaction is obtained when the rotor blade rows remove less swirl compared to the diffuser blade rows, that is $V_{w1} < C_{w2}$ .The swirl removing ability of a blade row is reflected in the static pressure rise across it. In a low-degree

reaction stage the diffuser blade rows are burdened by a comparatively larger static pressure rise which is not desirable for obtaining higher efficiencies.

4.1.6 Fifty Percent Reaction Stages

One of the ways to reduce the burden of a large pressure rise in a blade row is to divide the stages pressure rise equally between the rotor and diffuser. In this case $\Lambda=0.5$ and from Equation (4.25) we have:

$$\frac{U}{C_a} = \tan\beta_1 + \tan\beta_2$$

And it immediately follows from Equations (4.2) and (4.3) that:-

$$\begin{pmatrix} \tan\alpha_1=\tan\beta_2; & \text{that is,} & \alpha_1=\beta_2 \\ \tan\alpha_2=\tan\beta_1; & \text{that is,} & \alpha_2=\beta_1 \end{pmatrix}$$

Furthermore, from Figure 4.2, since Ca is constant through the stage, $C_a=C_1 \text{ Cos } \alpha_1=C_3 \text{ Cos } \alpha_3$

It was initially assumed that $C_1=C_3$ and hence $\alpha_1=\alpha_3$. Because of this equality of angles, namely $\alpha_1=\beta_2=\alpha_3$ and $\beta_1=\alpha_2$, the velocity diagram becomes symmetrical and blading designed on this bases is sometimes referred to as symmetrical blading. From the symmetry of the velocity diagram, it follows that $C_1=V_2$ and $V_1=C_2$. A stage designed with symmetrical blading will always be referred to as a 50 percent reaction stage.

4.1.7 High Reaction Stages

The static pressure rise in the rotor of a high reaction stage is larger compared to that in the diffuser that is $(\Delta P)_R>(\Delta P)_D$. For such a stage the quantity $(\tan\alpha_1-\tan\beta_2)$ in equation (4.27) is negative, giving $\Lambda>1/2$.

Therefore, for such a stage $\beta_2>\alpha_1$ and $V_{w1}>C_{w2}$.

The swirl component passed on to the diffuser blade row is relatively smaller, resulting in a lower static pressure rise there in. Since the rotor blade rows have relatively higher efficiencies, it is advantageous to have a slightly greater pressure rise in them compared to the diffuser.

4.1.8 Work Done Factor

From Equation (4.4):-

$$\left.\begin{array}{c} W=U\,C_a(\tan\beta_1-\tan\beta_2) \\ W=U\{C_a(\tan\alpha_1+\tan\beta_1)-C_a(\tan\alpha_1+\tan\beta_2)\} \end{array}\right)$$

Substituting from Equation (4.2) and (4.3):-

$$W=U\,\{U-C_a\,(\tan\alpha_1+\tan\beta_2)\} \qquad [4.30]$$

The air angles β_2 and α_1 are fixed by the cascade geometry of the rotor blades and the upstream blade row.

Therefore, assuming ($\tan\alpha_1 + \tan\beta_2$) and U as constant, Equation (4.30) relates work to the axial velocity at various sections along the blade height.

It may be seen from Equation (4.30), W, decreases with an increase in the axial velocity and vice versa.

Therefore, the work capacity of the stage is reduced in the central region expected increase in the work at the hub and tip regions. However, the expected increase in the work at the hub and tip is not obtained in actual practice on account of higher losses. Therefore, the net result is that the stage work is less than that given by Euler's equation based on a constant value of the axial velocity along the blade height. This reduction in the work absorbing capacity of the stage is taken into account by a "work-done factor" λ. This varies from 0.98 to 0.85 depending on the number of stages. [3,9].
Therefore, the work expressions are modified to:-

$$\left\{\begin{array}{l} h_{03}-h_{01}=\lambda\,U\,(C_{w2}-C_{w1}) \\ h_{03}-h_{01}=\lambda U C_a(\tan\alpha_2-\tan\alpha_1) \\ h_{03}-h_{01}=\lambda U\,C_a\,(\tan\beta_1-\tan\beta_2) \end{array}\right\} \qquad [4.31]$$

The actual stage temperature rise is then given by:

$$\Delta T_{os} = \frac{\lambda}{C_p} U C_a \left(\tan \beta_1 - \tan \beta_2\right) \qquad [4.32]$$

4.1.9 Factors Affecting Stage Pressure Ratio

A. Tip Speed

The centrifugal stress in the rotor blades depends on the rotational speed, the blade material and the length of the blade. The maximum centrifugal tensile stress, which occurs at the blade root, can be seen to be given by:

$$(\sigma_{ct})_{\max} = \frac{\rho_b \omega^2}{a_r} \int_r^t ar\, dr$$

Where 'ρ_b ' is the density of the blade material, ω is the angular velocity, 'a' is the cross-sectional area of the blade at any radius, and suffixes 'r' and 't' refer to root and tip of blade.

If, for simplicity, the blade cross-section is assumed to be constant from root to tip.

$$(\sigma_{ct})_{\max} = \frac{\rho_b}{2} (2\pi N)^2 \left(r_t^2 - r_r^2\right) = 2\pi N^2 \rho_b A$$

Where 'N' is the rotational speed and 'A' the annulus area. The tip speed, 'Ut,' is given by $2\pi N r_t$ so the equation for centrifugal tensile stress can be written also as

$$(\sigma_{ct})_{\max} = \frac{\rho_b}{2} U_t^2 \left[1 - \left(\frac{r_r}{r_t}\right)^2\right]$$

The ratio r_r/r_t is normally referred to as the hub-tip ratio. It is immediately apparent that the centrifugal stress is proportional to the square of the tip speed, and that a reduction of hub-tip ratio increases the blade stress. The first-stage blades, being the longest, are the most highly stressed, but the later stages often appear to be very moderately stressed. [6]

For tip speeds of around 350m/s, stress problems are not usually critical in the sizing of the annulus. Tip speeds of 450m/s, however, are common in the fans of high by-pass ratio turbofans, and with their low hub-tip ratios the design of disc to retain the long heavy blades becomes critical. The inner radius of the annulus may then be dictated by disc stressing constraints. [6]

B. Axial Velocity

Considering a first stage with no IGVs, the entry velocity will be purely axial in direction and the velocity diagram at entry to the rotor will be as shown by the right-angled triangle in figure 4.4.

The velocity relative to the rotor is given by $V_1^2=C^2_1 +U^2$ and, assuming the axial velocity to be constant over the blade height, the maximum relative velocities will occur at the tip, which is V_{1t}. The static temperature at the rotor entry, T_1 is given by $T_{01}-(C^2_1/2C_p)$ and the local acoustic velocity by $a= (\gamma RT_1)^{1/2}$.

The Mach number relative to the rotor tip is V_{1t}/a, and for a given speed U_t it is therefore determined by the axial velocity at entry to the stage as indicated by the curves in Figure 4.4. Axial velocities for an industrial gas turbine will usually be of the order of 150m/s whereas for advanced aero engines they could be up to 200m/s. [6]

The dotted velocity triangle in figure 4.4 shows how the Mach number at entry may be slightly reduced by means of IGVs.

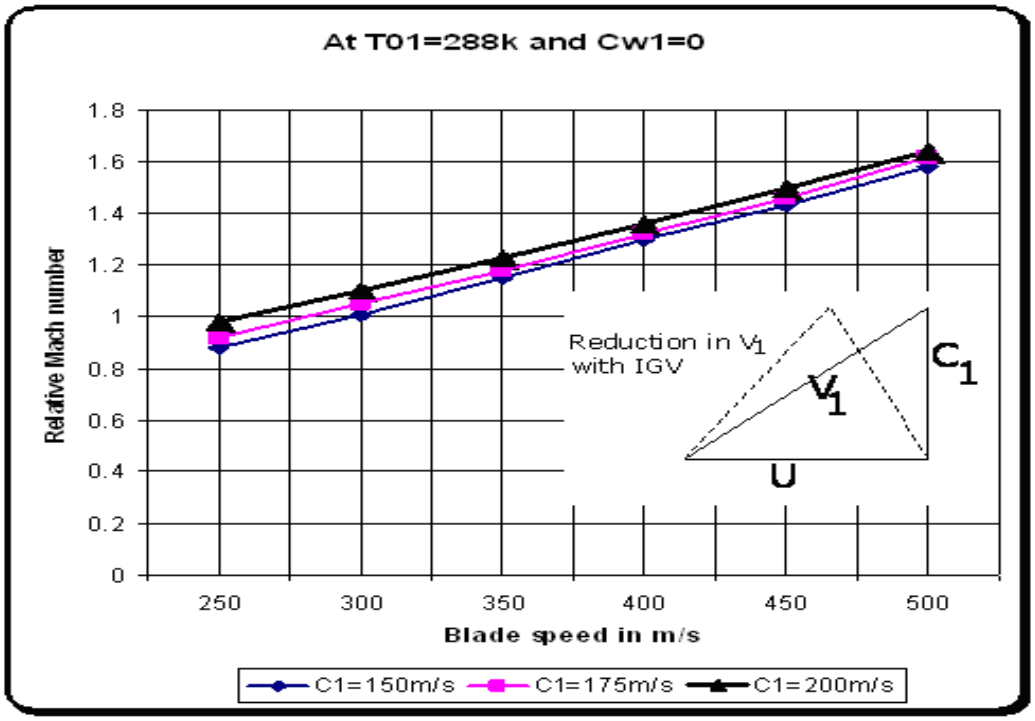

Figure 4.4 Relative Mach number at the rotor entry

C. High Fluid Deflections In the Rotor Blades

For most compressor stages it can be assumed with little error that the value of U is the same at inlet and out let of a rotor blade for any particular stream line, and the velocity triangles can conveniently be drawn on a common base as in figure 4.5 [6]

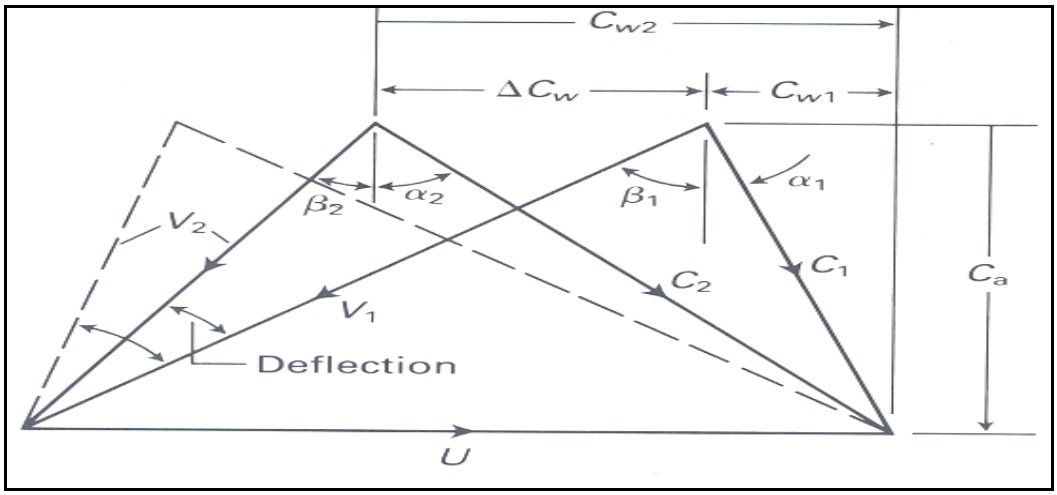

Figure 4.5 Effect of increasing fluid deflection, Howell [6]

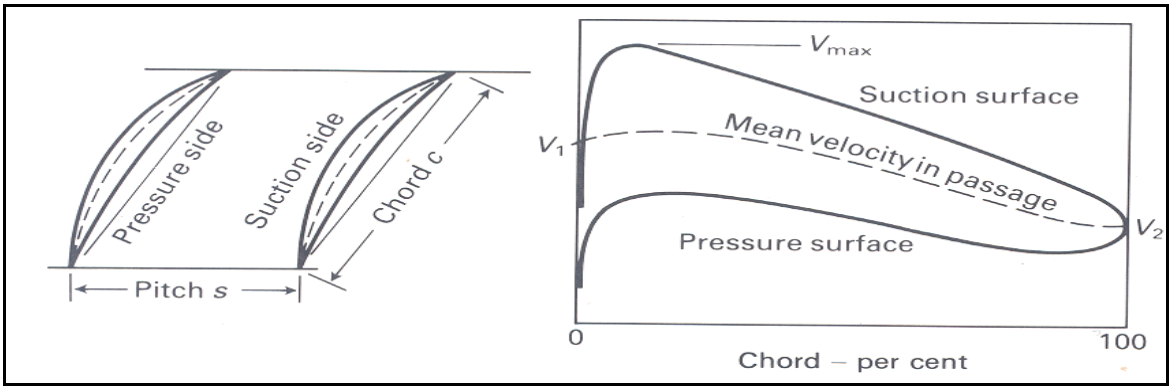

Figure 4.6 Blade spacing and velocity distribution through passage, Howell [6]

Figure 4.6 shows a pair of typical blades which have a pitch ‘S’ and a chord ‘C'. The air passing over an aerofoil will be accelerated to a higher velocity on the convex surface, and in a stationary row this will give rise to a drop in static pressure; for this reason the convex surface is known the suction side of the blade. [1, 6]

The amount of deflection required in the rotor is shown by the directions of the relative velocity vectors V_1 and V_2 and the change in whirl velocity is ΔC_w.

Considering a fixed value of β_1, it is obvious that increasing the deflection by reducing β_2 entails a reduction in V_2. In other words, high fluid deflection implies a high rate of diffusion. The designer must have some method for assessing the allowable diffusion, and one of the earliest criteria used was the de Haller number, defined as V_2/V_1; a limit of V_2/V_1 note less than 0.72 was set, lower values leading to excessive losses. Because of its extreme simplicity, the de Haller number is still used in preliminary design work, but for final design calculations a criteria called the diffusion factor is preferred. The latter concept was developed by NACA (the precussor of NASA). [1, 6]

On the concave surface, the pressure side, the fluid will be decelerated. The velocity distribution through the blade passage will be of the form shown; the maximum velocity on the suction surface will occur at around 10-15 percent of the chord from the leading edge and will then fall steadily until the outlet velocity is reached. Figure 4.6 would suggest that these would be most likely to occur on the suction surface. The derivation of the NASA diffusion factor is based on the establishment of the velocity gradient on the suction surface in terms of V_1, V_2 and V_{max} in conjunction with results from cascade tests. [1,6].

From the cascade tests it was deduced that the maximum velocity is:-

$Vmax=V_1+0.5(\Delta C_w\ S/C)$.

In simplified form, the diffusion factor, D, can be expressed as (REF1, 6)

$$D \approx \frac{V_{\max} - V_2}{V_1} \approx \frac{V_1 + \frac{\Delta C_w}{2}\frac{S}{C} - V_2}{V_1} \approx 1 - \frac{V_2}{V_1} + \frac{\Delta C_w}{2V_1}.\frac{S}{C} \qquad [4.33]$$

The variation of friction loss with D obtained from a large number of NASA tests (REF6) is shown in figure 4.7. These tests were carried out over a wide range of cascade geometries for a particular aerofoil section, and were found to be generally applicable as long as the maximum local mach numbers were subsonic or only slightly supersonic. It can be seen that for the rotor hub region and

stators the losses are unaffected by variation in D up to 0.6; in the rotor tip region, however, the losses increases rapidly at values of D above 0.4.

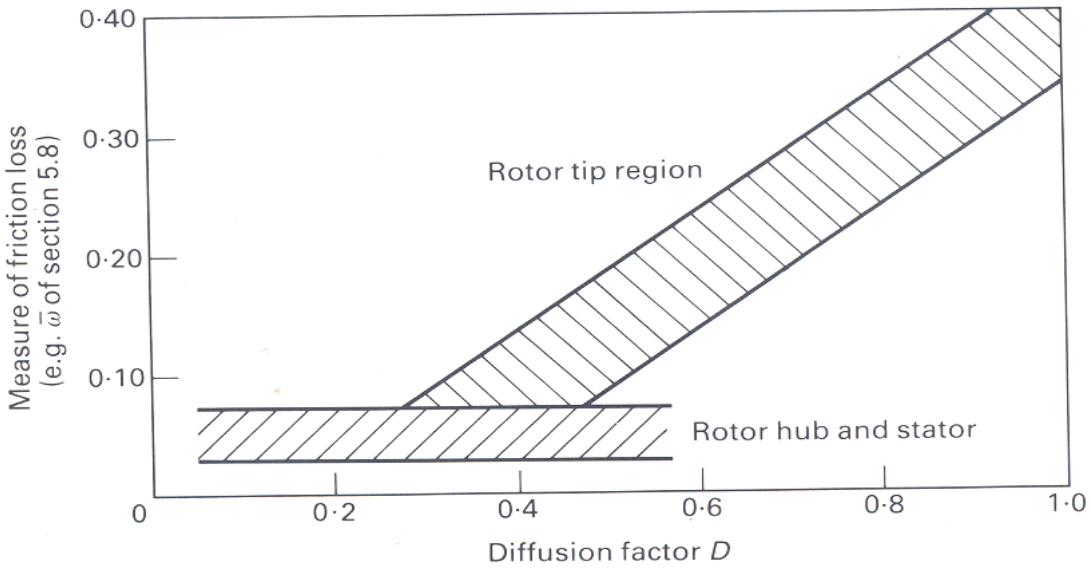

Figure 4.7 Variation of friction loss with diffusion factor [6]

4.2 Three-Dimensional Flow

In section 4.1 it is assumed that the flow in the compressor annulus is two –dimensional, meaning that any effect due to radial movement of the fluid is ignored. The assumption of two –dimensional flow is quite reasonable for stages in which the blade height is small relative to the mean diameter of the annulus, which is those of hub-tip ratio greater than about 0.8, which would be typical of the later stages of a compressor. [3]

The front stages, however, have lower values of hub-tip ratio, and values as low as 0.4 are used for the first stage of aero-engine compressors so that a high mass flow can be passed through a machine of low frontal area.[3]. For high efficiency it is essential that the blade angles match the air angles closely at all radii, and the blade must therefore be twisted from root to tip to suit the changing air angles.

The basic equation expressing the balance between pressure forces and inertia forces can be derived by considering the forces acting on the fluid element in Figure 4.8. The whirl component of velocity

is shown in Figure 4.8a and the axial component and much smaller radial component in the radial direction arise from the centripetal force associated with circumferential flow; the radial component of the centripetal force associated with the flow along the curved streamline.

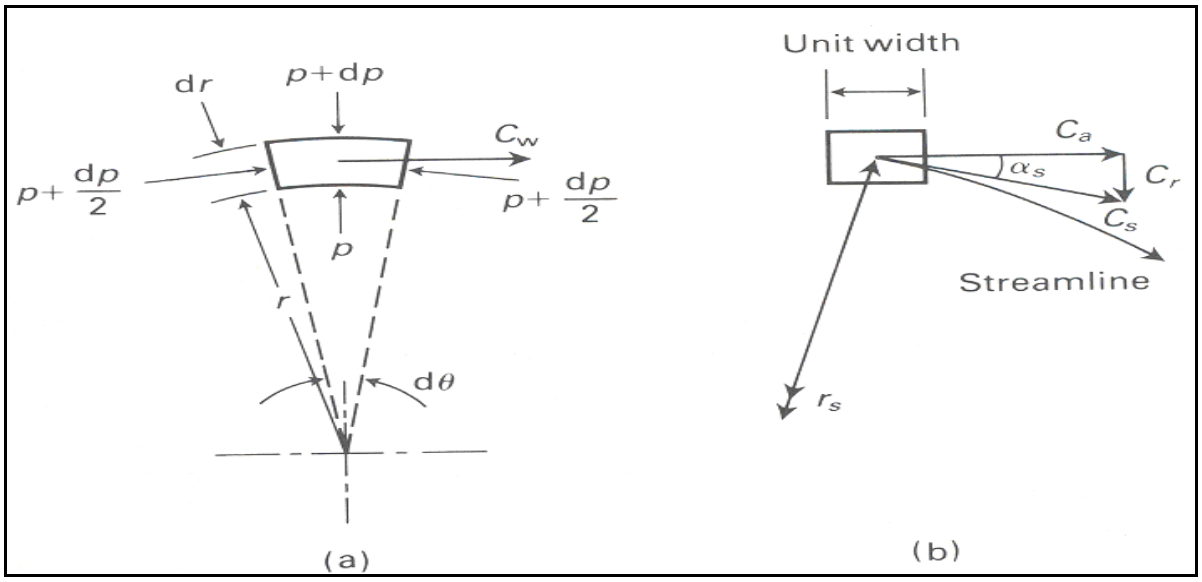

Figure 4.8 Radial equilibrium of fluid element [6]

The radial component of the force required to produce the linear acceleration along the stream line.

The total inertia force, F, must be produced by the pressure forces acting on the element in the direction. (The acceleration in the radial direction may amount to several thousand times the acceleration due to gravity so that gravitational forces can be neglected.)[3].

Considering a fluid element of unit width, having a density ρ, the three terms of the inertia force can be expressed as follows. The centripetal force associated with the circumferential flow is:-

$$F_{(i)} = \frac{mC_w^{\ 2}}{r} = (\rho r dr d\theta)\frac{C_w^{\ 2}}{r} \qquad [4.34]$$

For the flow along the curved streamline, the radial force is given by:-

$$F_{(ii)} = \frac{mC_s^{\ 2}}{r_s}\cos\alpha_s = (\rho r dr d\theta)\frac{C_s^{\ 2}}{r_s}\cos\alpha_s \qquad [4.35]$$

Where the suffix S refers to the component along the streamline and r_s is the radius of curvature of the streamline, the radial component of force is:-

$$F_{(iii)} = m\frac{dC_s}{dt}\sin\alpha_s = (\rho r dr d\theta)\frac{dC_s}{dt}a\sin\alpha_s \qquad [4.36]$$

With the curvature shown in Figure 4.8(b) the forces $F_{(ii)}$ and $F_{(iii)}$ are in the same direction as $F_{(i)}$. Thus the total inertia force, F_I, is given by:-

$$F_I = \rho r dr d\theta\left[\frac{C_w{}^2}{r} + \frac{C_s{}^2}{r_s}\cos\alpha_s + \frac{dC_s}{dt}\sin\alpha_s\right] \qquad [4.37]$$

The pressure force, F_P, producing this inertia force is obtained by resolving in the radial direction to give:-

$$F_p = (p+dp)(r+dr)d\theta - prd\theta - 2\left(p+\frac{dp}{2}\right)dr\frac{d\theta}{2} \qquad [4.38]$$

The third term in the equation results from the resolution of the pressure forces on the two sides of the element in the radial-axial plane, on which it is assumed that the pressure is the average of the two extremes, namely P+ (dP/2). Equating the forces F_I and F_P, and neglecting second-order terms, we are left with:-

$$\frac{1}{\rho}\frac{dp}{dr} = \frac{C_w{}^2}{r} + \frac{C_s{}^2}{r_s}\sin\alpha_s + \frac{dC_s}{dt}\sin\alpha_s \qquad [4.39]$$

This is the complete radial equilibrium equation which includes all contributory factors. For most design purposes it can be assumed that r_s is so large, and α_s so small, that the last two terms of Equation (4.39) can be ignored. Thus, finally, we have:

$$\frac{1}{\rho}\frac{dP}{dr} = \frac{C_w{}^2}{r} \qquad [4.40]$$

And this is what will be referred to as the radial equilibrium equation. In effect, the radial component of velocity is being neglected. Certainly in the spaces between the blade rows C_r is very much smaller than either Ca or C_w and can safely be assumed to be negligible.

Equation (4.40) enables us to deduce an energy equation which expresses the variation of enthalpy with radius. The stagnation enthalpy h_o at any radius r where the absolute velocity C is given by

$$h_o = h + \frac{C^2}{2} = h + \frac{1}{2}\left(C_a{}^2 + C_w{}^2\right)$$

And the variation of enthalpy with radius is therefore,

$$\frac{dh_o}{dr} = \frac{dh}{dr} + C_a \frac{dC_a}{dr} + C_w \frac{dC_w}{dr} \qquad [4.41]$$

From the thermodynamic relation TdS=dh-dp/ρ,

$$\frac{dh}{dr} = T\frac{dS}{dr} + dS\frac{dT}{dr} + \frac{1}{\rho}\frac{dP}{dr} - \frac{1}{\rho^2}\frac{d\rho}{dr}dP$$

Dropping second-order terms,

$$\frac{dh}{dr} = T\frac{dS}{dr} + \frac{1}{\rho}\frac{dP}{dr} \qquad [4.42]$$

Substituting for dh/dr in Equation (4.41)

$$\frac{dh_o}{dr} = T\frac{dS}{dr} + \frac{1}{\rho}\frac{dP}{dr} + C_a\frac{dC_a}{dr} + C_w\frac{dC_w}{dr}$$

Using the radial equilibrium equation (4.40), the second term of the right hand side of the above equation can be replaced by, leaving the basic equation for analysis of flow in the compressor annulus as:-

$$\frac{dh_o}{dr} = T\frac{dS}{dr} + \frac{C_w^{\,2}}{r} + C_a\frac{dC_a}{dr} + C_w\frac{dC_w}{dr} \qquad [4.43]$$

The term TdS/dr represents the radial variation of loss across the annulus, and may be significant in detailed design calculations; this is especially true if Mach numbers relative to the blade are supersonic and shock losses occur. For our purposes, however, it will be assumed that the entropy gradient term can be ignored and the final form of the equation is given by:-

$$\frac{dh_o}{dr} = \frac{C_w^{\,2}}{r} + C_a\frac{dC_a}{dr} + C_w\frac{dC_w}{dr} \qquad [4.44]$$

This will be referred to as the vortex energy equation. Apart from regions near the walls of the annulus, the stagnation enthalpy (and temperature) will be uniform across the annulus at entry to the compressor. If the frequently used design condition of constant specific work at all radii is applied, then although h_o will increase progressively through the compressor in the axial direction, its radial distribution will remain uniform. Thus dho/dr=0 in any plane between a pair of blade rows. Equation (4.44) then reduces to:

$$\frac{C_w^{\,2}}{r} + C_a\frac{dC_a}{dr} + C_w\frac{dC_w}{dr} = 0 \qquad [4.45]$$

A special case may now be considered in which Ca is maintained constant across the annulus, so that dCa/dr=0.Equation (4.46) then reduces to:-

$$-\frac{C_w}{r} = \frac{dC_w}{dr}$$

Which on integration gives, $C_w.r$=constant

Thus the whirl velocity varies inversely with radius, this being known as the free vortex condition.

In section 4.1 it was shown that for the case where $C_3=C_1$ and $Ca_1=Ca_2=Ca$. the degree of reaction can be expressed by:

$$\Lambda = 1 - \frac{C_a}{2U}\left(\tan\alpha_2 + \tan\alpha_1\right)$$

Which can readily be written in terms of whirl velocities as follows:

$$\Lambda = 1 - \frac{C_{w2} + C_{w1}}{2U} \qquad [4.46]$$

Remembering that $U=U_m\ r/r_m$, where U_m is the blade speed at the mean radius of the annulus r_m, Equation (4.46) can be written as:-

$$\Lambda = 1 - \frac{C_{w2} r + C_{w1} r}{2U_m r^2 / r_m}$$

For a free vortex design $C_w\ r$=constant

$$\Lambda = 1 - \frac{cons\tan t}{r^2} \qquad [4.47]$$

Evidently the degree of reaction increases markedly from root to tip of the blade. Even if the stage has the desirable value of 50 percent at the mean radius, it may well be too low at the root and too high at the tip for good efficiency. Because of the lower blade speed at the root section, more fluid deflection is required at the root section. It is, therefore, particularly undesirable to have a low degree of reaction in this region, and the problem is aggravated as the hub-tip ratio is reduced.

4.2.1 General Swirl Distribution

Compressor blade rows have also been designed by prescribing a general distribution of the tangential (swirl or whirl) velocity component along the blade height.

As an illustration we shall use the normal design condition that is:-

(A) Constant specific work input at all radii, together with,

(B) An arbitrary whirl velocity distribution which is compatible with (A), to obtain constant work input, $U(Cw_2\text{-}Cw_1)$ must remain constant across the annulus.

The general expression is:

$$C_w = a r^n \pm \frac{b}{r} \qquad [4.48]$$

At the rotor entry

$$C_{w1} = ar^n - \frac{b}{r} \qquad [4.49]$$

At the rotor exit,

$$C_{w2} = ar^n + \frac{b}{r} \qquad [4.50]$$

Where a, b and n are constants and R is the radius ratio r/r_m. At any radius r the blade speed is given by U=Um R. It is immediately seen that $(C_{w2}-C_{w1})2b/R$ and hence that:-

$U (C_{w2}-C_{w1}) = 2bUm$

This is independent of radius. The two design conditions (A) and (B) are therefore compatible.

We shall consider three special cases: where n=-1, 1 and 0 respectively. (It will be shown later that 'a 'and 'b' are not arbitrary constants but depending up on the chosen values of degree of reaction and stage temperature rise.)

When n=-1

The whirl distributions become

$$C_{w1} = \frac{a}{R} - \frac{b}{R} \qquad \text{And} \qquad C_{w2} = \frac{a}{R} + \frac{b}{R}$$

Which are of free vortex form, C_w r=constant. From what has gone before it should be clear that Ca=constant must be the third design condition required to ensure radial equilibrium, that is to

satisfy Equation (4.45). It also follows that the variation of Λ is given by Equation (4.47), which since (C_{w2} r +C_{w1} r) =2a r_m, can be written:-

$$\Lambda = 1 - \frac{2ar_m}{2U_m Rr} = 1 - \frac{a}{U_m R^2} \qquad [4.51]$$

When n=1

$$C_{w1} = aR - \frac{b}{R} \quad \text{And} \quad C_{w2} = aR + \frac{b}{R}$$

Rewriting Equation (4.45) in terms of the dimensionless R we have:-

$$C_a dC_a + C_w dC_w + \frac{C_w^{\ 2}}{R} dR = 0$$

Integrating from the mean radius (R=1) to any other radius,

$$-\frac{1}{2}\left[C_a^{\ 2}\right]_1^R = \frac{1}{2}\left[C_w^{\ 2}\right]_1^R + \int_1^R \frac{C_w^{\ 2}}{R} dR$$

At exit from the rotor, where, C_w=aR+ (b / R), the right-hand side of the equation becomes:

$$-\frac{1}{2}\left[a^2R^2 + 2ab + \frac{b^2}{R}\right]_1^R + \int_1^R \left[a^2R^2 + \frac{2ab}{R} + \frac{b^2}{R^3}\right] dR$$

And, finally, the radial distribution of Ca is given by:

$$C_{a2}^{\ 2} - (C_{a2}^{\ 2})_m = -2[a^2R^2 + 2ab\ln R - a^2] \qquad [4.52a]$$

Similarly, at inlet to the rotor,

$$C_{a1}^{\ 2} - (C_{a1}^{\ 2})_m = -2[a^2R^2 + 2ab\ln R - a^2] \qquad [4.52b]$$

Note that C_{a2} cannot equal C_{a1} except at the mean radius (R=1). It is not possible, therefore, to use the simple Equation (4.46) for the degree of reaction when finding the variation of Λ with radius. To do this it is necessary to revert to the original definition of Λ[=ΔTA/ (ΔTA+ΔTB)] and work from first principles as follows. We shall retain the assumption that the stage is designed to give $C_3=C_1$. Then ΔTs=ΔTos so that:-

$$C_p\left(\Delta T_A + \Delta T_B\right) = W = U\left(C_{w2} - C_{w1}\right)$$

$$C_p \Delta T_A = \frac{1}{2}\left(C_1{}^2 - C_2{}^2\right) + U\left(C_{w2} - C_{w1}\right)$$

$$= \frac{1}{2}\left[\left(C_{a1}{}^2 + C_{w1}{}^2\right) - \left(C_{a2}{}^2 + C_{w2}{}^2\right)\right] + U\left(C_{w2} - C_{w1}\right)$$

$$\Lambda = 1 + \frac{C_{a1}{}^2 - C_{a2}{}^2}{2U\left(C_{w2} - C_{w1}\right)} - \frac{C_{w2} + C_{w1}}{2U}$$

From Equations (4.52a) and (4.52b), assuming we choose to design with $(C_{a2})_m=(C_{a1})_m$,

$$C_{a1}{}^2 - C_{a2}{}^2 = 8ab \ln R$$

From the whirl distributions, $C_{w2} - C_{w1} = \frac{2b}{R}$ *and* $C_{w2} + C_{w1} = 2aR$

Substituting in the equation for, Λ, and writing $U=U_m R$, we get finally:

$$\Lambda = 1 + \frac{2a \ln R}{U_m} - \frac{a}{U_m} \qquad [4.46]$$

Designs with the exponent n=1 have been referred to as first power designs. At this point it can easily be made clear that the constants ‘a’ and ‘b’ in the whirl distributions are not arbitrary. Equation (4.53) shows that ‘a’ is fixed once the degree of reaction at the mean radius is chosen, that is at R=1:

$a=U_m(1-\Lambda_m)$

And 'b' is fixed when the stage temperature rise is chosen because,

$$C_p \Delta T_{os} = U\left(C_{w2} - C_{w1}\right) = 2bU_m$$

And hence $b = C_p \dfrac{\Delta T_{os}}{2U_m}$

When, n=0

Proceeding as in the previous case, but with:-

$$C_{w1} = a - \frac{b}{R} \quad and \quad C_{w2} = a + \frac{b}{R}$$

We find that:

$$(C_{a2}{}^2) - (C_{a2}{}^2)_m = -2\left[a^2 \ln R - \frac{ab}{R} + ab\right] \qquad [4.54]$$

$$(C_{a1}{}^2) - (C_{a1}{}^2)_m = -2\left[a^2 \ln R + \frac{ab}{R} - ab\right] \qquad [4.55]$$

Blading designed on this basis is usually referred to as exponential blading. Again proceeding as before, and assuming $(C_{a2})_m=(C_{a1})_m$, it can be shown that:

$$\Lambda = 1 + \frac{a}{U_m} - \frac{2a}{U_m R} \qquad [4.56]$$

It should be noted that for all three cases, at the mean radius (R=1), the expression $a=U_m(1-\Lambda_m)$ holds. If a value is specified for the reaction at the mean radius,Λ_m, the variation of reaction with radius can readily be obtained by substituting for 'a' in Equations (4.51), (4.53) and (4.56). The results can be summarized conveniently in the following table.

N	Λ	Blading
-1	$1-\frac{1}{R^2}(1-\Lambda_m)$	Free vortex
0	$1+\left[1-\frac{2}{R}\right](1-\Lambda_m)$	Exponential
1	$1+(2\ln R-1)(1-\Lambda_m)$	First power

It is instructive to evaluate the variation of Λ for all three cases assuming that Λ_m =0.5, and the results are given in Figure 4.9. It can be seen that the free vortex design gives the greatest reduction in Λ for low values of R while, the first power design gives the least reduction.

Furthermore, for all designs there is a lower limit to R below which the degree of reaction becomes negative. A negative value implies a reduction in static pressure in the rotor.

For the free vortex design, this limiting value of R is given by $0=1-\frac{1}{R^2}(1-\Lambda_m)$, from which R=0.71 when Λ_m=0.50.

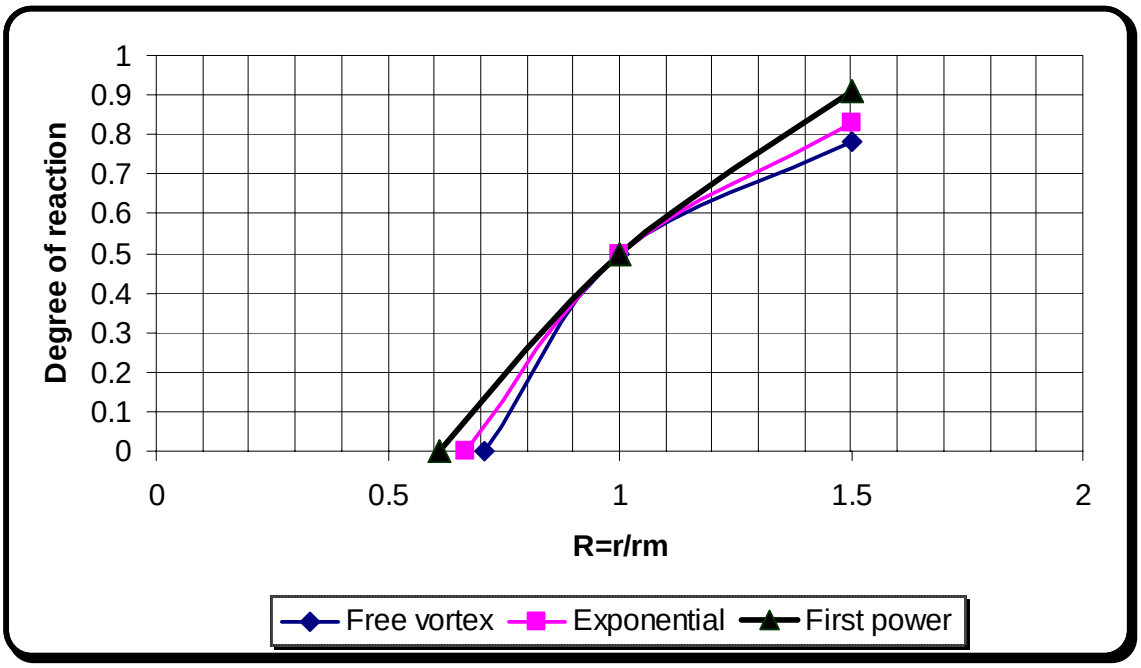

Figure 4.9 Radial variation of degree of reaction

4.3 Determination of Lift and Drag Coefficient

The resultant force due to the flow around an aerofoil blade acts at its center of pressure. It has two components-lift force, normal to the flow direction (or blade chord) and the drag force parallel to the flow. From the measured values of mean loss ϖ, two coefficients can be obtained. These are the lift and profile drag coefficient C_L and C_{DP}, formula for which may be obtained as follows. Referring to the diagram of forces acting on the cascade as shown in figure 4.10, the static pressure rise across the blades is given by the incompressible flow formula being used because the change of density is negligible.

$$\Delta P = P_2 - P_1 = \left(P_{02} - \frac{1}{2}\rho V_2^{\,2} \right) - \left(P_{01} - \frac{1}{2}\rho V_1^{\,2} \right)$$

Hence, still using cascade notation for velocities and angles, the axial velocity V_a being assumed the same at inlet and outlet.

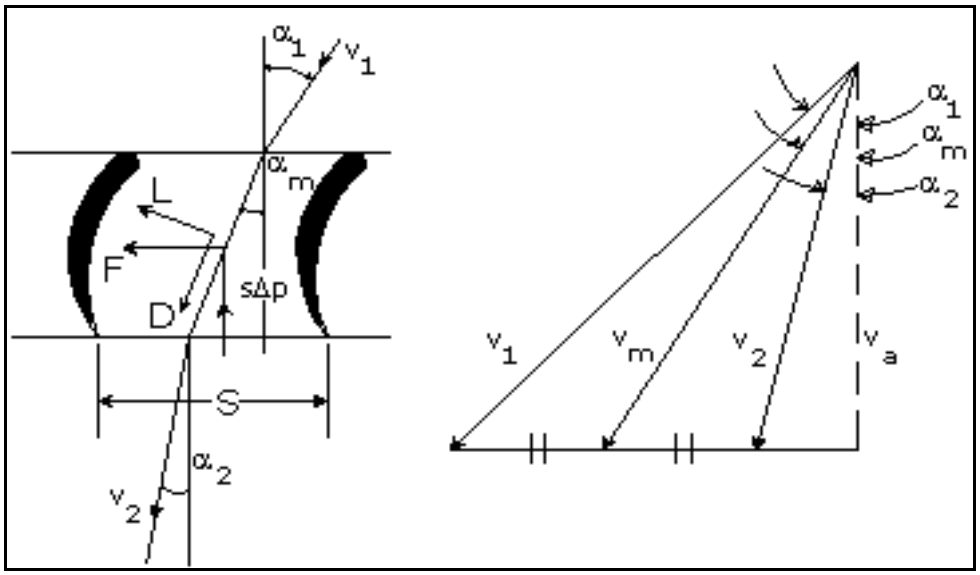

Figure 4.10 Applied and effective forces acting on cascade

$$\Delta P = \frac{1}{2}\left(V^2{}_1 - V_2^{\,2} \right) - \varpi \qquad [4.57]$$

$$= \frac{1}{2}\rho V_a^{\,2}\left(\tan^2 \alpha_1 - \tan^2 \alpha_2 \right) - \varpi$$

The axial force per unit length of each blade is SΔP and, from consideration of momentum changes, the force acting along the cascade per unit length is given by:-

F=S ρ V_a× change in velocity component along cascade

$=S\rho V_a^2 (\tan \alpha_1-\tan \alpha_2)$ [4.58]

The coefficients C_L and C_{DP} are based on a vector mean velocity V_m defined by the velocity triangles in Figure 4.10.

Thus,

$V_m=V_a \sec \alpha_m$ where α_m is given by:-

$$\tan \alpha_m = \frac{\left[\frac{1}{2}\left(V_a \tan \alpha_1 - V_a \tan \alpha_2\right) + V_a \tan \alpha_2\right]}{V_a} = \frac{1}{2}\left(\tan \alpha_1 + \tan \alpha_2\right)$$

If D and L are the drag and lift forces along and perpendicular to the direction of vector mean velocity, then resolving along the vector mean gives:-

$$D = \frac{1}{2}\rho V_m^{\ 2} C C_{Dp}$$ (By definition of C_{DP})

$=F \sin \alpha_m-S\Delta P \cos \alpha_m$

Hence from equations (4.57) and (4.58)

$$\frac{1}{2}\rho V_m^{\ 2} C C_{DP} = S\rho V_a^{\ 2}\left(\tan \alpha_1 - \tan \alpha_2\right)\sin \alpha_m - \frac{1}{2}\rho V_a^{\ 2} S\left(\tan^2 \alpha_1 - \tan^2 \alpha_2\right)\cos \alpha_m + \varpi S \cos \alpha_m$$

Since $\tan^2 \alpha_1 - \tan^2 \alpha_2 = (\tan \alpha_1 - \tan \alpha_2)(\tan \alpha_1 + \tan \alpha_2)$

$=2(\tan \alpha_1 - \tan \alpha_2) \tan \alpha_m$

The first two terms in the expressions for C_{DP} are equal and the equation reduces to

$$C_{DP} = \left(\frac{S}{C}\right)\left(\frac{\varpi}{1/2\rho}\right)\left(\frac{\cos \alpha_m}{V^2{}_m}\right)$$

$$C_{DP} = \left(\frac{S}{C}\right)\left(\frac{\varpi}{1/2\rho}\right)\left(\frac{\cos^3 \alpha_m}{V^2{}_a}\right)$$

$$C_{DP} = \left(\frac{S}{C}\right)\left(\frac{\varpi}{1/2\rho V_1^{\ 2}}\right)\left(\frac{\cos^3 \alpha_m}{\cos^2 \alpha_1}\right) \quad [4.59]$$

Also, resolving perpendicularly to the vector mean,

$L = \frac{1}{2}\rho V_m{}^2 C C_L$ (By definition of C_L)

$=F \cos \alpha_m + S\Delta P \sin \alpha_m$

Therefore,

$$\frac{1}{2}\rho V_m{}^2 C C_L = S\rho V_a{}^2 (\tan\alpha_1 - \tan\alpha_2)\cos\alpha_m + \frac{1}{2}\rho V_a{}^2 S(\tan{}^2\alpha_1 - \tan{}^2\alpha_2)\sin\alpha_m - \varpi S \sin\alpha_m$$

This on reduction finally gives:-

$$C_L = 2(S/C)(\tan\alpha_1 - \tan\alpha_2)\cos\alpha_m - C_{Dp}\tan\alpha_m \qquad [4.60]$$

Since α'_1 is known from the geometry of the blade row, the following data may be found for any incidence angle i:

$\alpha_1=\alpha'_1+i$

$\alpha_2= \alpha_1- \varepsilon^*$

$\alpha_m=\tan^{-1}[1/2(\tan \alpha_1+\tan \alpha_2)]$

CHAPTER FIVE

AERO-THERMODYNAMIC ANALYSIS FOR AXIAL FLOW AIRCRAFT GAS TURBINE ENGINE COMPRESSOR DESIGN

5.1 Introduction

The theory and experimental result made in many literatures presented in the previous sections will now be applied to the aerothermodynamics analysis of axial flow aircraft gas turbine engine compressor design. For the complete analysis of the compressor, a design point under sea-level static condition (with Pa=1.01bar and Ta=288K) are assumed as follows:

Compressor pressure ratio, P_{02}/P_{01}	4.15
Air-mass flow rate, $\dot{m}$	20kg/s
The tip speed of the first stage blade	355.3 m/s

With these data specified, it is now necessary to investigate the aero-thermodynamic analysis of the compressor. It will be assumed that the compressor has no inlet guide vanes, to keep weight, and noise down.

5.2 Preliminary Analysis for Compressor Design

The general objective of this analysis is to determine the blade geometry of the axial compressor based on the above conditions so that the geometry of the blade can be used for:-

- Detail analysis using FLUENT software.
- Developing a small scale computer program using C++ to calculate the power (work) required by the compressor and to determine other performance (explained later) measuring parameters at the design and off-design conditions.

5.2.1 Determination of Rotational Speed and Annulus Dimensions

Section 4.1.9 will suggest that a tip speed, U_t, of around 355.3 m/s will lead to acceptable stresses and that the axial velocity, Ca, could range from 150 to 200m/s. Without IGVs there will be no whirl component of velocity at inlet, and this will increase the Mach number relative to the blade (see Figure.4.4), so it may be advisable to use a modest value of 150 m/s for Ca.

To satisfy continuity

$$\dot{m} = \rho A C_{a1} = \rho_1 \pi\ r_t^{\,2}\left[1-\left(\frac{r_r}{r_t}\right)^2\right]C_a \qquad [5.1]$$

$$r_t^{\,2} = \frac{\dot{m}}{\pi\rho_1 C_{a1}\left[1-\left(\frac{r_r}{r_t}\right)^2\right]} \qquad [5.2]$$

At sea-level static conditions, $T_{01}=T_a=288K$. Assuming no loss in the intake, $P_{01}=Pa=1.01bar$. With $C_1=C_{a1}=150m/s$ ($C_{w1}=0$).

$$T_1 = T_{01} - \frac{C_a^{\,2}}{2\times C_p}$$

$$T_1 = 288 - \frac{150^2}{2\times 1.005\times 10^3} = 276.8K$$

$$P_1 = P_{01}\left[\frac{T_1}{T_{01}}\right]^{\frac{\gamma}{\gamma-1}} = 1.01\left[\frac{276.8}{288}\right]^{3.5} = 0.879bar$$

$$\rho_1 = \frac{P_1}{RT_1} = \frac{100\times 0.879}{0.287\times 276.8} = 1.106\,kg/m^3$$

$$r_t^{\,2} = \frac{20}{\pi\times 1.106\times 150\left[1-\left(r_r/r_t\right)^2\right]} = \frac{0.03837}{\left[1-\left(r_r/r_t\right)^2\right]}$$

The tip speed, U_t is related to r_t by $U_t=2\pi r_t N$, and hence if U_t is chosen to be 355.3 m/s,

$$N = \frac{355.3}{2\pi r_t}$$

Choosing a hub-tip ratio of 0.5 would give a compatible compressor tip radius of 0.2262m and the rotational speed becomes 250rev/s. It should be realized that the choice of 0.50 for hub-tip ratio is arbitrary, and merely provides a sensible starting point; and a considerable amount of design optimization is called for.

With the geometry selected, that is a hub-tip ratio of 0.50 and a tip radius of 0.2262m, it follows that the root radius is 0.1131m and the mean radius is 0.1697m.

The compressor delivery pressure is, $P_{02}=(\frac{P_{02}}{P_{01}})P_{01}=4.15\times1.01=4.19$bar. To estimate the compressor delivery temperature it will be assumed that the polytropic efficiency of the compressor is 0.90 (reasonable assumption based on Figure 2 in Appendix 'A' for a small pressure ratio of the stage). Thus,

$$T_{02}=T_{01}\left[\frac{P_{02}}{P_{01}}\right]^{\frac{\gamma-1}{\gamma\eta_{pc}}}, \text{ where } \quad \frac{\gamma-1}{\gamma\eta_{pc}}=\frac{1.4-1}{1.4}\times\frac{1}{0.9}=0.3175$$

So that,

$T_{02}=288.0\ (4.15)^{0.3175}=452.5$K

Assuming that the air leaving the stator of the last stage has an axial velocity of 150m/s and no swirl, the static temperature, pressure and density at exit can readily be calculated as follows:

$$T_2=452.5-\frac{150^2}{2\times1.005\times10^3}=441.3K$$

$$P_2=P_{02}\left[\frac{T_2}{T_{02}}\right]^{\gamma/(\gamma-1)}=4.19\left[\frac{441.3}{452.5}\right]^{3.5}=3.838bar$$

$$\rho_2=\frac{100\times3.838}{0.287\times441.3}=3.03kg/m^3$$

The exit annulus area is thus given by:

$$A_2 = \frac{20}{3.03 \times 150} = 0.0440 m^2$$

With r_m =0.1697m, the blade height at exit, h, is then given by:-

$$\boxed{h = \frac{0.044}{2\pi r_m} = \frac{0.044}{2\pi \times 0.1697} = 0.0413 m}$$

The radii at exit from the last stator are then,

r_t=0.1697+(0.0413/2)=0.1903m

r_r=0.1697-(0.0413/2)=0.1491m

5.2.2 Estimation of Number of Stages

With the assumed polytropic efficiency of 0.9, the overall stagnation temperature rise through the compressor is $\Delta T_{os}= T_{02}-T_{01}= 452.5-288=164.5K$.

Rather than choosing a value at random, it is instructive to estimate a suitable ΔT_{os} based on the mean blade speed.

$U=2\pi \times r_m \times N=2\pi \times 0.1697 \times 250=266.6 m/s$

We will adopt the simple design condition $C_{a1}=C_{a2}=C_a$ throughout the compressor, so that temperature rise from equation (4.32) is given by:-

$$\Delta T_{os} = \frac{\lambda U C_a (\tan \beta_1 - \tan \beta_2)}{C_p} = \frac{\lambda U (C_{w2} - C_{w1})}{C_p}$$

With a purely axial velocity at entry to the first stage, in the absence of IGVs, we have:

$$\tan \beta_1 = \frac{U}{C_a} = \frac{266.6}{150}, \quad \Longrightarrow \quad \beta_1 = 60.64^0$$

$$V_1 = \frac{C_a}{\cos \beta_1} = \frac{150}{\cos 60.64} = 305.9 m/s$$

In order to estimate the maximum possible deflection in the rotor, we will apply the de Haller criteria $V_2/V_1 \leq 0.72$. On this basis the minimum allowable value of V_2, and the corresponding rotor blade outlet angle are given by:-

$V_2=305.9\times0.72=220$m/s

$$\cos\beta_2 = \frac{C_a}{V_2} = \frac{150}{220}, \qquad \Longrightarrow \qquad \beta_2=47.01^0$$

Using this deflection and neglecting the work-done factor for this crude estimate:

$$\Delta T_{0s} = \frac{266.6\times150(\tan 60.64 - \tan 47.01)}{1.005\times10^3} \approx 28K$$

A temperature rise of 28K per stage implies 164.5/28=5.9 stages. It is likely, then, that the compressor will require six or seven stages and, in view of the influence of the work-done factor, seven is more likely. An attempt will therefore be made to analyze a seven-stage compressor.

It is normal to design for a somewhat lower temperature rise in the first and last stages, for reasons of compressibility effects. Compressibility effects will be most important at the front and at the last stage of the compressor where at the front of the compressor the inlet temperature, and hence the acoustic velocity, are lowest. Compressibility effect occurs on the last stage due to the increase of the relative velocity at the last stage there by increasing the Mach number relative to the blade. Therefore, a good starting point would be to assume $\Delta T_0=20$K for the first and the last stages, leaving a requirement for $\Delta T_0=24$K or 25 K in the remaining stages [3].

5.2.3 Stage-By-Stage Design Analysis

Having determined the rotational speed, annulus dimensions, and estimated the number of stages required, the next step is to evaluate the air angles for each stage at the mean radius.

From the velocity diagram, Figure 4.5, it is seen that $C_{w1}=C_a \tan\alpha_1$ and $C_{w2}=C_{w1}+\Delta C_w$. For the first stage $\alpha_1=0$, because these are no inlet guide vanes. The stator outlet angle for each stage, α_3, will be the inlet angle α_1 for the following rotor.

The work-done factors will vary through the compressor and reasonable values shall be assumed based on Figure 3.3 for the seven stages would be 0.98 for the first stage, 0.93 for the second, 0.88 for the third and 0.83 for the remaining four stages

Stages 1 and 2

Recalling the equation for the stage temperature rise in terms of change in whirl velocity $\Delta C_w = C_{w2} - C_{w1}$, we have:-

$$\Delta C_w = \frac{C_p \Delta T_0}{\lambda U} = \frac{1.005 \times 10^3 \times 20}{0.98 \times 266.6} = 76.9\, m/s$$

Since $C_{w1}=0$, $C_{w2}=76.9$ m/s and hence

$$\tan \beta_1 = \frac{U}{C_a} = \frac{266.6}{150} = 1.7773, \quad \Longrightarrow \quad \beta_1 = 60.64^0$$

$$\tan \beta_2 = \frac{U - C_{w2}}{C_a} = \frac{266.6 - 76.9}{150} = 1.264, \quad \Longrightarrow \quad \beta_2 = 51.67^0$$

$$\tan \alpha_2 = \frac{C_{w2}}{C_a} = \frac{76.9}{150} = 0.513, \quad \Longrightarrow \quad \alpha_2 = 27.14^0$$

The deflection in the rotor blades is $\beta_1 - \beta_2 = 8.98^0$, which is modest. The diffusion can readily be checked using the de Haller number as follows:

$$\frac{V_2}{V_1} = \frac{C_a / \cos \beta_2}{C_a / \cos \beta_1} = \frac{\cos \beta_1}{\cos \beta_2} = \frac{0.490}{0.260} = 0.790$$

Referring to Figure 3.4 this value of de Haller number indicates a relatively light aerodynamic loading, which is a low rate of diffusion.

At this point it is convenient to calculate the pressure ratio of the stage $(P_{03}/P_{01})_1$, the suffix outside the parenthesis denoting the number of the stage, and then the pressure and temperature at exit which will also be the values at inlet to the second stage.

The isentropic efficiency of the stage is approximately equal to the polytropic efficiency of the compressor, which has been assumed to be 0.90, so we have from Equation (4.18):-

$$\left(\frac{P_{03}}{P_{01}}\right)_1 = \left(1+\frac{\eta_s \times \Delta Tos}{T_{01}}\right)^{3..5}$$

$$\left(\frac{P_{03}}{P_{01}}\right)_1 = \left(1+\frac{0.90\times 20}{288}\right)^{3..5} = 1.236$$

$$\left(P_{03}\right)_1 = 1.01\times 1.236 = 1.249 bar$$

$$\left(T_{03}\right)_1 = 288+20 = 308K$$

We have finally to choose a value for the air angle at outlet from the stator row, α_3, which will also be the direction of flow, α_1, into the second stage. Here it is useful to consider the degree of reaction. For this first stage, with the prescribed axial inlet velocity, C_3 will not equal C_1 (Unless α_3 is made zero).

Whereas our equations for Λ were derived on the assumption of this equality of inlet and outlet velocities. Nevertheless, C_3 will not differ markedly from C_1, and we can arrive at an approximate value of Λ by using Equation (4.39).

$$\Lambda \approx 1-\frac{C_{w2}+C_{w1}}{2U} = 1-\frac{76.9}{2\times 266.6} = 0.856$$

Using 50 percent reaction stages from the third or fourth stage onwards, and an appropriate value of Λ for the second stage may be about 0.70.

For the Second stage ΔT_{os}=25K and λ =0.93 and we can determine β_1 and β_2 using Equations (4.32) and (4.25) from (4.32)

$$25 = \frac{0.93\times 266.2\times 150}{1.005\times 10^3}\left(\tan\beta_1 - \tan\beta_2\right)$$

$(\tan\beta_1-\tan\beta_2)$=0.6756 and from Equation (4.25)

$$0.70 \approx \frac{150}{2 \times 266.6}\left(\tan \beta_1 + \tan \beta_2\right)$$

$(\tan \beta_1 - \tan \beta_2) = 2.4883$

Solving these simultaneous equations we can get:

$\beta_1 = 57.70^0$ and $\beta_2 = 42.19^0$

Finally, using Equations (4.2) and (4.3)

$\alpha_1 = 11.06^0$, and $\alpha_2 = 41.05^0$

The whirl velocities at inlet and out let are readily found from the velocity diagram,

$C_{w1} = C_a \tan \alpha_1 = 150 \tan 11.06 = 29.3$ m/s

$C_{w2} = C_a \tan \alpha_2 = 150 \tan 41.05 = 130.6$m/s

It appears that α_3 for the first stage should be 11.06 degrees. This design gives a de Haller number for the second – Stage rotor blades of cos 57.70/cos 42.19 = 0.721, which is satisfactory.

The outlet pressure and temperature from the 2nd stage become:

$$\left(\frac{P_{03}}{P_{01}}\right)_2 = \left(1 + \frac{0.90 \times 25}{308}\right)^{3.3} = 1.280$$

$(P_{03})_2 = 1.249 * 1.280 = 1.599$ bar

$(T_{03})_2 = 308 + 25 = 333$k

At this point we do not know α_3 for the second stage, but it will be determined from the fact that it is equal to α_1 for the third stage, which we will now proceed to consider.

Stage 3

Using a stage temperature rise of 24K and a work-done factor of 0.88, an attempt will be made to use a 50 percent reaction design for the third stage.

Proceeding as before:-

$$\tan\beta_1 - \tan\beta_2 = \frac{\Delta T_{os} C_p}{\lambda U C_a} = \frac{24 \times 1.005 \times 10^3}{0.88 \times 266.6 \times 150} = 0.6854$$

$$\tan\beta_1 + \tan\beta_2 = \Lambda \frac{2U}{C_a} = \frac{0.5 \times 2 \times 266.6}{150} = 1.7773$$

Yielding $\beta_1=50.92^0$, $\beta_2=28.63^0$ and a de Haller number of 0.718, which is satisfactory for this preliminary design.

With a stage temperature rise of 24K, the performance of the third stage is then given by

$$\left(\frac{P_{03}}{P_{01}}\right)_3 = \left(1 + \frac{0.90 \times 24}{333}\right)^{3.5} = 1.246$$

$(P_{03})_3=1.599*1.246=1.992$ bar

$(T_{03})_3=333+24=357$K

From the symmetry of the velocity diagram, $\alpha_1=\beta_2=28.63^0$ and $\alpha_2=\beta_1=50.92^0$.

The whirl velocities are given by:-

$C_{w1}=150 \tan 28.63=81.9$m/s

$C_{w2}=150 \tan 50.92=184.7$m/s

At entry to the 3rd stage:-

$$T_1 = T_{01} - \frac{C^2 a}{2 \times Cp} = 333 - \frac{150^2}{2 \times 1005} = 321k$$

$$P_1 = P_{01}\left[\frac{T_1}{T_{01}}\right]^{3.5} = 1.599\left[\frac{321}{333}\right]^{3.5} = 1.42\,bar$$

$$\rho_1 = \frac{P_1}{RT_1} = \frac{100 \times 1.42}{0.287 \times 321} = 1.54kg/m^3$$

At exit to the 3rd stage:-

$$T_1 = T_{01} - \frac{C^2 a}{2 \times Cp} = 357 - \frac{150^2}{2 \times 1005} = 346k$$

$$P_1 = P_{01}\left[\frac{T_1}{T_{01}}\right]^{3.5} = 1.992\left[\frac{346}{357}\right]^{3.5} = 1.78\,bar$$

Stages 4, 5 and 6

A work-done factor of 0.83 is appropriate for all stages from the fourth on wards, and 50 percent reaction can be used. The design can be simplified by using the same mean diameter velocity diagrams for stages four to six. Reducing the stage temperature rise to 24K increases the de Haller number to 0.705, which will be consider to be just acceptable for the preliminary design by referring Figure 3.4.

$$\tan\beta_1 - \tan\beta_2 = \frac{24 \times 1.005 \times 10^3}{0.83 \times 266.6 \times 150} = 0.7267$$

$$\tan\beta_1 + \tan\beta_2 = 0.5 \times 2 \times \frac{266.6}{150} = 1.7773$$

Yielding $\beta_1=51.38^0$ $(=\alpha_2)$ and $\beta_2=27.71^0$ $(=\alpha_1)$.

It is not necessary to repeat all the calculations of stages 4-6, it is just summarized in Table 5.1.

Table 5.1

The performance of stages 4, 5 and 6:

Stages	4	5	6
P_{01}(bar)	1.992	2.447	2.968
T_{01}(K)	357	381	405
ρ(kg/m^3)	1.78	2.077	2.381
(P_{03}/P_{01})	1.228	1.213	1.199
P_{03} (bar)	2.447	2.968	3.56
T_{03} (K)	381	405	429
P_{03}-P_{01}	0.455	0.521	0.592

Stage 7

At entry to the final stage the pressure and temperature are 3.560 bar and 429K. The required compressor delivery pressure is 4.15*1.01=4.192 bar.

The pressure ratio of the seventh stage is thus given by: $\left(\frac{P_{03}}{P_{01}}\right)_7 = \frac{4.192}{3.560} = 1.177$

The temperature rise required to give this pressure ratio can be determined from

$$\left(1+\frac{0.90\times\Delta T_{os}}{429}\right)^{3.5} = 1.177$$

Giving, ΔTos=22.8K

The corresponding air angles, assuming 50 percent reaction, are then $\beta_1=50.98^0$ ($=\alpha_2$), $\beta_2=28.52^0$ ($=\alpha_1$) with a satisfactory de Haller number of 0.717.

With a 50 percent reaction design used for the final stage, the fluid will leave the last stator with an angle $\alpha_3=\alpha_1=28.52^0$, whereas ideally the flow should be axial at entry to the combustion chamber. The flow can be straightened by incorporating vanes after the final compressor stage and these can form part of the necessary diffuser at entry to the combustion chamber.

At entry to the 7th stage:-

$$T_1 = T_{01} - \frac{Ca^2}{2Cp} = 427.8 - \frac{150^2}{2 \times 1005} = 416.61K$$

$$P_1 = P_{01}\left[\frac{T_1}{T_{01}}\right]^{3.5} = 3.56\left[\frac{416.61}{429}\right]^{3.5} = 3.21bar$$

$$\rho_1 = \frac{P_1}{RT_1} = \frac{100 \times 3.21}{0.287 \times 416.61} = 2.685 kg/m^3$$

All the preliminary calculations have been carried out on the basis of a constant mean diameter. Another problem now arises: A sketch, approximately to scale, of the compressor annuli (see Appendix" A" Figure 1 for the sketch of the 7th stage compressor).

5.2.4 Variation of Air Angles from Root to Tip

As an example let our attention turned to the design analysis of the third stage which is typical of the later stages, recalling that the mean radius design was Λ_m=0.50.

P_{01}=1.599bar, P_{03}/P_{01}=1.246

T_{01}=333K T_{03} (=T_{02})=357K

α_1=28.63^0(=β_2=α_3) β_1=50.92^0

C_{w1}=81.9m/s C_{w2}=184.7m/s, ΔC_w=102.8m/s

$$C_3 = \frac{150}{\cos 28.63} = 170.9 m/s$$

$$T_3 = 357 - \frac{170.9^2}{2 \times 1.005 \times 10^3} = 342.9K$$

$$P_3 = 1.3923\left(\frac{342.9}{357}\right)^{3.5} = 1.7303bar$$

$$\rho_3 = \frac{100 \times 1.7303}{342.9 \times 0.287} = 1.758 kg/m^3$$

$$A_3 = \frac{m}{\rho_3 C_{a3}} = \frac{20}{1.758 \times 150} = 0.0076 m^2$$

$$\boxed{h = \frac{0.0076}{2\pi \times 0.1697} = 0.0711 m}$$

$$r_t = 0.1697 + \frac{0.0711}{2} = 0.2032 m,\ r_r = 0.1697 - \frac{0.0711}{2} = 0.1341 m$$

These radii refer to the conditions at the stator exit.

With negligible error it can be assumed that the radii at exit from the rotor blades are the mean of those at rotor inlet and stator exit. [3].

Thus at the exit of the rotor, $r_t = \frac{0.2115 + 0.2032}{2} = 0.2073 m$, $r_r = \frac{0.1341 + 0.1279}{2} = 0.131 m$

It is not necessary to repeat the calculations for rotor radii and blade speed at root and tip for this stage, and it will be sufficient to summarize the results as follows:

Table 5.2

Summarization of the Result for the Third Stages

	r_r(m)	r_t(m)	r_r/r_t	U_r(m/s)	U_t(m/s)
Inlet to the rotor blade	0.1279	0.212	0.605	200.9	332.2
Exit to the stator blade	0.131	0.207	0.653	205.71	325.6

The resulting air angles for a free vortex design are obtained from the calculations tabulated in Table 5.3, and the values already obtained at the mean radii are included for completeness.

Table 5.3

Result of Air Angles for Free Vortex Design, Third Stages

	Root	Mean	Tip
$C_{w1}=C_{w1}\ r_m/r$(m/s)	108.7	81.9	65.7
Tan $\alpha_1=C_{w1}/C_a$	108.7/150		65.7/150
α_1	35.93	28.63	23.65
Tan$\beta_1=(U-C_{w1})/C_a$	(200.9-108.7)/150		(332.2-65.7)/150
β_1	31.58	50.92	60.63
$C_{w2}=C_{w2}\ r_m/r$(m/s)	233.7	184.7	152.7
Tan $\alpha_2=C_{w2}/C_a$	233.7/150		152.7/150
α_2	57.31	50.92	45.51
Tan$\beta_2=(U-C_{w2})/C_a$	(205.8-233.7)/150		(322.5-152.7)/150
β_2	-10.54	28.63	48.54
$\beta_1-\beta_2$	42.12	22.29	12.09
$\Lambda=1-(1-\Lambda_m)/R^2$	0.161	0.5	0.668

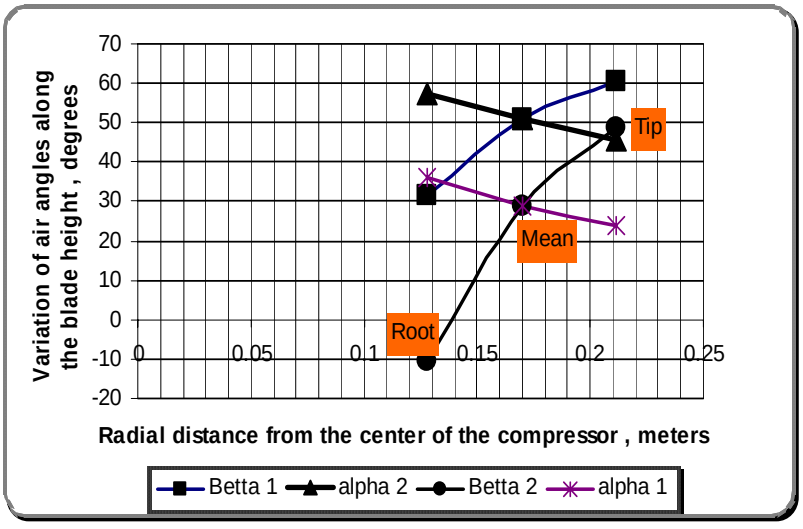

Figure 5.1 Radial variation of air angles: free vortex, 3rd stage.

The radial variation of air angles shown in Figure 5.1 clearly indicates the very large fluid deflection (β_1- β_2) required at the root and the substantial blade twist from root to tip.

In this section we have been deciding on the air angles likely to lead to a satisfactory design of the compressor. It is now necessary to discuss methods of obtaining the blade shapes which will lead to these air angles being achieved, and this will be done in the next section.

5.2.5 Blade Design

Having determined the air angle distributions which will give the required stage work, it is now necessary to convert these into blade angle distributions from which the correct geometry of the blade forms may be determined.

As an example, consider the design of the third-stage rotor blade required for free vortex design carried out in the previous section.

At the mean radius of 0.1697m, where $\beta_1=50.92^0$ and $\beta_2=28.63^0$, $\varepsilon^*=\beta_1-\beta_2=22.29^0$ and from Figure 3.7, with an air outlet angle of 28.63^0, S/C=0.9

For this thesis we can assume an aspect ratio of three (h/C).

The blade height can be obtained from the previously determined annulus dimensions as 0.0836m (Table 5.2 $h=r_t-r_r$), so that the chord becomes $\boxed{C=\frac{0.0836}{3}=0.0279m}$ and the pitch is $S=0.9\times0.0279=0.0251m$.

The blade number of an annular cascade is chosen in such a way that the azimuthal distance of two adjacent blades at the mean radius has the value of the pitch of the linear cascade: Therefore, the number of blades n is then given by:-

$$\boxed{n=\frac{2\pi\times0.1697}{0.0251}=42.5}$$

It is desirable to avoid numbers with common multiples for the blades in successive rows to reduce the likelihood of introducing resonant forcing frequencies.[3] One method of doing this is to choose an even number for the stator blades and a prime number for the rotor blades. An appropriate number for the rotor blades in this stage would therefore be 43, and recalculation in the reverse order gives: S=0.0248m, C=0.0276m and h/C=3.03

Then by using values of $\varpi/1/2\rho V_1^2$ read from the curve of Figure 3.6 and the known value of S/C for the cascade, C_{DP} and C_L may be calculated from Equations (4.51) and (4.52) and plotted against incidence as in Figure 5.2 .

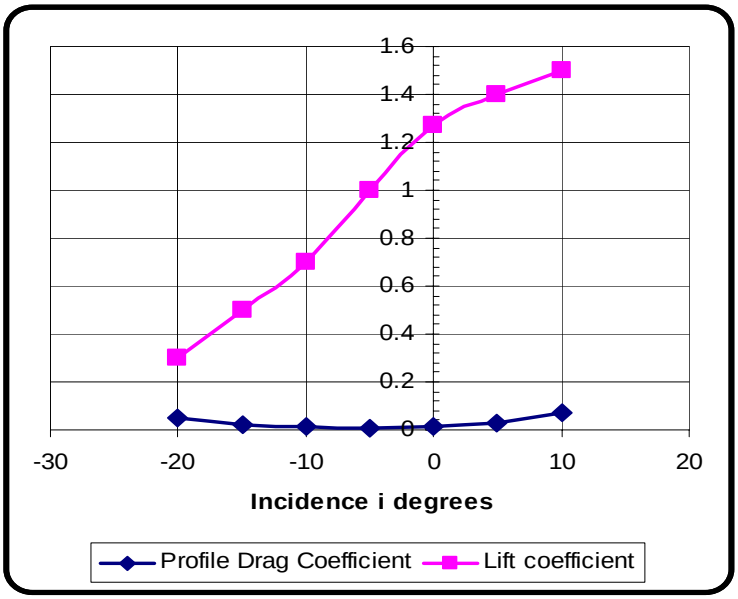

Figure 5.2 Lift and Drag coefficient for cascade of fixed geometrical form (S/C=0.9).

A similar procedure could also be carried out for the stator blades and using the same chord, C=0.0276m we can find that a stator blades of 42, S=0.0254, on the third stage. The use of prime numbers for rotor blades is less common than used to be the case. This is a result of developments in mechanical design which have resulted in the ability to replace damaged rotor blades in the field without the need for re-balancing the rotor system. [3]

5.2.6 Construction of Blade Shape

On the assumption of a circular arc camber-line, the deviation in the current example will be:-

$\delta = [0.23+0.1\times 28.63/50]\ (0.9)^{1/2}\theta = 0.273\theta$

With this information it is now possible to fix the main geometrical parameters of the rotor blade row of our example. The procedure is as follows.

Since $\theta = \alpha'_1 - \alpha'_2$ and $\alpha'_2 = \alpha_2 - \delta$

$\theta = \alpha'_1 - \alpha'_2 + \delta = \alpha'_1 - \alpha_2 + 0.273\theta$

$0.727\theta = \alpha'_1 - \alpha_2 = 50.92 - 28.63$ (assuming zero incidence, $\alpha'_1 = \alpha_1$)

It follows that $\theta = 30.64^0$ and $\alpha'_2 = \alpha'_1 - \theta = 20.28^0$. The deviation angle is 8.63^0. The position of the blade chord can be fixed relative to the axial direction by the stagger angle ζ given by:-

$\zeta = \alpha'_1 - \theta/2 = 50.92 - (30.64/2) = 35.60^0$

Referring to Figure 5.3, the chord line AB is drawn 0.0276m long at 35.60^0 to the axial direction. The lines AC and BD at angles α'_1 and α'_2 are then added and a circular arc constructed tangential to these lines and having AB as chord. This arc will now be the camber-line of the blade around which an airfoil section can be built up.

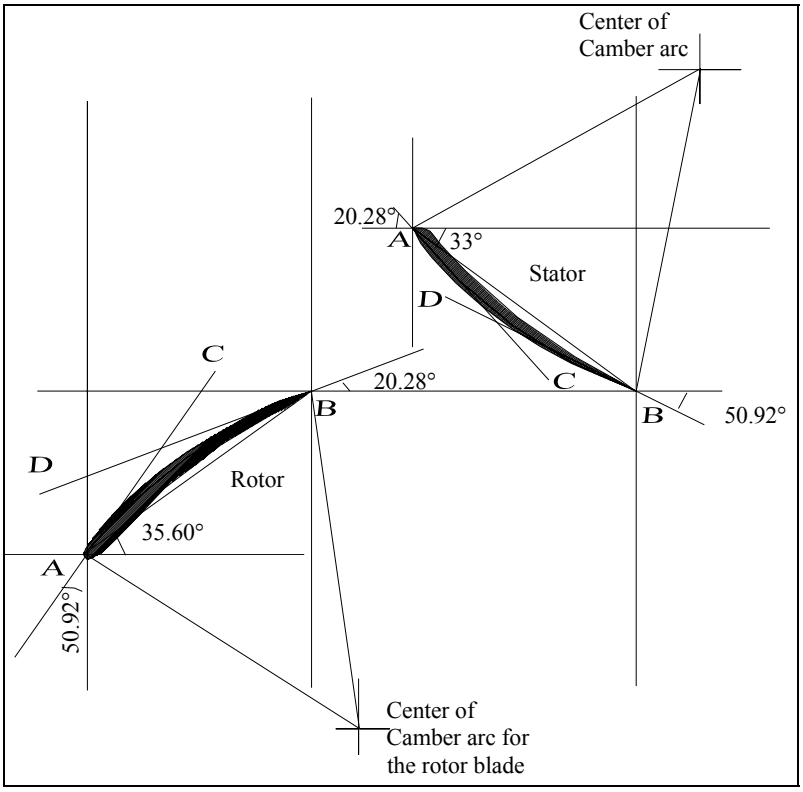

Figure 5.3 Construction of the blade shape.

The method outlined could now be applied to a selected number of points along the blade length, bearing in mind that having once fixed the pitch at the mean diameter by the choice of a particular number of blades, the pitch at all other radii is determined. As the S/C ratio is derived from the air angles, the length of the chord of the blade at any particular radius will be determined from the pitch.

CHAPTER SIX

CFD ANALYSIS AND PERFORMANCE EVALUATION OF AXIAL FLOW AIRCRAFT GAS TURBINE ENGINE COMPRESSOR

6.1 Computational Fluid Dynamic (CFD) Analysis

Computational Fluid Dynamics (CFD) is the science of predicting fluid flow, heat and mass transfer, chemical reactions, and related phenomena by solving numerically the set of governing mathematical equations such as conservation of mass, momentum, energy and species. CFD analysis complements testing and experimentation and reduces the total effort required in the experiment design and data acquisition. The results of CFD analyses are relevant in conceptual studies of:-

- New designs,
- Detailed product development,
- Trouble shooting and redesign.

FLUENT is a computational fluid dynamics (CFD) software package to simulate fluid flow problems. It uses the finite-volume method to solve the governing equations for a fluid.

In this section the necessary governing equations that FLUENT uses to solve the flow in axial flow compressor along with the method of numerical computation of the flow variables and the basic program structure will be discussed. It is based on the FLUENT documentation [15] and REF [7, 14, 17] which describes the numerical approach to solve the flow variables during CFD simulation and finally present work of the thesis using FLUENT will be presented.

6.1.1 Basic Program Structure

An important step of any CFD processing, which is also the first one to be done, is the pre-processing. The results of the pre-processing represent an ordered sequence of data that refer to the geometry, aerodynamic loads, external forces, stresses, local velocity field, pressure field, temperature field, rotational speed and constraints which is done using GAMBIT which is the preprocessor bundled with FLUENT.

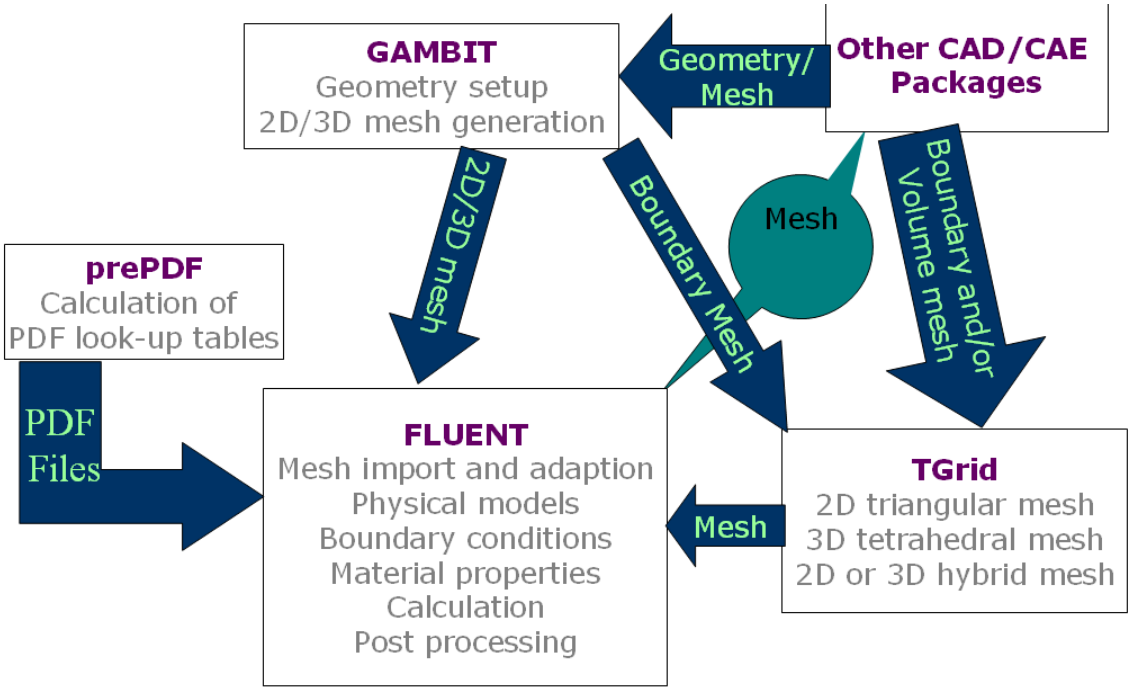

Figure 6.1 Basic program structures of FLUENT [14]

- FLUENT package includes the following products:-
  - FLUENT, the solver.
  - PrePDF, the preprocessor for modeling non-premixed combustion in FLUENT.
  - GAMBIT, the preprocessor for geometry modeling and mesh generation.
  - TGrid, an additional preprocessor that can generate volume meshes from existing boundary meshes.

6.1.2 Governing Equations

For flows, FLUENT solves numerically the conservation equations for Mass and Momentum. In axial flow compressor (AFC) since the flow involves compressibility an additional equation for energy conservation is solved.

A. **The Mass Conservation Equation**

The equation for conservation of mass, or continuity equation, can be written as follows:

$$\frac{\partial \rho}{\partial t} + \nabla . \left(\rho \vec{v} \right) = S_m$$

[6.1]

Equation 6.1 is the general form of the mass conservation equation and is valid for all flows. The source, S_m is the mass added to the continuous phase from the dispersed second phase (e.g., due to vaporization of liquid droplets) and any user-defined sources. This equation can be written to a reduced form for the flow in AFC as:

$$\nabla . \left(\rho \vec{v} \right) = 0 \qquad [6.2]$$

B. **Momentum Conservation Equations**

Conservation of momentum in an inertial (non-accelerating) reference frame is described by:

$$\frac{\partial \left(\rho \vec{v} \right)}{\partial t} + \nabla . \left(\rho \vec{v} \vec{v} \right) = -\nabla P + \nabla . \left(\bar{\bar{\tau}} \right) + \rho \vec{g} + \vec{F}$$

[6.3]

Where, *p* is the static pressure, τ is the stress tensor given as:-

$$\bar{\bar{\tau}} = \mu \left[\left(\nabla \vec{v} + \nabla \vec{v}^{T} \right) - \frac{2}{3} \nabla . \vec{v} I \right]$$

[6.4]

Where μ is the molecular viscosity, *I* is the unit tensor, and the second term on the right hand side is the effect of volume dilation. And ρ, *g* and *F* are the gravitational body force and external body forces (e.g., that arise from interaction with the dispersed phase), respectively. Also *F* contains other model dependent source terms such as porous-media and user-defined sources. These terms can be ignored in the analysis of AFC hence the equation is reduced to;

$$\nabla . \left(\rho \vec{v} \vec{v} \right) = -\nabla P + \nabla . \left(\bar{\bar{\tau}} \right) \qquad [6.5]$$

C. The Energy Equation

The energy equation solved by FLUENT correctly incorporates the coupling between the flow velocity and the static temperature, and should be activated whenever we are solving a compressible flow. FLUENT solves the energy equation in the following form:

$$\frac{\partial(\rho E)}{\partial t}+\nabla.\left(\vec{v}(\rho E+P)\right)=\nabla.\left(k\nabla T-\sum h_j J_j+\left(\bar{\bar{\tau}}.\vec{v}\right)\right)+S_h \qquad [6.6]$$

Where k is the effective conductivity (which includes the turbulent thermal conductivity, defined according to the turbulence model being used), and J_i is the species diffusion flux. The first three terms on the right-hand side of Equation 6.6 represent energy transfer due to conduction, species diffusion, and viscous dissipation, respectively. S_h includes heat of chemical reaction, and any other volumetric heat sources defined.

For the analysis of AFC the equation is reduced to;

$$\nabla.\left(\vec{v}(\rho E+P)\right)=\nabla.\left(k\nabla T+\left(\bar{\bar{\tau}}.\vec{v}\right)\right)$$

[6.7]

In Equation 6.7, E is the total energy given as:-

$$E=h-\frac{P}{\rho}+\frac{v^2}{2}$$

[6.8]

Equation 6.7 includes viscous dissipation terms, which describe the thermal energy created by viscous shear in the flow.

D. **Equations for Rotating Reference Frame**

When the equations of motion (see Section 3.5) are solved in a rotating frame of reference, the acceleration of the fluid is augmented by additional terms that appear in the momentum equations. **FLUENT** allows you to solve rotating frame problems using the absolute velocity, C, or the relative velocity, V, as the dependent variable. The two velocities are related by the following equation: $V_r=C-\omega\times r$ .Here ω is the angular velocity vector (that is, the angular velocity of the rotating frame) and **r** is the position vector in the rotating frame as shown in the Figure 4.3. The left-hand sides of the momentum equations appear as follows for an inertial reference frame:-

$$\frac{\partial}{\partial t}(\rho C)+\nabla.(\rho CC) \qquad [6.9]$$

For a rotating reference frame, the left-hand side written in terms of absolute velocities becomes:

$$\frac{\partial}{\partial t}(\rho C)+\nabla.(\rho V_r C)+\omega\times C \qquad [6.10]$$

In terms of relative velocities the left-hand side is given by:-

$$\frac{\partial}{\partial t}(\rho V_r)+\nabla.(\rho V_r V_r)+2\omega\times V_r+\omega\times\omega\times r+\rho\frac{\partial\omega}{\partial t}\times r \qquad [6.11]$$

Note that, **FLUENT** neglects the term, $\rho\frac{\partial\omega}{\partial t}\times r$ so it cannot accurately model a time-varying angular velocity using the relative velocity formulation.

6.1.3 Spatial Discretization (Interpolation Methods)

- Field variables must be interpolated to the faces of the control volumes in the FVM:
- Interpolation schemes for the convection term are:
  - **First-Order Upwind Scheme: -** Easiest to converge, only first order accurate.
  - **Power Law Scheme: -** More accurate than first-order for flows when Re < 5 (low Re flows).
  - **Second-Order Upwind Scheme:-** uses larger 'stencils' for 2nd order accuracy, essential with tri/tet mesh or when flow is not aligned with grid; convergence may be slower
  - **Quadratic Upwind Interpolation (QUICK):-** Applies to quad/hex and hybrid meshes (not applied to tri mesh), useful for rotating/swirling flows, 3rd order accurate on *uniform* mesh.

6.1.4 Pressure-Based Segregated Algorithm

The pressure-based solver uses a solution algorithm in FLUENT where the governing equations are solved sequentially (that is segregated from one another). Because the governing equations are non-linear and coupled, the solution loop must be carried out

iteratively in order to obtain a converged numerical solution. With the segregated algorithm, each iteration consists of the steps illustrated in the Figure and outlined below:

1. Update fluid properties (e.g., density, viscosity, specific heat) on the current solution.
2. Solve the momentum equations (*u*, *v*, and *w*) one after another, using the recently updated values of pressure and face mass fluxes.
3. Solve the pressure correction equation using the recently obtained velocity field and the mass-flux.
4. Correct face mass fluxes, pressure, and the velocity field using the pressure correction obtained from Step 3.

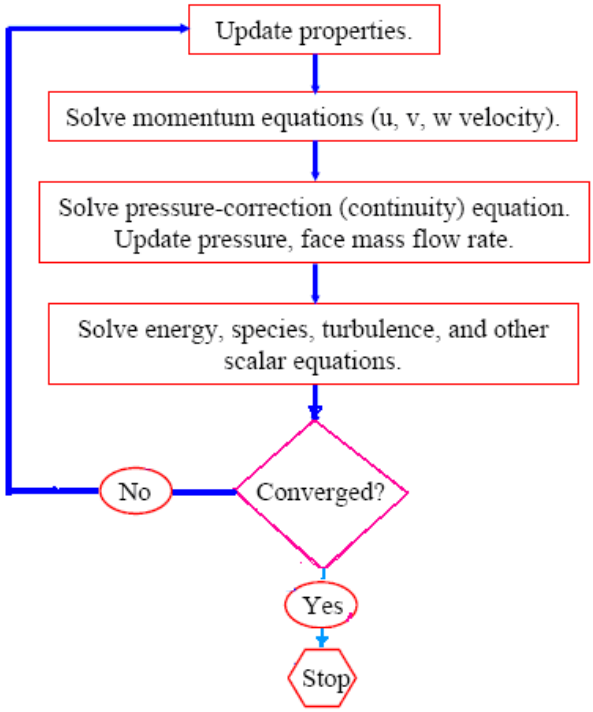

Figure 6.2 Overview of the pressure-based solution methods [14]

- At convergence:
  - All discrete conservation equations (momentum, energy, etc.) are obeyed in all cells *to a specified tolerance*.
  - Solution no longer changes with more iteration.
  - Overall mass, momentum, energy, and scalar balances are achieved.

6.2 Present Study Using FLUENT

Two-dimensional air flow through the third stage blades of axial compressor will be studied in this analysis by using the manner of specifying the base profile as shown in Figure 5.3, ordinates being given at definite positions along the camber line. The NASA 65 series profiles which have been widely used for axial flow compressor blade profile is selected. The selected profile thickness along the blade camber is given in Appendix B Table 1. As discussed in the previous section the results of the analysis in FLUENT can be shown by using graphical display. The outputs here are to illustrate such graphical displays for third stage compressor and similar analysis can be obtained for the other stages based on the same methodology.

6.2.1 Computational Methodology

- A two-dimensional model of computational domain (blade profiles, camber line, upstream and down stream of blade) created in GAMBIT 2.3.16. using the following procedure:-
  - Import selected airfoil vertices data from reference [13].
  - Create vertices using a grid system.
  - Create straight edges between vertices.
  - Split an arc on the blades using a vertex point.
  - Create faces from edges.
  - Specify the distribution of nodes on an edge.
  - Create unstructured meshes on faces (Unstructured grids permit automatic adaptive refinement based on the pressure gradient (FLUENT)).
  - Set boundary types.
  - Prepare the mesh to be read into FLUENT.
- The meshed domain is shown in Figure 6.3. This mesh is exported to FLUENT 6.3.26. In FLUENT 6.3.26 pressure-based solver is selected.

6.2.2 Study Description

There are two sections of flow created by this third stage of the compressor. In the first section, flow is created by a 43 bladed rotor, which rotates at 250rev/s (1570 rad/s). In the second section, the flow is "straightened out" by means of a 42 bladed stator section located just downstream of the rotor section, as shown in Figure 6.3.

Previous computational work showed that the application of inlet boundary conditions approximately 10 percent of axial chord length upstream of the blade and exit conditions 20 percent of axial chord lengths downstream of the blade would not interfere with any flow phenomena within the passage. [14, 17] For this reason, the sketch and the essential details of the original blade row geometry are provided in Figure 6.3, Figure 6.4 and Table 6.1 based on the design value in chapter 5 for third stage compressor.

Table 6.1

Cascade Geometric Data for Third Stage Compressor

	Rotor blades	**Stator blades**
Chord length, c	27.6 mm	28 mm
Axial chord, b	22.4 mm	22.8mm
Pitch-chord ratio, s/c	0.9	0.9
Inlet blade angle, α'_1	50.92 deg	20.28 deg
Outlet blade angle, α'_2	20.28 deg	50.92 deg
Incidence, i	0 deg	0 deg
Stagger angle, γ	35.60 deg	33 deg
Number of blades	43	42

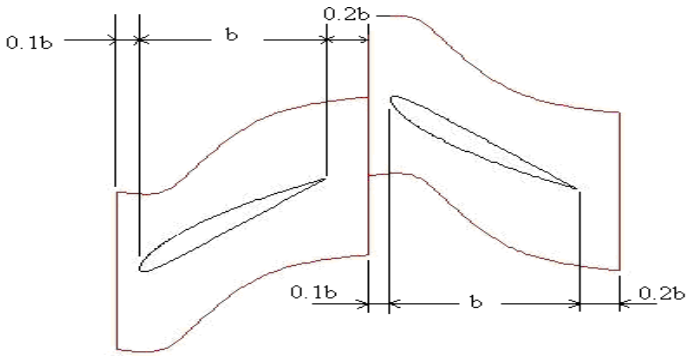

Figure 6.3 Profile of the third stage compressor

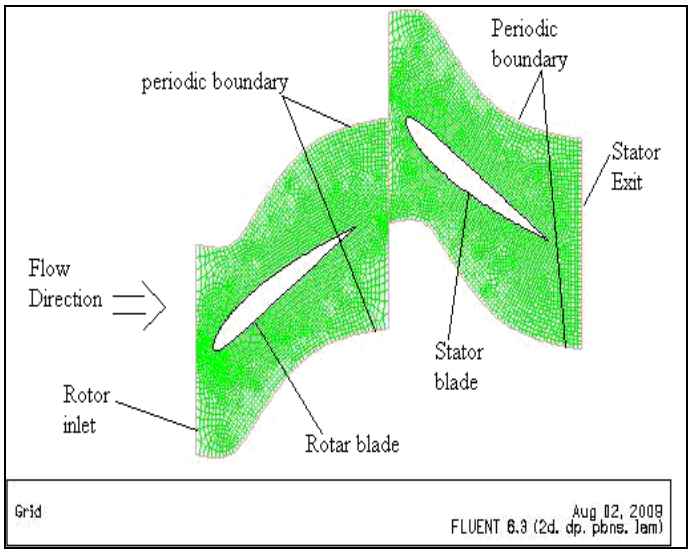

Figure 6.4 Profile of the third stage with the grid mesh generation and boundaries

6.2.3 Turbulence Modeling

A flow having high Reynolds numbers usually involves turbulence length scales that are much smaller than the size of the control volumes. Therefore, it is common to employ statistical models to simulate the turbulence. The standard *k*-ε turbulence model offered in FLUENT was used for the purpose of these simulations. This semi-empirical model is adequate for fully turbulent flows. This model is based on the transport equations of the turbulence kinetic energy *k* and on the turbulence dissipation rate ε [14].

6.2.4 Boundary Conditions

The boundary types for the case illustrated in Figure 6.4 are as follows:

A. ***Periodic boundary***, Periodicity is a flow condition that plays an integral role in turbo machinery research. A periodic flow field is defined as the repetition of small domains to create a larger domain. Axial compressor blades are usually evenly spaced in the circumferential direction. This means that the blade row can be broken into smaller domains including just one blade or one passage (space between blades). So the boundaries separating each individual blade have the same values of velocity and other fluid properties. For this case the assumption is that the blades are stacked on top of each other creating an endless

row of blades. The annulus or blade row is accurately modeled in this manner because it really is an endless loop of blades. In this thesis, since each section of the stage is symmetric, only a portion of each section is needed for modeling in order to obtain a solution for the entire geometry. Use of the periodic boundary condition is required to do this. That is to say, since there are 43 rotor blades and 42 stator blades, 1/43 of the rotor section and 1/42 of the stator section will be modeled. The periodic boundary is drawn at the middle line of the flow channel between two adjacent blade row profiles. The surfaces of the periodic boundary conditions were constructed from the middle line of the blade and connected smoothly to the inlet and outlet walls. The effective representation of this model is also shown in Figure 6.4. Creation of periodic zone is done in FLUENT by entering the following command line in the command prompt: > **grid/modify-zones/make-periodic**.

B. ***Inlet boundary***, which is located at the blade row inlet and its length, equals the blade row pitch. The flow at inlet to the third stage that is total temperature (321K), a static pressure of 142000pa and flow direction (normal to boundary) are specified based on the calculated values in chapter 5.
C. ***Outlet boundary***, which is located at the blade row exit and its length, equals the blade row pitch. A constant mass flow rate of (20/42) 0.4762kg/s is set out let to the stator blade.
D. ***Rotating Reference Frame*:** the rotating boundaries become stationary relative to the rotating frame. That is, on imposing the boundary conditions for the third stage AFC, the rotor blades are made stationary while the surrounding fluid appears to move with a specified rotational speed in opposite direction relative to the actual rotor motion. An angular speed of 250rev/s (1570 rad/s) is set for the third stage rotor blade.
E. ***Wall boundary conditions (Airfoil boundary):*** are used to bound fluid regions of the flow domain. The rotor and stator blades are represented as walls in the flow simulation of the third stage. In viscous flows, the no-slip boundary condition which means that the fluid remains attached to the solid surface, i.e. the fluid's velocity equals the velocity of the solid surface is enforced at walls by default and a tangential velocity component is incorporated in terms of the rotational motion of the wall boundary. Fixed temperature condition is selected at the walls.

F. ***Mixing Plane boundary Condition:*** The moving cell zone capability in **FLUENT** provides a powerful set of features for solving problems in which the domain or parts of the domain are in motion, for example, in turbo machinery applications where rotor and stator blades are in close proximity (and hence rotor-stator interaction is important). **FLUENT** provides the mixing plane model to address this class of problems. The mixing plane model is applicable in the following conditions of axial flow compressor stage:-

- When the number of blades is different for each blade row, a large number of blade passages are required within the model in order to maintain circumferential periodicity.
- When each fluid zone is treated as a steady-state problem; flow-field data from adjacent zones are passed as boundary conditions that are spatially averaged or \mixed" at the mixing plane interface. This mixing plane model removes any unsteadiness that would arise due to variations in the zone-to-zone flow field (e.g., wakes, shock waves, separated flow), and thus the mixing plane model yields a steady-state or \quasi-steady-state" result. At the interface of the rotor and stator. Observing the flow path through the compressor, the outlet of flow from the rotor section essentially becomes the inlet of flow for the stator section. Since each section has different geometry, the Mixing Plane boundary condition must be applied in order to develop a solution.

Some examples of specifying the above boundary conditions in the fluent window are shown in the figure below. Figure 6.5 shows that how mixing plane model is created in the analysis.

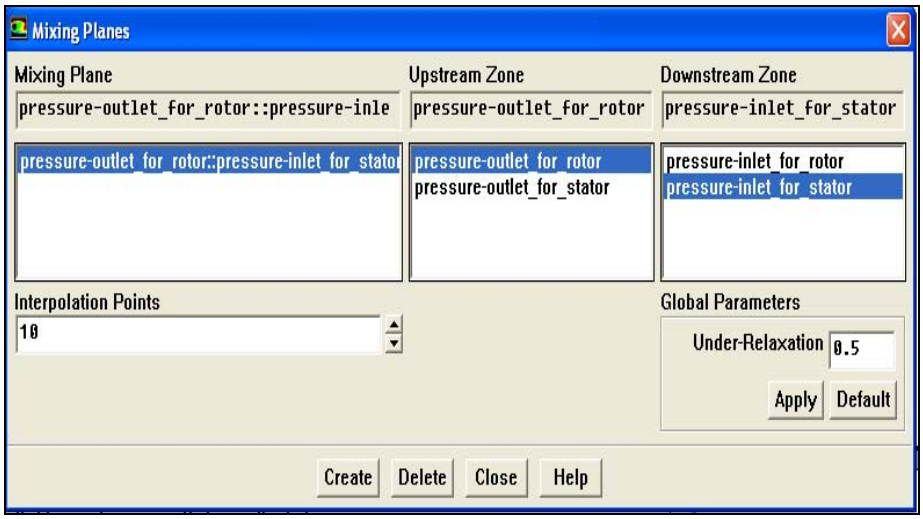

Figure 6.5 Creating of mixing plane boundary conditions

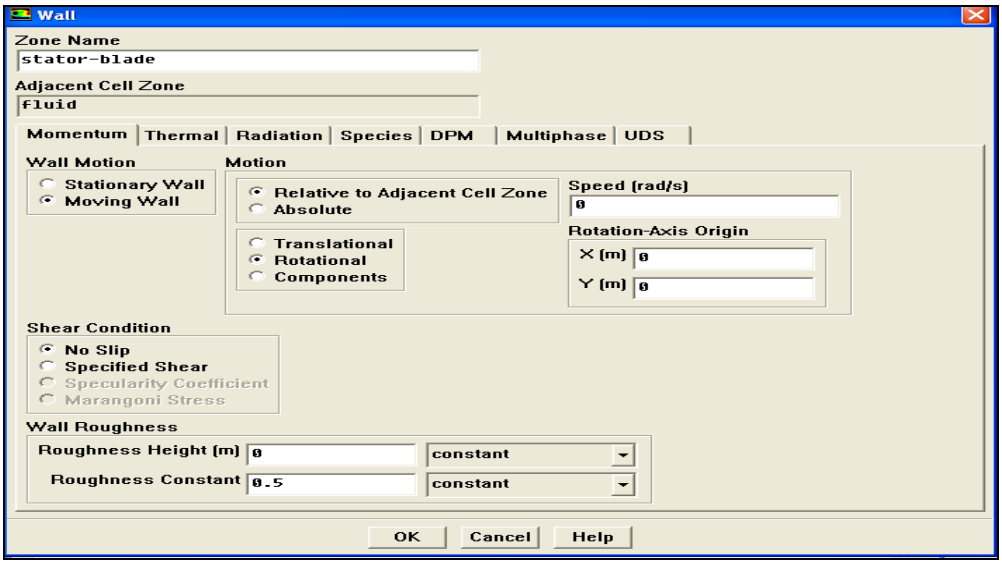

(a)

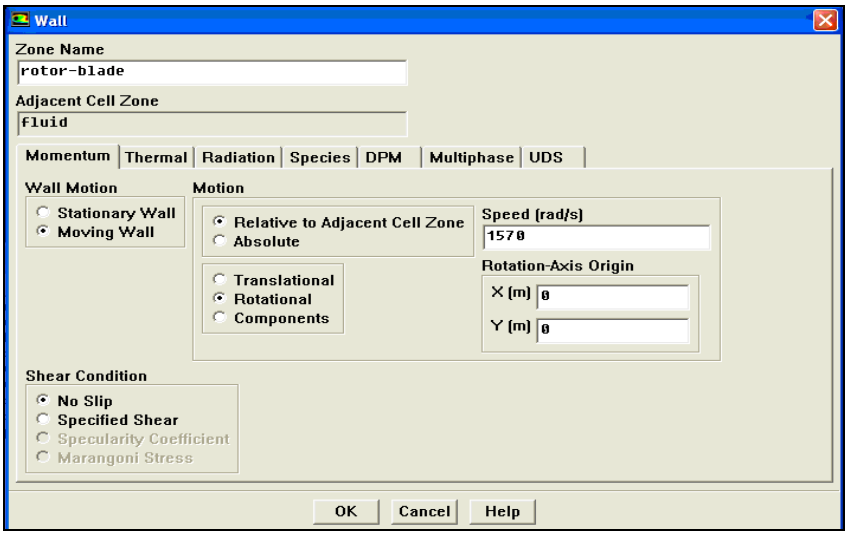

(b)

Figure 6.6 (a), (b) Specification of wall boundary conditions.

Figure 6.6 (a) and (b) shows that how the wall boundary condition for stator and rotor blades are specified during the analysis.

6.2.5 Solution Controls

The solution controls were modified from the default settings to better suit this flow study. They are explained as follows:-

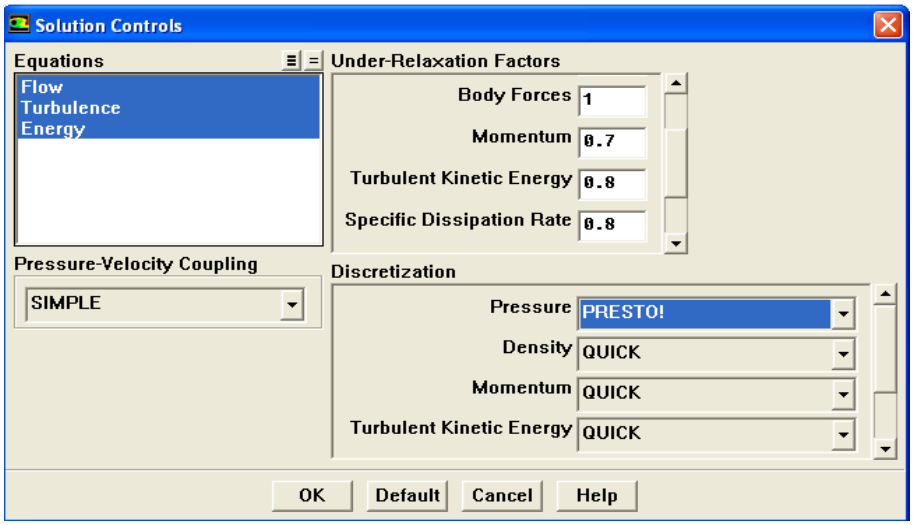

Figure 6.7 Solution control property window

A. **Under-relaxation factors:-**These factors control the calculations of computed variables during each iteration. Either higher or lower values can give result, might higher values give solver failures that is to say solution is diverged or etc, and might lower values can take long time to get good residuals. It is recommended to use the default under-relaxation factors. If the residuals continue to increase, relaxation factors can be decreased accordingly.

B. **Pressure-velocity Coupling:-**Pressure –velocity coupling can be read for details by using 26.3.5 from FLUENT user guide. SIMPLE is a fluent default scheme. The SIMPLE algorithm utilizes an interaction between velocity and pressure corrections to enforce mass conservation and to obtain the pressure field.

C. **Discretization:-**The PRESTO! (Pressure staggering option) scheme can be used for all kind of meshes. This scheme is recommended for swirl flows, high-speed rotating flows and flows in strongly curved. This scheme is highly recommended for the steep pressure gradients with swirling flows.

After all the above steps the solution was initialized and the **Continuity** value falls below 1e-6, the simulation will have converged, and the fluent display will look as follows.

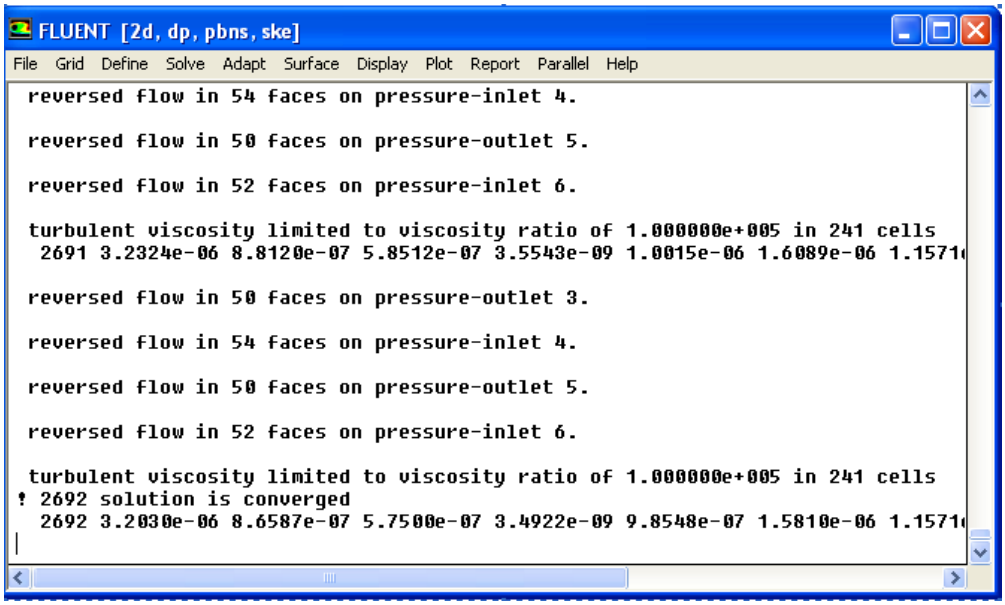

Figure 6.8 Fluent displays window for the convergence of the solution.

Once the **Continuity** value falls below 1e-6, the simulation will have converged, and the FLUENT display will look as Figure 6.8. The mass flow rate history, lift and drag coefficient history are shown in the plots below.

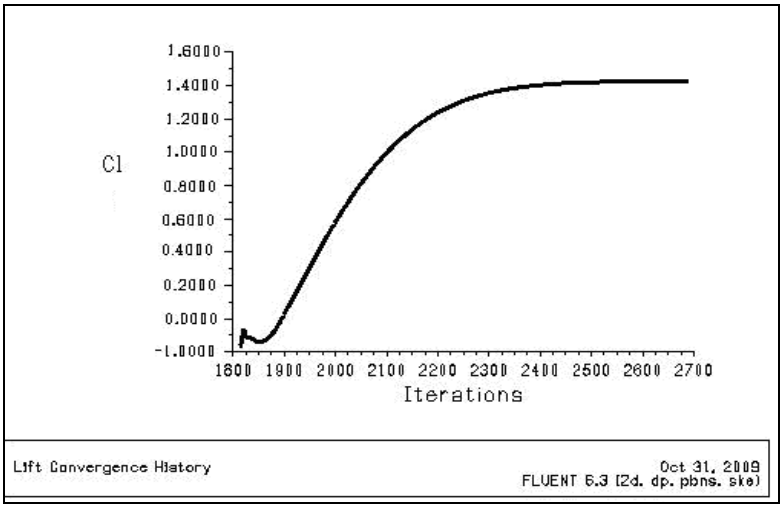

Figure 6.9 Convergence history of Lift Coefficient on the rotor blade

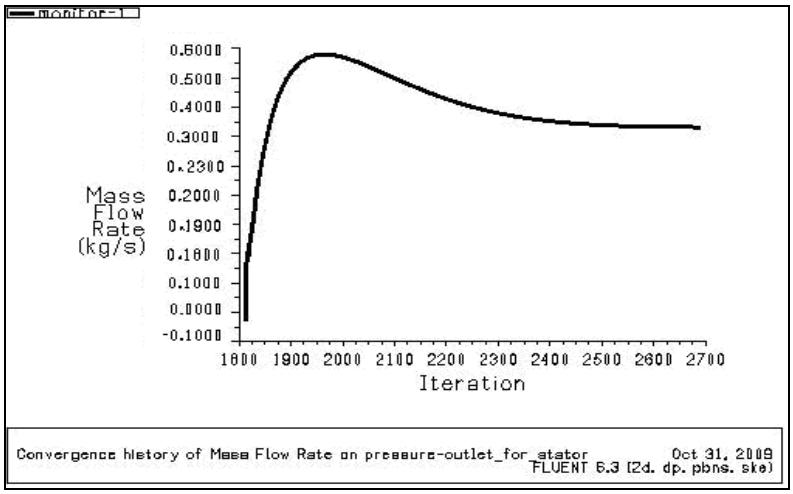

Figure 6.10 Convergence history of Mass flow rate on pressure-outlet for stator

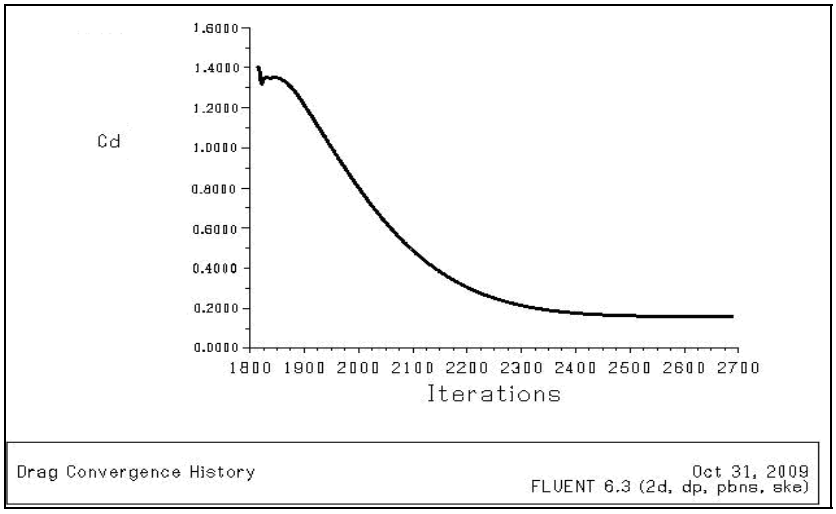

Figure 6.11 Convergence history of drag Coefficient on the rotor blade

6.2.6 Simulations, Results and Discussion

The simulation through a stage of compressor is very important for aerospace applications and research and development department. For example Figure 6.12 show the stagnation region near to leading edge of the rotor airfoil and as well as show the low-pressure region which is lower than the total pressure.

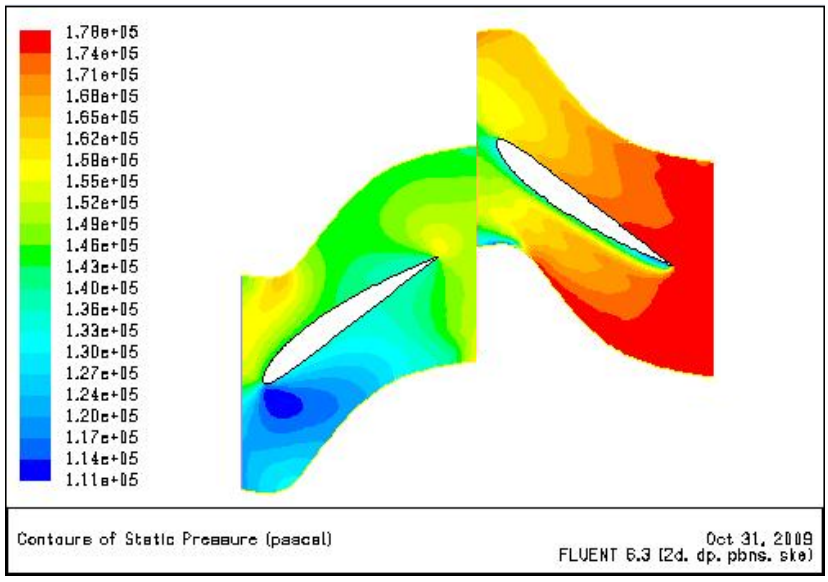

Figure 6.12 Contours of static pressure on the third stage compressor

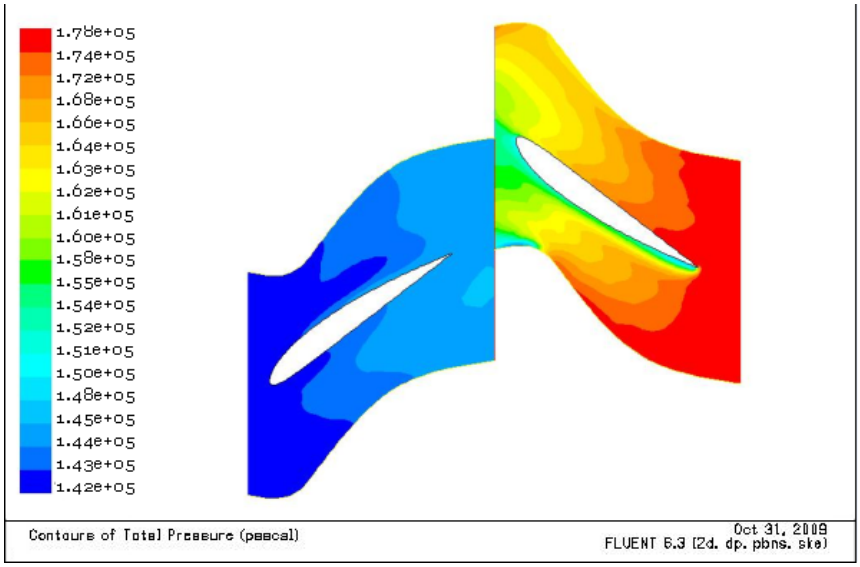

Figure 6.13 Contours of Total pressure on the third stage compressor

From the changing of color in Figure 6.13 we can see that, there is an increase in pressure from inlet to outlet section of the stage (a total pressure change of 0.36 bars is seen).

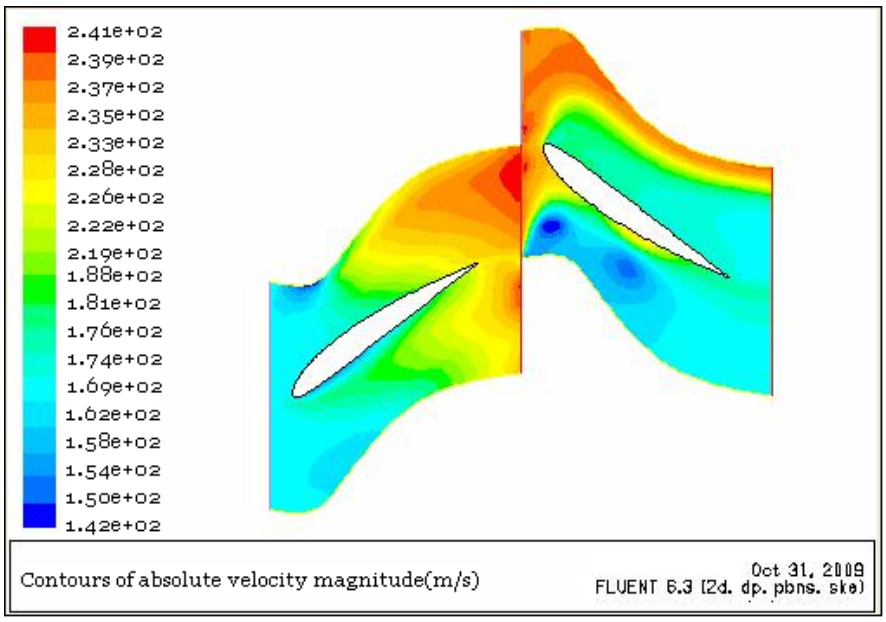

Figure 6.14 Contours of absolute velocity magnitude on the third stage compressor

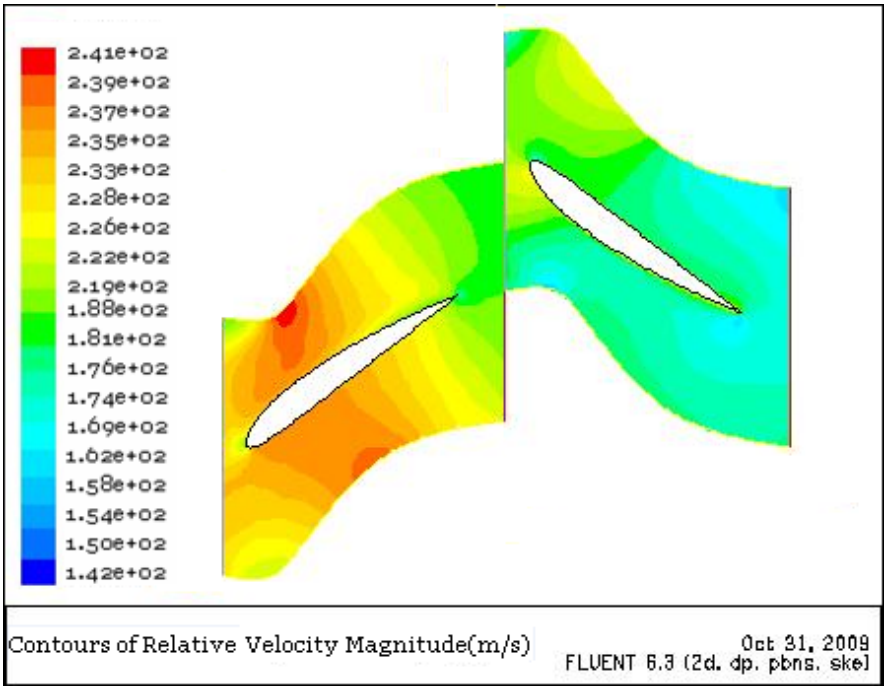

Figure 6.15 Contours of relative velocity magnitude on the third stage compressor

Figure 6.14 and Figure 6.16 show that, the absolute velocity of air is increased due to its passage through the ring of moving blades but, it decreased during its passage in the stator sections.

Figure 6.15 shows, air passing over the rotor surface will be accelerated to a higher velocity on the convex surface. The velocity distribution through the blade passage will be of the form shown; the

maximum relative velocity on the suction surface of the rotor blade will occur at around 10-15 percent of the chord from the leading edge of the rotor blade and will then fall steadily until the outlet velocity is reached.

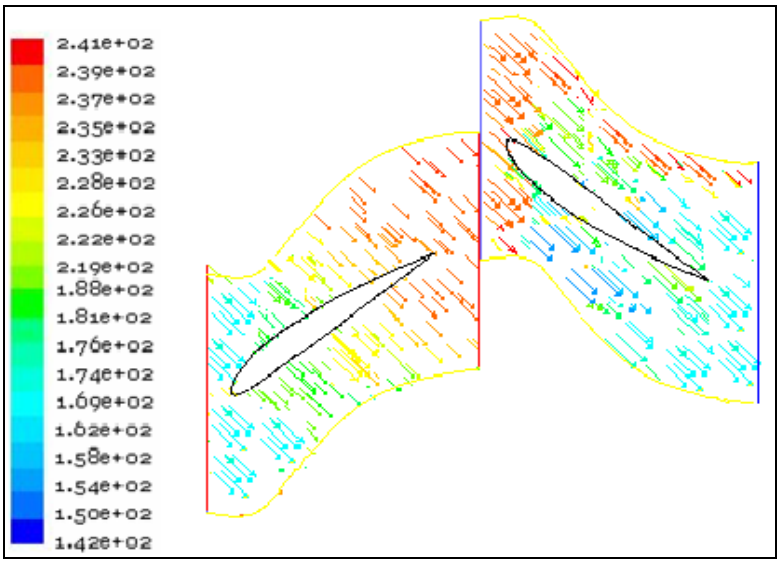

Figure 6.16 Velocity Vector Colored by Absolute velocity Magnitude (m/s)

6.2.7 Compressibility Effect

Compressibility effects are encountered in gas flows at high velocity and/or in which there are large pressure variations.

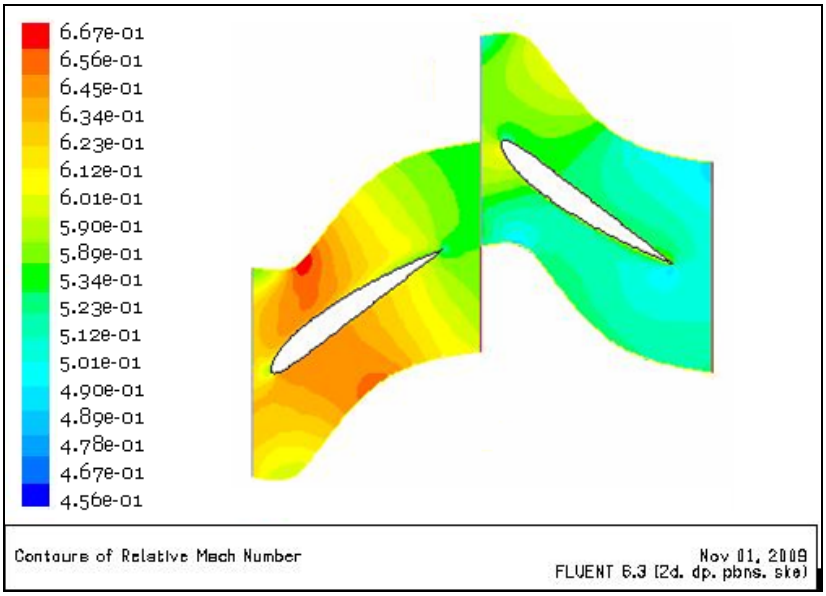

Figure 6.17 Contours of relative Mach number on the third stage compressor

Compressible flows can be characterized by the value of the relative Mach number, *M* given as $\frac{V}{a} = M$ .Where '*V*' is the relative velocity and '*a*' is the speed of sound in the gas given as ($a = \sqrt{\gamma RT}$). If the Mach number is less than 1.0, the flow is termed subsonic. Generally at Mach numbers much less than 1.0 (M < 0.32), compressibility effects are negligible and the variation of the gas density with pressure can safely be ignored in flow modeling. As the Mach number approaches 1.0 (which is referred to as the transonic flow regime), compressibility effects become important. When the Mach number exceeds 1.0, the flow is termed supersonic, and may contain shocks which can impact the flow pattern significantly. In FLUENT compressible flow is enabled when you choose ideal gas for fluid density. Figure 6.17 emphasized that in areas of high relative velocity, the Mach number is rather large; the effect has an influence on the flow field inside the stage.

6.2.8 Experimental and Theoretical Validation

As explained in the literature assumptions need to be made to simplify the conditions that are to be modeled. These introduce approximation errors into the simulations. In an attempt to reduce the effect of such simplifications and approximations, the models first need to be verified and validated against experimental data to ensure their accuracy. Therefore, Validation is defined as "the process of determining the degree to which a model is an accurate representation of the real world from the perspective of the intended uses of the model". On the other hand, a validation process is necessary in order to confirm that our design analysis meets the specified requirements. This process made with verifying lift and profile drag coefficient using the available data as follows:-

We can get lift and drag coefficient in FLUENT by using the following step:-

To display lift and drag coefficient start by selecting the following menus

Report → Forces…

This will cause the drag data to appear in Fluent's main window and the final number displayed on the first row, labeled **total coefficient**, is the **drag coefficient** which is **Drag = 0.0119.**

Similarly, Set the Force Vector components for the lift.

1. To find **lift coefficient** open the **Force Reports** window.
2. In the **Force Vector** field change **X=0, Y=1** for incidence angle 0^0 and set X to -sin (5°) = -0.087 and Y to cos (5°) =0.996 for incidence angle 5^0. And **Left Click** on **Print**

Scroll the window all the way the right, and the final number displayed on the bottom row, labeled **total coefficient**, is the **lift coefficient** as shown in Figure 6.18.

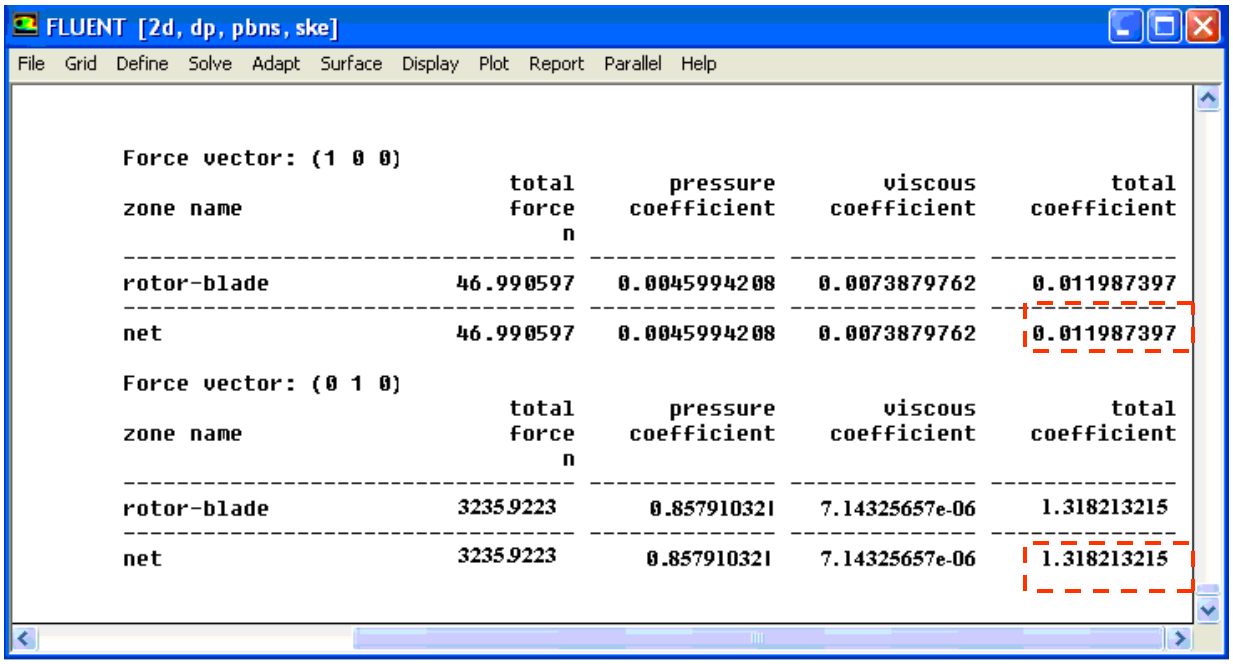

Figure 6.18 Result of FLUENT console window on the surface of the rotor blade for nominal incidence angle 0^0

With this simulation data for this study, we can now compare the FLUENT result with the theoretical calculated values and experimental data. The summary of result is shown in the Table 6.2

Table 6.2

Comparison of lift and profile drag coefficient on the third stage rotor blade

	C_L	C_{DP}
FLUENT (At zero incidence angle)	1.32	0.0119
Theory (From Figure 5.2 at zero incidence angle)	1.26	0.014
Experimental (From figure 3.5 and 3.8 at zero incidence angle)	1.23	0.016
FLUENT (At five incidence angle)	1.48	0.0278
Theory (From Figure 5.2 at five incidence angle)	1.40	0.03
Experimental (From Figure 3.5 and 3.8 at five incidence angle)	1.37	0.02

Note that: - the performance at $i=0^0$ can be determined as follows:

Nominal deflection=$\varepsilon^*= 22.92^0$, Nominal incidence=$i^*= 0^0$, and S/C=0.9

Referring to Figure 3.8 and with (i- i*)/ε*= 0 obtain C_{DP}=0.016. Similarly, the performance at incidence angle (i) =5^0 can be obtained as above. From the above table we can see that lift coefficient and profile drag coefficient of FLUENT results are pretty close to their respective theoretically calculated values. The experimental result that is made by Howell (1, 9 and 16) on the profile drag coefficient shows also a good agreement with the FLUENT result.

6.2.9 Limitations

- The built in, Gambit Turbo machinery module is not used because of the non-availability of license.
- The all picture of the blade is not analyzed, so that one can estimate secondary loss occurred due to the blade height.
- It does not give a detailed interpretation of flow behaviors due to the lack of validation data.
- The simulations have only been carried out on one stage of compressor.

6.3 Performance Evaluation of Compressor Using C++ High Programming Language

The performance characteristics of axial compressors or their stages at various speeds can be presented in terms of the plots of the following parameters:

I. Pressure rise vs. mass flow rate, $\Delta P=f(\dot{m})$
II. Loading coefficient vs. flow coefficient, $\psi = f(\phi)$
III. Power (work) absorbed by the compressor vs mass flow rate, $P=f(\dot{m})$

I have developed small scale computer programming that used to evaluate the performance of the aero-thermodynamically treated axial flow compressor which is done in chapter 5.

The main objective of developing computer program using previously developed equation is:-

- To evaluate the design and off-design performance of the 7^{th} stage axial flow compressor at each stages for different flight conditions very easily.
- To determine which portion of the blades are heavily loaded and which are slightly loaded.

The flow chart of the program is as follows:

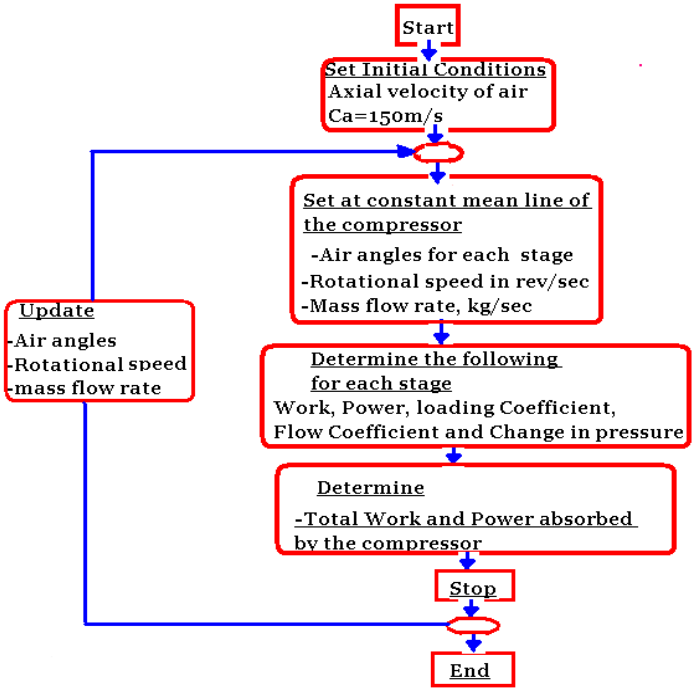

Figure 6.19 Flow Chart of C++ programming

6.3.1 Performance of the Compressor at Design Point Operation

The following result will appear after running the above program at the design condition and based on constant mean radius.

Table 6.3

The performance of the compressor at the design condition

Stage	Work(kJ)	Power(kW)	Torque(N.m)	Blade loading coefficient(BLC)	Flow Coefficient(FC)	Change in Pressure(bar)
1	20.041	400.827	255.304	0.28	0.56	0.2217
2	20.041	400.827	255.304	0.28	0.56	0.2585
3	25.074	501.491	319.421	0.35	0.56	0.3861
4	24.072	481.431	306.644	0.33	0.56	0.4285
5	24.072	481.431	306.644	0.34	0.56	0.4997
6	24.072	481.431	306.644	0.34	0.56	0.5731
7	24.072	481.431	306.644	0.32	0.56	0.6144
Total	161.444	3228.869	2056.605			0.2982

At the mean diameter of the compressor, the third stage is heavily loaded than the first and the second stages. The last stage mean sections are slightly more heavily loaded than the mean sections of the front stages. The values of flow coefficient are in the range of that are put for modern axial flow aircraft engine compressors which is 0.45 to 0.57 [3].

6.3.2 Performance of the Compressor at off –Design operation

Attention so far has focused on the aero-thermodynamic analysis of axial flow compressors to meet a particular design point of mass flow, pressure ratio and efficiency. It must be realized at the outset, however, that any compressor will be required to operate at conditions far removed from the design point including engine starting, idling, reduced power, maximum power, acceleration and deceleration. Thus, it is clear that the compressor must be capable of satisfactory operation over a wide range of rotational speeds and inlet conditions. Therefore, in this section we can see the off-design performance of the compressor using graphical interpretation which resulted after running the C++ programming at different flight conditions of the aircraft. Figure 6.20 depicts theoretical characteristics curves for some values of constant $A = \tan\beta_2 + \tan\alpha_1$. For positive values of A, the curves are falling, while for negative values rising characteristics are obtained. The actual curves will be modified forms of these curves on account of losses. The line in Figure 6.20 is drawn for the case where the efficiency is a maximum at the design flow coefficient,ϕ_d=0.563002.

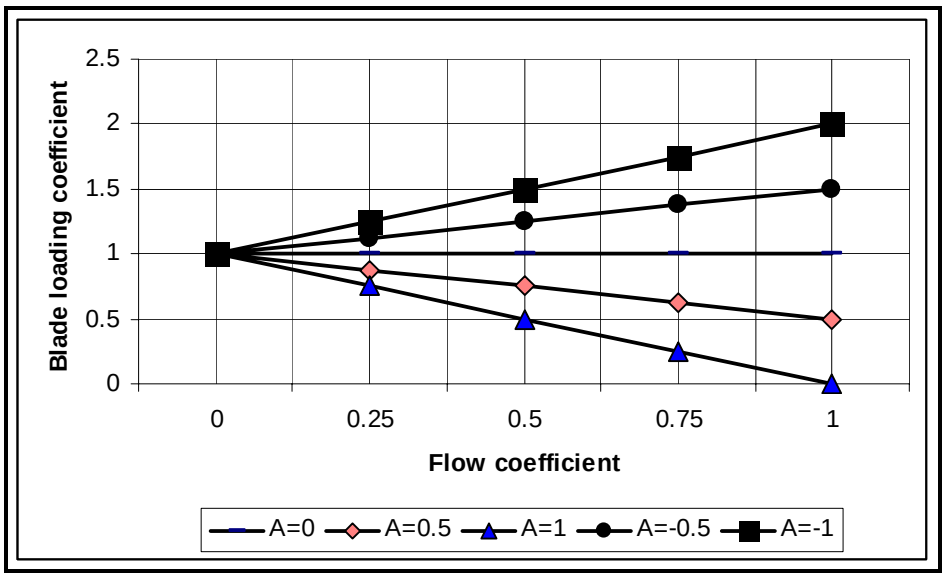

Figure 6.20 Off-design characters tics curve for an axial compressor stage

It is already known that moving away from ϕ_d=0.563002 results in a change in incidence and increased losses. Reducing ϕ(flow coefficient) results in increased positive incidence and stall at a certain value of flow coefficient this has to be determined during compressor testing; increasing eventually results in chocking of the stage and a sever drop in efficiency. It is essential that all individual stages of a compressor operate in the region of high efficiency without encountering either stall or choke at normal operating conditions.

A compressor gives its best performance while operating at its design point, that is at rotational speed, N=250rev/s and mass flow rate, Ma=20kg/s for which it has been designed. However, it also expected to operate away from the design point. Therefore, knowledge about its behavior at off-design operation is also necessary. Figure 6.21 and 6.22 show the off-design performance of the compressor. There is also a limit of operation on the extreme left and right of Figure 6.21 characteristics curve when the mass-flow rate cannot be further increased due to choking. This has to be determined during compressor testing.

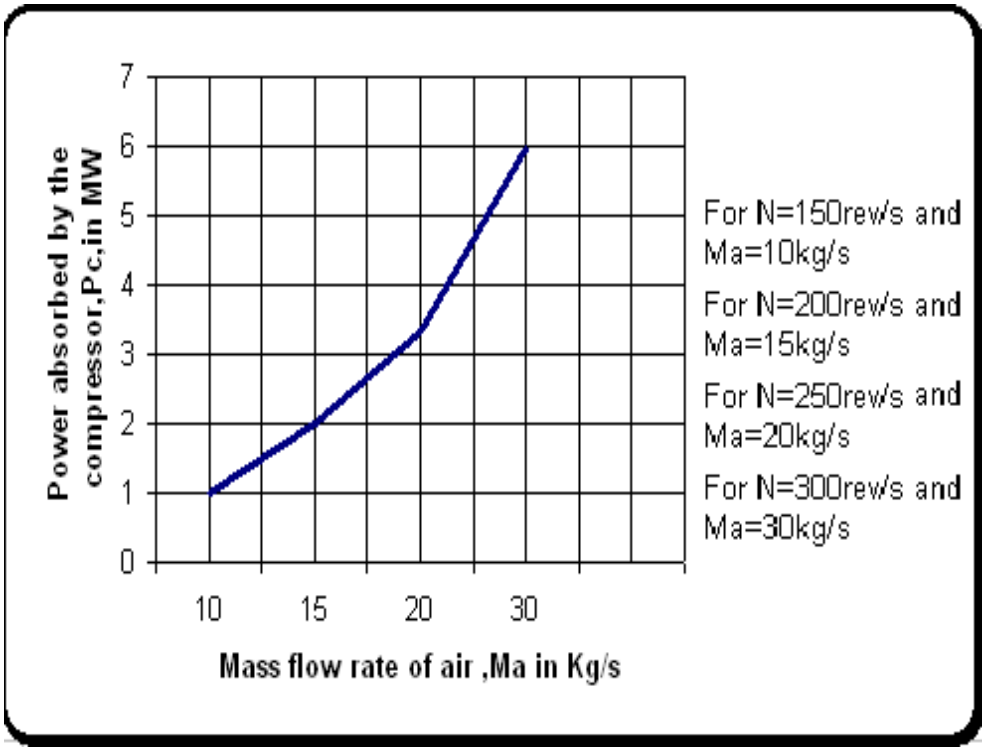

Figure 6.21 Power absorbed by the compressor vs mass flow rate of air at constant mean diameter

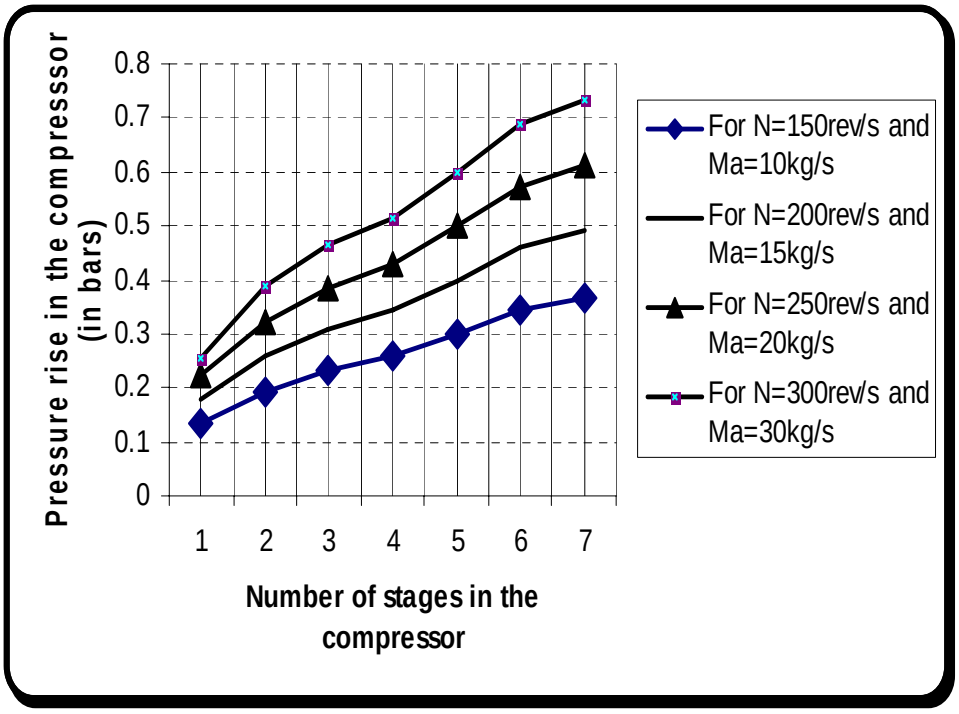

Figure 6.22 Pressure rise vs number of stages in the compressor at constant mean diameter

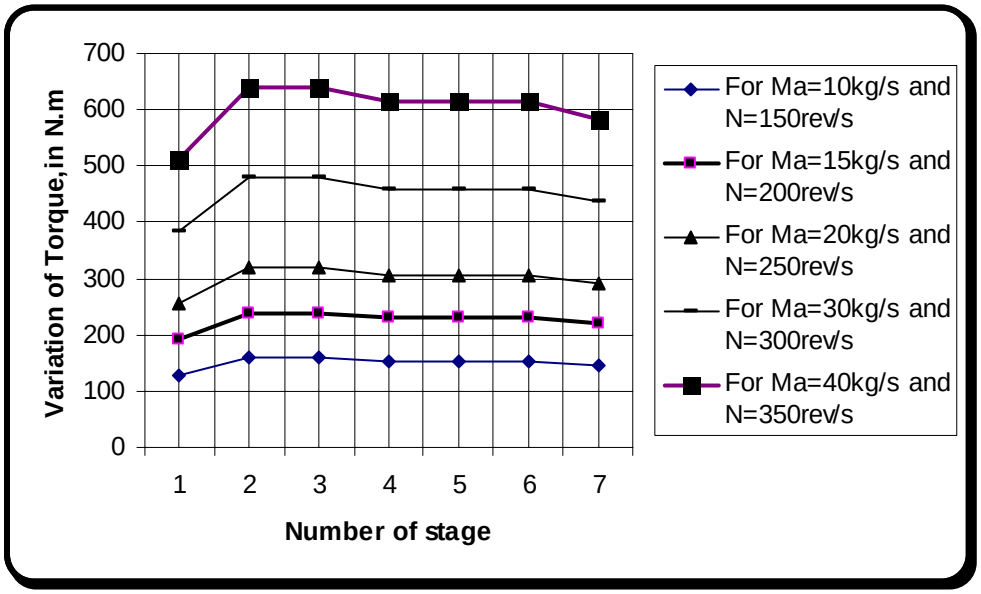

Figure 6.23 Variation of Torque absorbed by the compressor with number of stages

From Figure 6.23 we can see that high Torque is absorbed by the second and third stages for different operational conditions of the compressor.

CHAPTER SEVEN
SUMMARY, CONCLUSIONS AND RECOMMENDATIONS FOR FUTURE WORK

7.1 SUMMARY

Before, coming to conclusion and recommendation, it may be helpful to summarize the main steps in the aerothermodynamics analysis described in the previous sections.

Having made appropriate assumption about the efficiency, tip speed, axial velocity, and so on, it was possible to size the annulus at inlet and outlet of the compressor and calculate the air angles required for each stage at the mean diameter. A choice was then made of a suitable vortex theory to enable the air angles to be calculated at various radii from root to tip. Throughout this work it was necessary to ensure that limitations on blade stresses, rates of diffusion and Mach number were not exceeded. Cascade test data were used to determine a blade geometry which would give these air angles, and also the lift and drag coefficients for a two-dimensional row of blades of this form. Finally, computational fluid dynamic work using FLUENT and C++ programming were done to analyze the compressor.

7.2 CONCLUSIONS

The paper addresses a design optimization problem for axial flow aircraft engine compressor. Although the particular example presented in detail corresponds to the third stage compressor model, it is quite obvious that both the methodologies, as well as the optimization criteria, are valid for any axial compressor design. The optimization criterion considered in this paper is the minimization of weight for aircraft engine compressor by avoiding the inlet guide vane of the compressor and by choosing a suitable axial velocity of air (that does not bring any effect on the flow) which is constant throughout the compressor in the axial direction.

The detailed CFD model of the compressor and its comparison with Howell [9] experimental data were explained as a sample and shown in this work. The computed lift coefficient and drag

coefficient along the blade surfaces using FLUENT were compared with the theoretical (calculated in chapter 5) and experimental values (Howell's data) and the predictions of FLUENT were found to agree very well. Overall, the CFD gave a good prediction of the performance and resolved enough of the local flow details. Using this information of flow phenomena, it is possible to improve compressor performance, or make a new design (low cost and low weight) of axial flow aircraft gas turbine engine compressor.

The final work of the thesis is developing of small scale computer programming software. This will enable us to determine (calculate or identify) the preliminary design and off-design performance of the compressor very easily. Therefore, one may consider this paper as a successful attempt to be a useful guide of the first steps in axial compressor design.

7.3 RECOMMENDATIONS

There are many areas where the work in this thesis can be further developed. The following list outlines some of the critical areas where future research is needed:

- In practice, the process will be one of continued refinement, coupled with feedback from other groups such as the designers of the combustion system and turbine, metallurgists and stress analysts, and those concerned with mechanical problems associated with whirling speeds, bearing, stiffens of structural members and so on.
- The program could be extended and improved to predict the flow characteristics for turbine.
- At the same time the turbine designer will be examining a suitable turbine and the compressor and turbine designers must keep in close contact while establishing preliminary designs. It would be important to minimize the number of turbine stages, again for reasons of cost.
- For a fixed blade speed, then, the rotational speed will also be a function of hub–tip ratio. Thus the designer will, in very short order, be presented with a wide range of solutions and must use his judgment to select the most promising.
- Mesh algorithm improvement, FLUENT setup, and automatic relational database creation.

REFERENCE:

[1]. HORLOCK.J.H: 'Axial flow compressors: fluid mechanics and Thermodynamics (1958).

[2]. GOSTELOW,J.P., HORLOCK,J>H> and MARSH,H., Recent developments in the aerodynamic design of axial flow compressors. Symposium at war wick university. Proc.Instn.Mech.Engs. London, 183, Pt.3N (1969).

[3].SM YAHYA Turbines, Compressors and Fans. Indian Institute of Technology New Delhi.

[4]. Holtzmann, charl. Lehrbuch Der Theoretischen Mechanik, J.B.Metzler, Stuttgart, 1861.

[5]. HOWELL, A.R., Fluid dynamics of axial flow compressors. Proc.Instn.Mech.Engrs.London, 153 (1943).

[6]. HOWELL, A.R. and BONHAM, R.P., overall and stage characteristics of axial flow compressors. Proc.Instn.Mech.Engrs.London, 163 (1950).

[7] http://www. Tutorial-10 the flow in an axial fan using the Mixing plane model

[8].TODD,K.W., Practical aspects of cascade wind tunnel research.

Proce.Instn.Mech.Engrs.London, 157(1947).

[9]. HOWELL, A.R., The present basis of axial compressor design: Part I-Cascade theory and performance. A.R.C.R. and M.2095 (1942).

[10]. HOWELL, A.R. Design of Axial Flow compressors. Proc.Instn.Mech.Engrs.London 153(1945).

[11]. HORLOCK,J.P., Axial flow compressors, Butter worth, London (1958).

[12]. http://www.pagendarm.de/trapp/programming/java/profiles/NACA4.html

[13]. http://www.airfoil analyzer software.

[14]. Special topics on map meshing in turbo machinery, periodical poly technical ser. transp. eng. vol. 34, no. 1–2, pp. 59–68 (2006)

[15]. Fluent Inc.: FLUENT 6.3.26 Documentation – User's Guide, 2006.

[16]. Dixon S.L.: Fluid Mechanics and Thermodynamics of Turbo machines, Fourth Edition, University of Liverpool, 2005.

[17].http://www.GAMBIT 2.2 tutorials

APPENDIX A

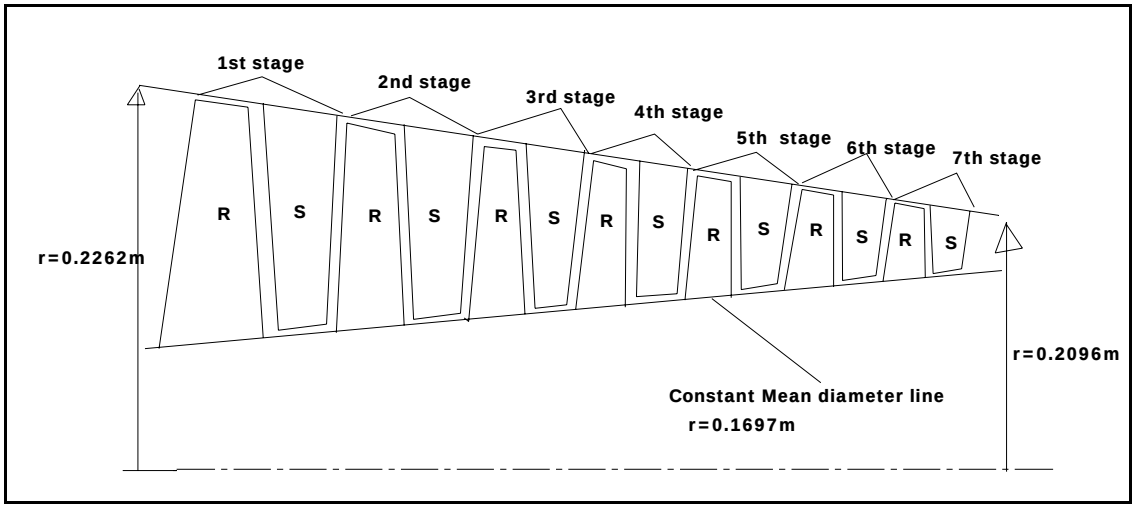

Figure-1 Annulus shape of the seven stages single spool axial flow aircraft engine compressor-schematic diagram

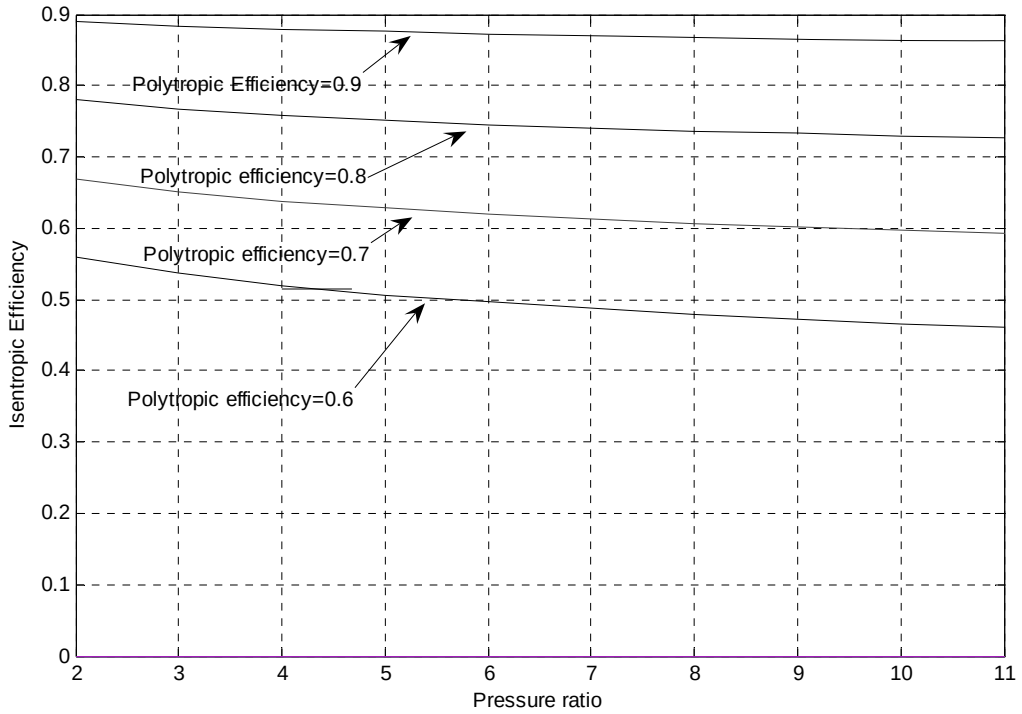

Figure 2 Relationship between overall efficiency, pressure ratio and small stage (polytropic) efficiency for a compressor (γ=1.4)

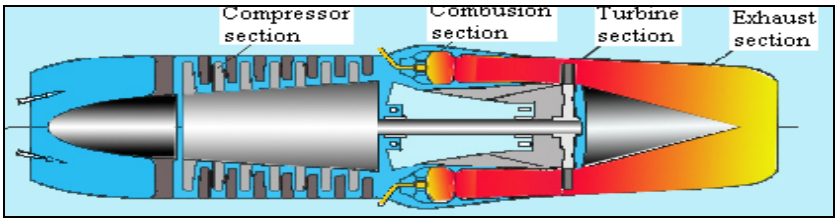

Figure 3 Construction of Turbojet engine-schematic diagram

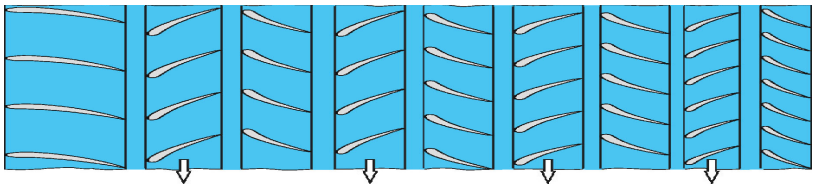

Figure 4 Two dimensional cascade representation of compressor-schematic diagram.

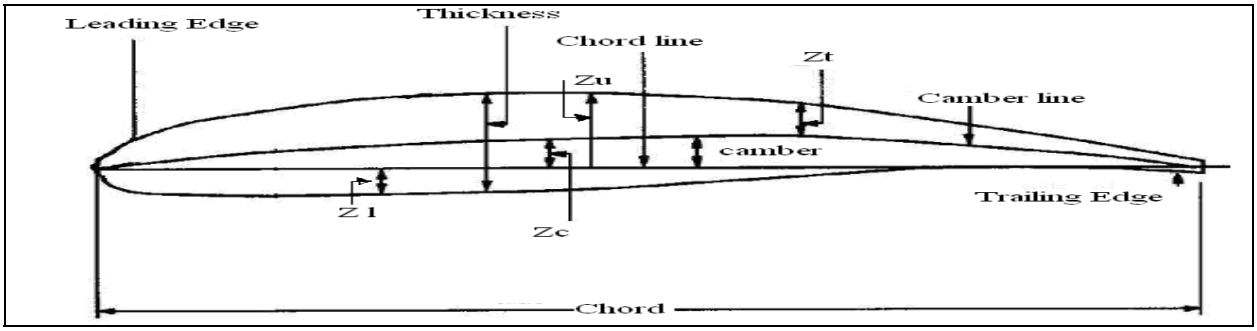

Figure 5 Schematic Diagram of Airfoil Theory [2]

The constant Z_U, Z_t, Z_l, Z_c can be calculated by the following formula:

$$Z_c = \left(\frac{Z_u + Z_l}{2}\right), Z_t = \left(\frac{Z_u - Z_l}{2}\right), Z_l = \left(\frac{Z_c + Z_t}{2}\right) \text{ and } Z_C = \left(\frac{Z_c - Z_t}{2}\right)$$

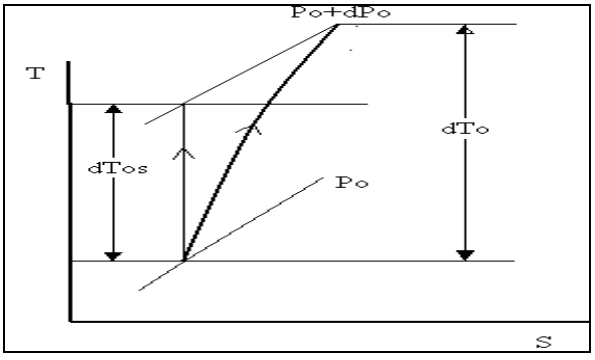

Figure 6 A T-S diagram which shows incremental change of state in a compression process.

APPENDIX B

Table 1 Selected thickness of NASA 65 -410 series airfoils [13]

NACA Mean Line 65-410					
(Stations and ordinates given in percent of airfoil chord)					
x	Y	dy/dx	x	Y	dy/dx
0	0	0.24	45	5.94	0.024
0.5	0.1194	0.2376	50	6	0
0.75	0.1786	0.2364	55	5.94	-0.024
1.25	0.2963	0.234	60	5.76	-0.048
2.5	0.585	0.228	65	5.46	-0.072
5	1.14	0.216	70	5.04	-0.096
7.5	1.665	0.204	75	4.5	-0.12
10	2.16	0.192	80	3.84	-0.144
15	3.06	0.168	85	3.06	-0.168
20	3.84	0.144	90	2.16	-0.192
25	4.5	0.12	95	1.14	-0.216
30	5.04	0.096	100	0	-0.24
35	5.46	0.072			
40	5.76	0.048			

APPENDIX C Used Software

In this work, commercially available and free software was used. The Free Software used was published under the Gnu Public License (GPL). The programs used were as shown below to select the different airfoil geometry.

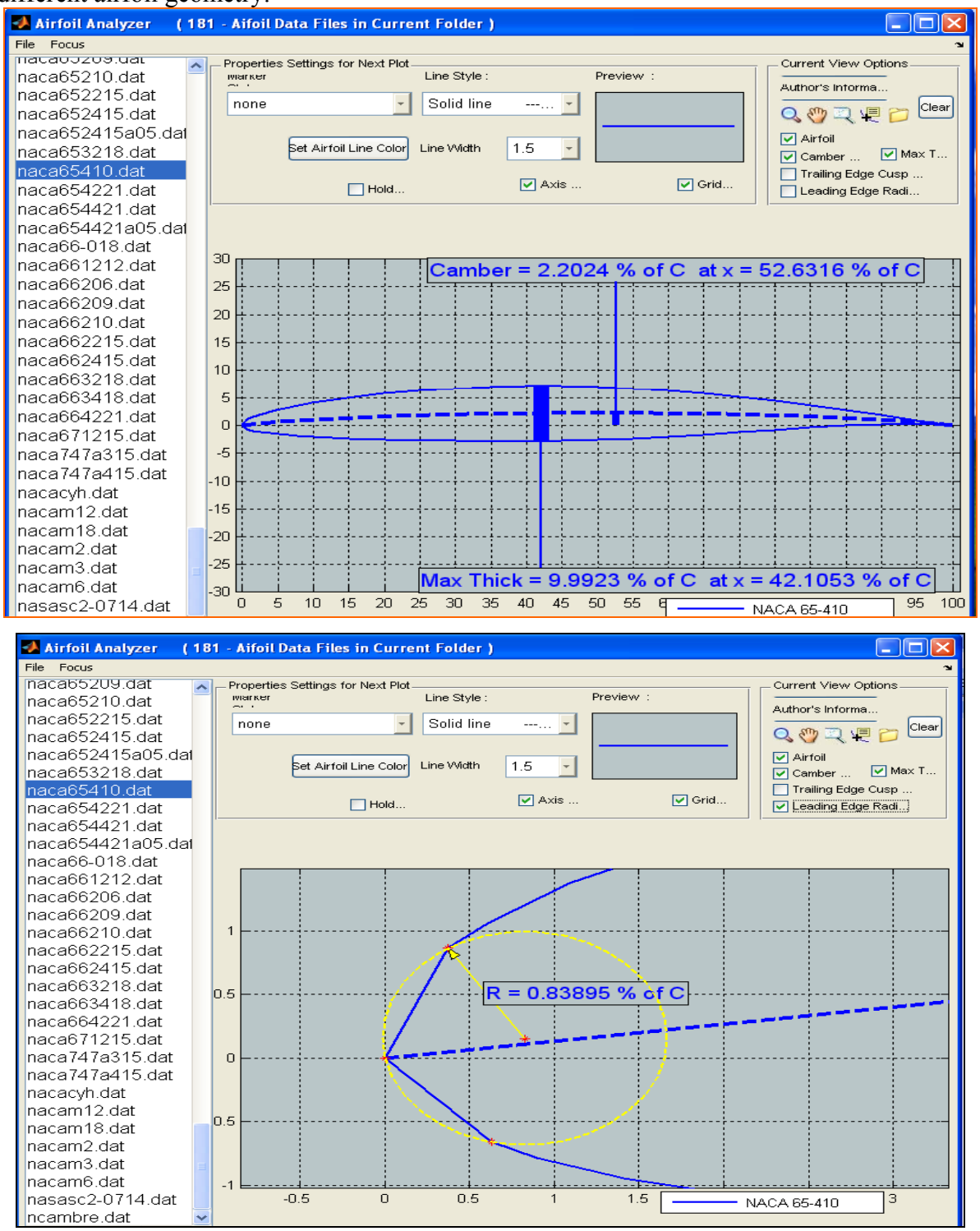

Figure 7 Airfoil data file analyzer software [13]

APPENDIX D

Developed C++ Program For Performance Evaluation Of The Compressor.

```
#include<iostream.h>

#include<iomanip.h>

#include<math.h>

#include<stdlib.h>

#include<conio.h>

const float Ca=150;

int i;

float Ma, N, r, Wc, Pc, Tc;

struct m

{

int stage;

float Work, Power, Flowcoeff, Torque, V, Change in pressure;

double  beta1;

double beta2;

double lamda;

double Density;

}

arr[20];

void give stage()

{

for(int i=0;i<7;i++)

arr[i].stage=i+1;

}
```

```
void getdata()

{

give stage();

arr[0].beta1=60.64;arr[0].beta2=51.67;arr[0].lamda=0.98;arr[0].Density=1.106;

arr[1].beta1=60.64;arr[1].beta2=51.67;arr[1].lamda=0.98;arr[1].Density=1.29;

arr[2].beta1=51.24;arr[2].beta2=28.00;arr[2].lamda=0.88;arr[2].Density=1.54;

arr[3].beta1=51.38;arr[3].beta2=27.71;arr[3].lamda=0.83;arr[3].Density=1.78;

arr[4].beta1=51.38;arr[4].beta2=27.71;arr[4].lamda=0.83;arr[4].Density=2.077;

arr[5].beta1=51.38;arr[5].beta2=27.71;arr[5].lamda=0.83;arr[5].Density=2.381;

arr[6].beta1=50.98;arr[6].beta2=28.52;arr[6].lamda=0.83;arr[6].Density=2.685;

cout<<"\n Enter the mass flow rate of air in the compressor, Kg/sec.\n=>";

cin>>Ma;

cout<<"\n Enter the rotational speed of the rotor shaft in terms of revolution per second.\n=>";

cin>>N;

cout<<"\n Enter the radial distance from the center of the compressor in meter.\n=>";

cin>>r;

} void display()

{

for(i=0;i<7;i++)

{arr[i].Work=arr[i].lamda*2*3.14*N*r*Ca*(tan(arr[i].beta1*3.14/180)-tan(arr[i].beta2*3.14/180));

 arr[i].Power=Ma*arr[i].Work;  arr[i].Flowcoeff=Ca/(2*3.14*N*r); arr[i].change in pressure=arr[i].Work*arr[i].Density

 arr[i].Torque=arr[i].lamda*Ma*r*Ca*(tan(arr[i].beta1*3.14/180)-tan(arr[i].beta2*3.14/180));

arr[i].V=(arr[i].lamda*2*3.14*N*r*Ca*(tan(arr[i].beta1*3.14/180)-
tan(arr[i].beta2*3.14/180)))/(2*3.14*N*r*2*3.14*N*r);

 Wc=Wc +arr[i].Work; Pc=Pc+ arr[i].Power; Tc=Tc+ arr[i].Torque;

 }
```

```
 cout<<"\n\n";

cout<<"\nstage"<<"\t Work (KJ)"<<"\tpower (KW)"<<"\tTorque (N.m)"<<" \tBLC"<<"\change in pressure (bar)"<<"
\tFC\n";

cout<<"\n================================================================================";

  for(i=0;i<7;i++)

  {

cout<<"\n"<<arr[i].stage<<""<<arr[i].Work<<""<<arr[i].Power<<""<<arr[i].Torque<<""<<arr[i].V<<"
"<<arr[i].Flowcoeff;

  }

  cout<<"\n--------------------------------------------------------------------------\n";

cout<<" "<<Wc<<" "<<Pc<<" "<<Tc;

}void main()

{

clrscr();

cout<<"\n\t\t\t Enter the following number";

cout<<"\n\t\t\t================================================================================";

getdata();

cout<<"\n\t\t The performance of the compressor for the above data";

cout<<"\n\t\t================================================================================";

display();

getch();

  }
```

DECLARATION

I hereby declare that the work which is presented in this thesis entitled *"**Aerothermodynamics Analysis of Axial Flow Aircraft Gas Turbine Engine Compressor**"* is original work of my own, has not been presented for a degree in any other university and that all sources of material used for the thesis have been duly acknowledged.

TILAHUN NIGUSSIE GEMECHU DATE